

SUPPLEMENTAL MATERIAL TO:

Atypical epigenetic and small RNA control of degenerated transposons and their fragments in clonally reproducing *Spirodela polyrhiza*

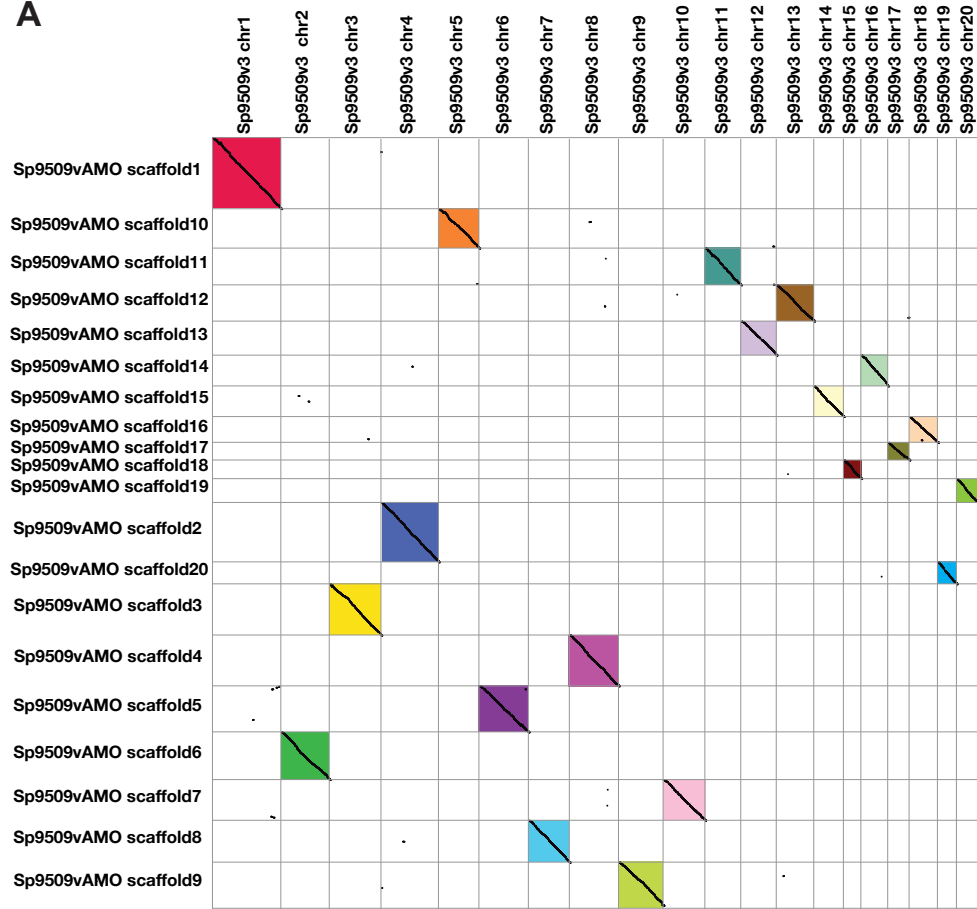
Rodolphe Dombey, Daniel Buendía-Ávila, Verónica Barragán-Borrero, Laura Diezma-Navas, Arturo Ponce-Mañe, José Mario Vargas-Guerrero, Rana Elias and Arturo Marí-Ordóñez.

Table of contents:

Page	
2	Supplemental Figure 1: Genetic differences between Sp9509 from RDSC and Landolt collection
3	Supplemental Figure 2: Phylogenetic position of <i>Spirodela</i> within flowering plants
4	Supplemental Figure 3: Small RNA profiles of <i>Arabidopsis</i> WT, <i>nrdp1</i> and <i>Spirodela</i>
5	Supplemental Figure 4: Gene body methylation in <i>Spirodela</i>
6	Supplemental Figure 5: List of gene IDs shown in Figure 2
7	Supplemental Figure 6: Phylogenetic analysis of <i>Spirodela polyrhiza</i> DRB proteins
8	Supplemental Figure 7: Phylogenetic analysis of <i>Spirodela polyrhiza</i> RDR proteins
9	Supplemental Figure 8: Phylogenetic analysis of <i>Spirodela polyrhiza</i> DCL proteins
10	Supplemental Figure 9: Phylogenetic analysis of <i>Spirodela polyrhiza</i> AGO proteins
12	Supplemental Figure 10: <i>Spirodela</i> #9509 AGO5 cluster
13	Supplemental Figure 11: Phylogenetic analysis of <i>Spirodela polyrhiza</i> SHH proteins
14	Supplemental Figure 12: Phylogenetic analysis of <i>Spirodela polyrhiza</i> Snf2 chromatin remodelers
16	Supplemental Figure 13: Phylogenetic analysis of <i>Spirodela polyrhiza</i> SUVH and SUVR proteins
18	Supplemental Figure 14: Phylogenetic analysis of <i>Spirodela polyrhiza</i> DNA methyltransferases
19	Supplemental Figure 15: Phylogenetic analysis of <i>Spirodela polyrhiza</i> RNA Pol. large subunit (NRP) proteins
21	Supplemental Figure 16: Phylogenetic analysis of <i>Spirodela polyrhiza</i> SPT5 and SPT5L proteins
23	Supplemental Figure 17: Phylogenetic analysis of <i>Spirodela polyrhiza</i> VIM proteins
24	Supplemental Figure 18: Phylogenetic analysis of <i>Spirodela polyrhiza</i> SUVH5/6 and ASI1 proteins
25	Supplemental Figure 19: Genome-wide distribution of DNA methylation in <i>Spirodela polyrhiza</i>
26	Supplemental Figure 20: Distribution of CHH DNA methylation in <i>Spirodela polyrhiza</i>
27	Supplemental Figure 21: Transposon classification, nomenclature and codes used in this study
28	Supplemental Figure 22: Transposon composition of <i>Arabidopsis</i> (Col-0) and <i>Spirodela</i> (9509) genomes
29	Supplemental Figure 23: mCHH levels across TE sizes and RLC and RLG length distribution
30	Supplemental Figure 24: Mass-spectrometry (MS) quantification of H3K9me1/2 abundance in <i>Spirodela</i>
31	Supplemental Figure 25: Chromatin immunoprecipitation (ChIP) workflow and quality control in <i>Spirodela</i>
32	Supplemental Figure 26: Genome-wide distribution of H3K9me1, H3K9me2 and H3K27me3 in <i>Spirodela</i>
33	Supplemental Figure 27: <i>Spirodela</i> chromatin organization in interphase nuclei
34	Supplemental Figure 28: Distribution of H3K9me1/2 in <i>Spirodela</i> TEs
35	Supplemental Figure 29: Relative position of H3K9me1 and H3K9me2 peaks to each other in <i>Spirodela</i>
36	Supplemental Figure 30: Analysis of H3K9me1/2 association to DNA methylation in <i>Arabidopsis</i> and <i>Spirodela</i>
37	Supplemental Figure 31: Patterns of H3K27me1 and H3K9me1/2 distribution in <i>Spirodela polyrhiza</i> transposons
38	Supplemental Figure 32: Analysis of the epigenetic and small RNA landscape of 5S rRNA repeats in <i>Spirodela</i>
39	Supplemental Figure 33: Distribution of silencing marks and sRNAs in <i>Arabidopsis</i> RLC and RLG complete TEs
40	Supplemental Figure 34: LTR identification for complete TEs in Figure 6
41	Supplemental Figure 35: Defects in <i>SpAGO4a</i> splicing in <i>N. benthamiana</i> prevent its transient expression
42	Supplemental Figure 36: Additional examples of siRNA producing TEs in <i>Spirodela</i>
43	Supplemental Figure 37: TAS3 tasiRNAs in <i>Spirodela</i>
44	Supplemental Figure 38: Transient expression procedure in <i>Spirodela</i>
46	Supplemental Figure 39: Oligos used in this study
47	Supplemental Methods
58	References to Supplemental Methods

SUPPLEMENTAL FIGURE S1

A



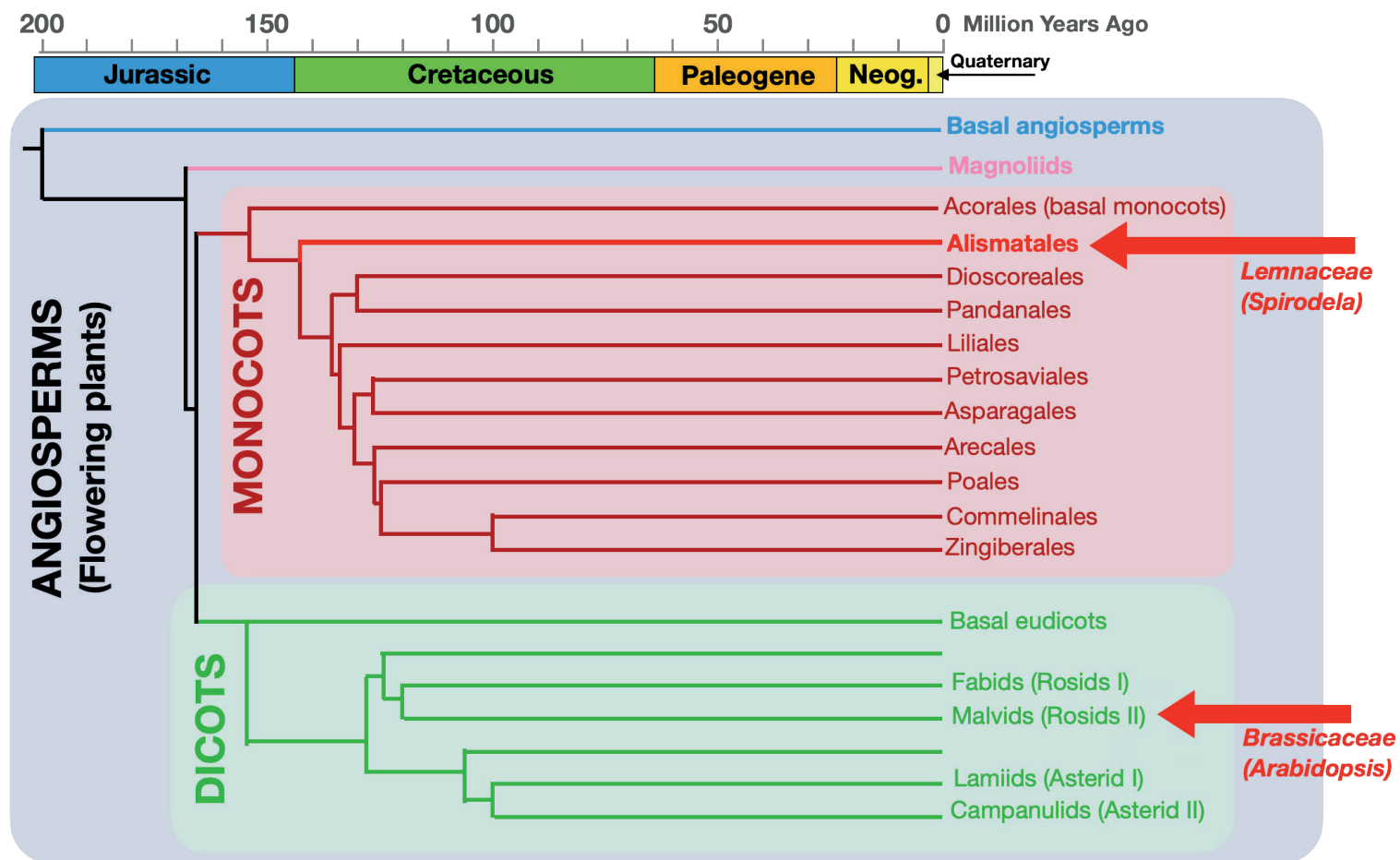
B

Chr	SNPs	INDELs	Mixed
1	37731	12583	95
2	29937	9288	68
3	38448	11399	68
4	29164	10081	85
5	23655	8101	66
6	28412	10142	91
7	26706	9233	85
8	32969	9520	70
9	19155	7873	53
10	33311	9768	78
11	28157	8431	65
12	23193	8181	82
13	19514	7285	51
14	20716	6278	28
15	30989	7471	71
16	24749	6791	44
17	17239	5592	56
18	13502	6255	23
19	22995	5061	41
20	12333	4364	44
Total	512875	163697	1264

Supplemental Figure S1: Genetic differences between Sp9509 from RDSC and Landolt collection.

(A) Syntenic dotplot between Sp9509 from RDSC and Landolt collection, the analysis was generated with SynMap from genomevolution.org using default parameters. **(B)** Summary table of identified variations between Sp9509 from RDSC and Landolt collection, using gatk (version 3.8-1).

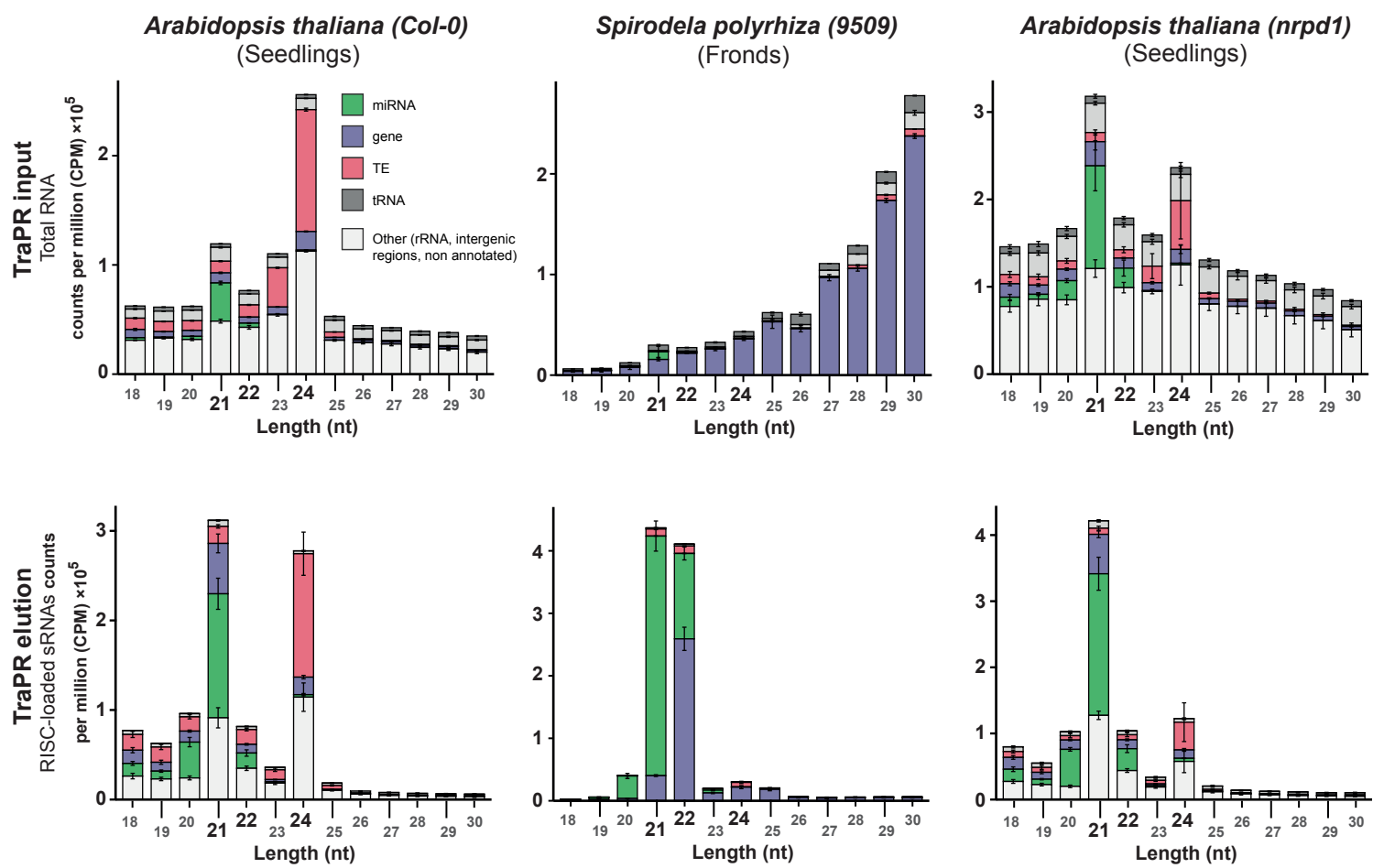
SUPPLEMENTAL FIGURE S2



Supplemental Figure S2: Phylogenetic position of *Spirodela* within flowering plants.

Summary of the phylogenetic placement of *Spirodela* and *Arabidopsis* within angiosperms.

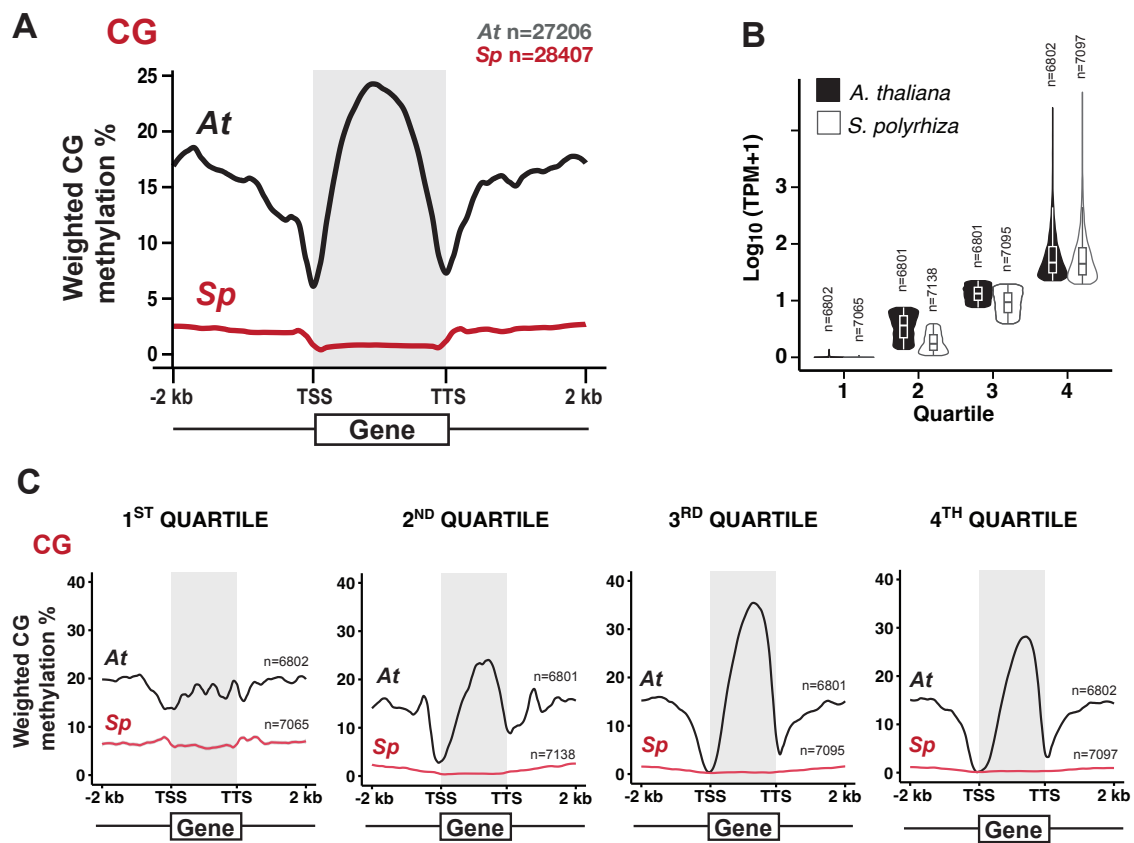
SUPPLEMENTAL FIGURE S3



Supplemental Figure S3: Small RNA profiles of *Arabidopsis* WT, *nrpd1* and *Spirodea*.

Size distribution and genomic feature annotation of small RNA extracted from TraPR Input (lysate) and elution from *Arabidopsis* Col-0 WT, *nrpd1* seedlings and *Spirodea* fronds. Error bars represent standard deviation of the mean from three biological replicates

SUPPLEMENTAL FIGURE S4



Supplemental Figure S4: Gene-body Methylation in *Spirodela*.

(A) Metaplots of average weighted CG DNA methylation over protein coding genes and ± 2 kb flanking regions in *Arabidopsis* and *Spirodela*. (B) Violin and box plots of *Spirodela* and *Arabidopsis* gene expression sorted into quartiles based on transcript levels. In boxplots, median is indicated by solid bar, the boxes extend from the first to the third quartile and whiskers stretch to the furthest value within 1.5 times the interquartile range for each set. (C) Metaplots of average weighted CG DNA methylation over protein coding genes and ± 2 kb flanking regions in *Arabidopsis* and *Spirodela* within each set of genes sorted by expression quartiles set in (B). At: *Arabidopsis*, Sp: *Spirodela*.

SUPPLEMENTAL FIGURE S5

miRNA biogenesis

<i>Arabidopsis (Col-0)</i>		<i>Spirodelia (9509)</i>	
GENE	AGI	GENE	Sp9509GI
AtSE	AT2G27100	SpSE	Sp9509d012g007660
AtHYL1	AT1G09700	SpHYL1	Sp9509d001g003860
AtDRB2	AT2G28380	SpDRB2a	Sp9509d002g000320
		SpDRB2b	Sp9509d014g000150
AtHEN1	AT4G20910	SpHEN1	Sp9509d017g000460
AtDCL1	AT1G01040	SpDCL1	Sp9509d002g008800

24-nt siRNA/RdDM

<i>Arabidopsis (Col-0)</i>		<i>Spirodelia (9509)</i>	
GENE	AGI	GENE	Sp9509GI
AtSHH1	AT1G15215		
AtCLSY1	AT3G42670		
AtCLSY2	AT5G20420		
AtCLSY3	AT1G05490	SpCLSY3	Sp9509d011g003360
AtCLSY4	AT3G24340		
AtNRPD1	AT1G63020	SpNRPD1	Sp9509d0013g000080
AtRDR2	AT4G11130	SpRDR2	Sp9509d002g008450
AtDCL3	AT3G43920	SpDCL3	Sp9509d005g001240
AtSUVH2	AT2G33290	SpSUVH2	Sp9509d020g001160
AtSUVH9	AT4G13460		
AtDRD1	AT2G16390	SpDRD1	Sp9509d007g000370
AtNRPE1	AT2G40030	SpNRPE1	Sp9509d003g010520
AtSPT5L	AT5G04290	SpSPT5L	Sp9509d001g003550
AtDRM2	AT2G33830	SpDRM2	Sp9509d008g003000
AtDRM1	AT1G28330		
AtDRM3	AT3G17310		

21-22-nt siRNA biogenesis

<i>Arabidopsis (Col-0)</i>		<i>Spirodelia (9509)</i>	
GENE	AGI	GENE	Sp9509GI
AtSGS3	AT5G23570	SpSGS3	Sp9509d004g006000
AtRDR1	AT1G14790	SpRDR1a	Sp9509d018g002090
		SpRDR1b	Sp9509d018g002070
AtRDR6	AT3G49500	SpRDR6	Sp9509d006g004830
AtRDR3	AT2G19910		
AtRDR4	AT2G19920		
AtRDR5	AT2G19930		
AtDRB4	AT3G62800	SpDRB4	Sp9509d001g004790
AtDRB7.1	AT1G80650		
AtDRB7.2	AT4G00420		
AtDCL4	AT5G20320	SpDCL4	Sp9509d005g008560
AtDCL2	AT3G03300		
RTL1	AT4G15417		

Argonautes

<i>Arabidopsis (Col-0)</i>		<i>Spirodelia (9509)</i>	
GENE	AGI	GENE	Sp9509GI
AtAGO1	AT1G48410	SpAGO1	Sp9509d020g001530
AtAGO10	AT5G43810	SpAGO10	Sp9509d008g011640
AtAGO5	AT2G27880	SpAGO5a	Sp9509d007g002750
		SpAGO5b	Sp9509d007g002760
		SpAGO5c	Sp9509d007g002770
		SpAGO5d	Sp9509d007g002790
		SpAGO5e	Sp9509d007g002800
		SpAGO5f	Sp9509d007g002810
		SpAGO5g	Sp9509d007g002820
		SpAGO5h	Sp9509d007g002830
AtAGO2	AT1G31280		
AtAGO3	AT1G31290		
AtAGO7	AT1G69440	SpAGO7	Sp9509d009g009840
AtAGO4	AT2G27040	SpAGO4a	Sp9509d001g011250
		SpAGO4b	Sp9509d006g000640
AtAGO8	AT5G21030		
AtAGO9	AT5G21150		
AtAGO6	AT2G32290		

DNA methylation maintenance

<i>Arabidopsis (Col-0)</i>		<i>Spirodelia (9509)</i>	
GENE	AGI	GENE	Sp9509GI
AtDDM1	AT5G66750	SpDDM1	Sp9509d003g002770
AtMET1	AT5G49160	SpMET1	Sp9509d003g004910
AtVIM1	AT1G57820	SpVIM	Sp9509d004g007270
AtVIM2	AT1G66050		
AtVIM3	AT5G39550		
AtVIM4	AT1G66040		
AtVIM5	AT1G57800		
AtCMT3	AT1G69770		
AtCMT2	AT4G19020	SpZMET	Sp9509d003g011020
AtSUVH4	AT5G13960	SpSUVH4	Sp9509d004g011450
AtSUVH5	AT2G35160		
AtSUVH6	AT2G22740	SpSUVH6(5)	Sp9509d008g010000

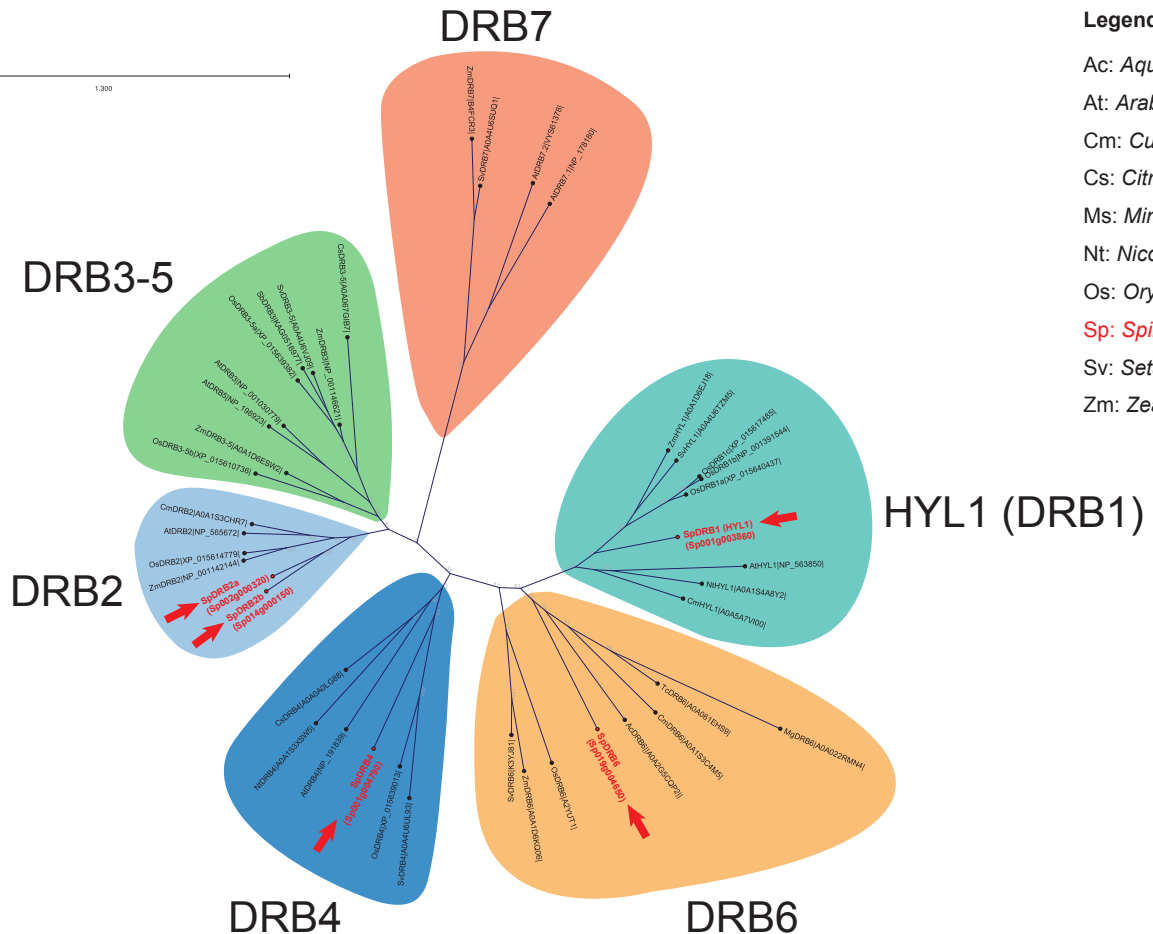
Other

<i>Arabidopsis (Col-0)</i>		<i>Spirodelia (9509)</i>	
GENE	AGI	GENE	Sp9509GI
AtSHH2	AT3G18380	SpSHH2a	Sp9509d020g005890
		SpSHH2b	Sp9509d009g007120
		SpDRB6	Sp9509d019g004650
AtASI1	AT5G11470	SpASI1	Sp9509d005g000050

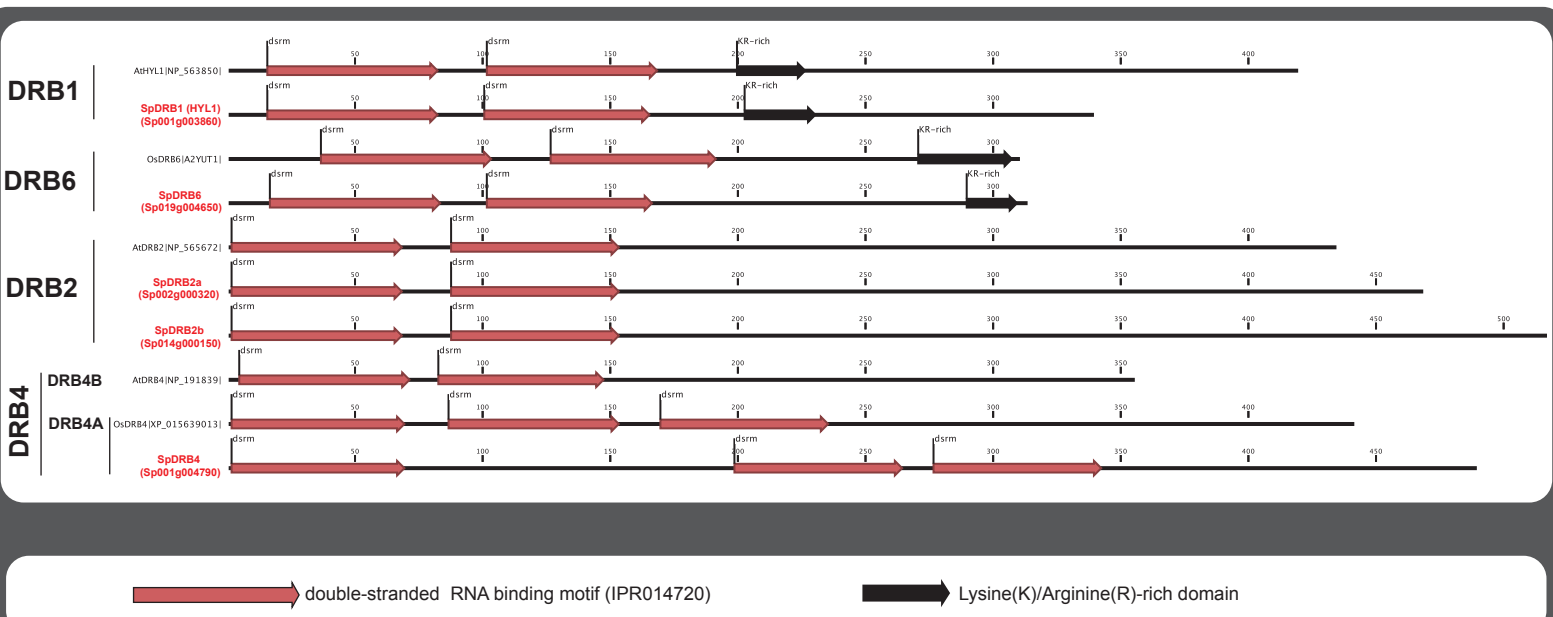
Supplemental Figure S5: List of gene IDs shown in Figure 2.

SUPPLEMENTAL FIGURE S6

A



B

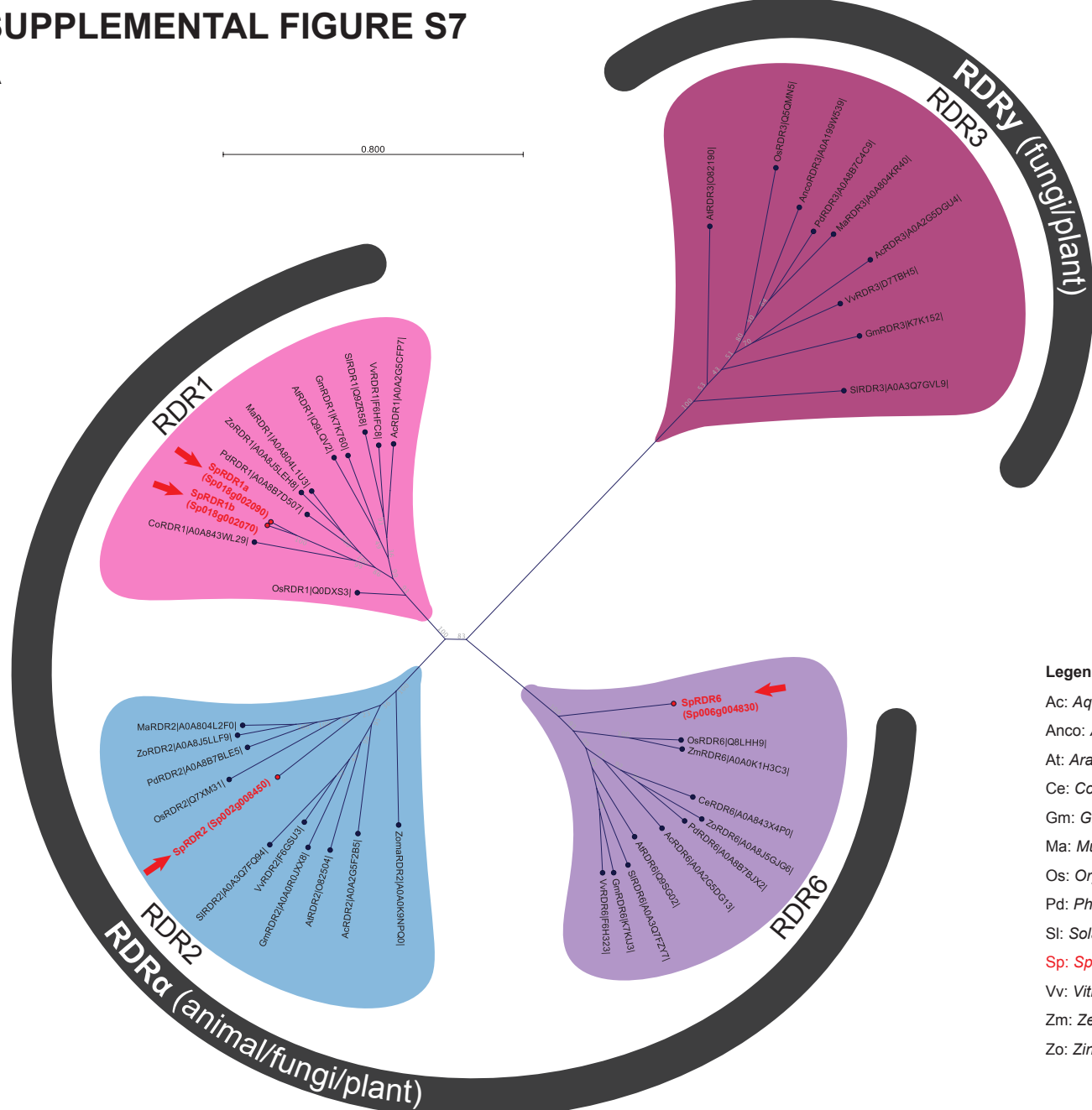


Supplemental Figure S6: Phylogenetic analysis of *Spirodela polyrhiza* DRB proteins.

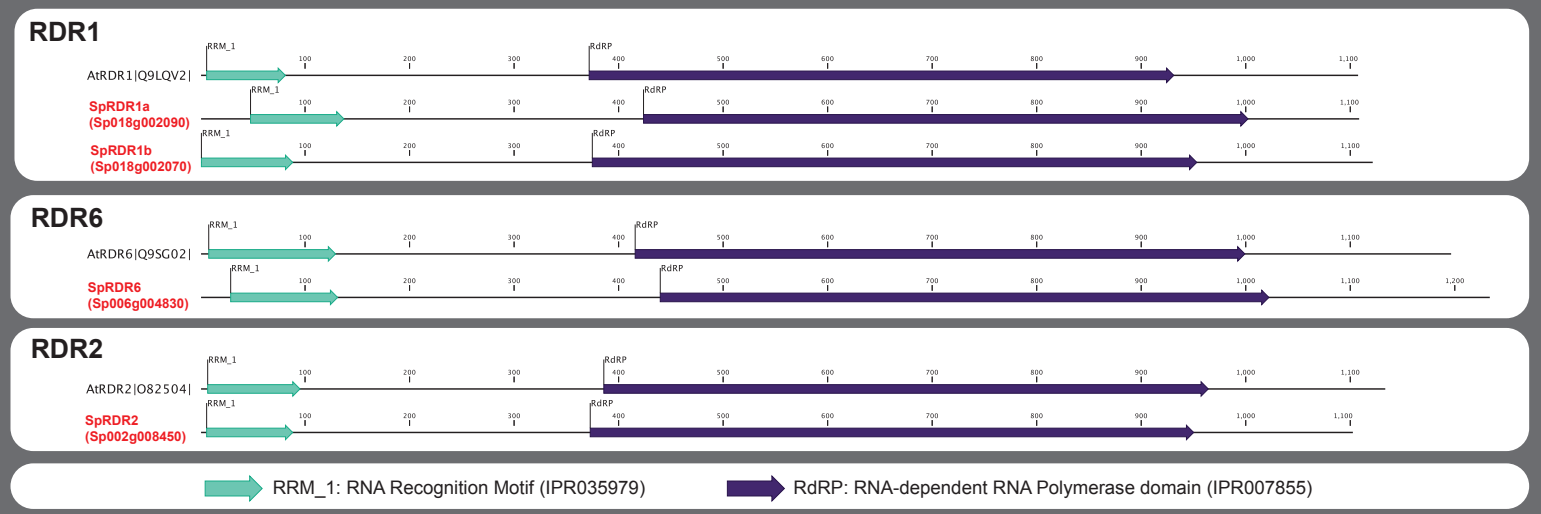
(A) Unrooted phylogenetic tree of DRB proteins from several angiosperms including those identified in the *Spirodela polyrhiza* genome. The maximum likelihood tree was constructed with 1000 bootstrap replications. Protein families are highlighted in bubbles of different colors. Arrows point to *Spirodela* proteins. *Spirodela* proteins and annotations were named accordingly to their position in the tree. Uniprot entry codes appear next to the name of proteins in the tree. For *Spirodela*, the gene annotation ID is shown instead. The sequence of all proteins used to build the tree, their alignment and tree files can be found in the raw data files corresponding to this figure. (B) Domain annotation of *Spirodela* proteins in (A) along those of their orthologues in other plant species. Numbers along linear protein representations indicate positions in amino acids. Domain annotations were obtained using Interpro and Pfam databases, their integrated InterPro ID codes are display in the graphical legend. Filled arrows indicate significant domain predictions, empty arrows indicate non-significant predictions. For simplicity, Sp9509 gene identifiers have been shortened from Sp9509d(xxx)g(yyyyyy) to Sp(xxx)g(yyyyyy) (where (xxx) is chromosome number, and (yyyyyy) gene number).

SUPPLEMENTAL FIGURE S7

A



B



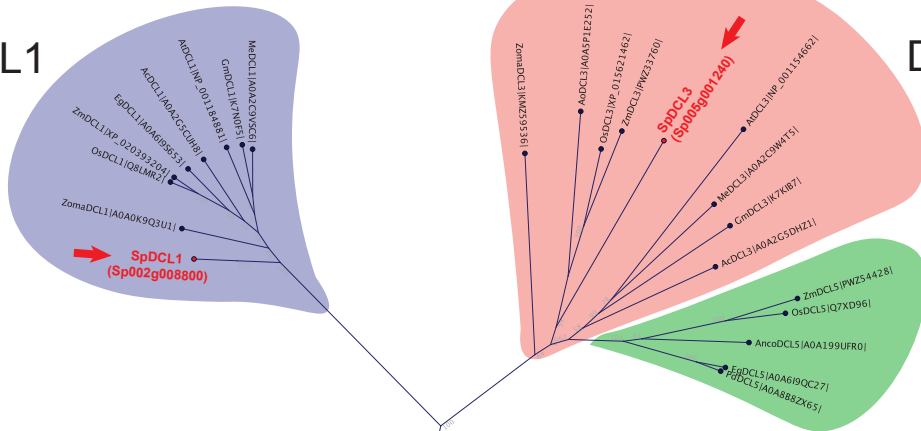
Supplemental Figure S7: Phylogenetic analysis of *Spirodela polyrhiza* RDR proteins.

(A) Unrooted phylogenetic tree of RNA-dependent RNA Polymerases, RdRPs (RDRs), proteins from several angiosperms, including those identified in the *Spirodela polyrhiza* genome. The maximum likelihood tree was constructed with 1000 bootstrap replications. Protein families are highlighted in bubbles of different colors. Arrows point to *Spirodela* proteins. *Spirodela* proteins and annotations were named accordingly to their position in the tree. Uniprot entry codes appear next to the name of proteins in the tree. For *Spirodela*, the gene annotation ID is shown instead. The sequence of all proteins used to build the tree, their alignment and tree files can be found in the raw data files corresponding to this figure. (B) Domain annotation of *Spirodela* proteins in (A) along those of their orthologues in other plant species. Numbers along linear protein representations indicate positions in amino acids. Domain annotations were obtained using Interpro and Pfam databases, their integrated InterPro ID codes are display in the graphical legend. Filled arrows indicate significant domain predictions, empty arrows indicate non-significant predictions. For simplicity, Sp9509 gene identifiers have been shortened from Sp9509d(xxx)g(yyyyyy) to Sp(xxx)g(yyyyyy) (where (xxx) is chromosome number, and (yyyyyy) gene number).

SUPPLEMENTAL FIGURE S8

A

DCL1



DCL3

DCL5

Legend:

- Ac: *Aquilegia coerulea*
- Anco: *Ananas comosus*
- Ao: *Asparagus officinalis*
- At: *Arabidopsis thaliana*
- Eg: *Elaeis guineensis*
- Gm: *Glycine max*
- Me: *Manihot esculenta*
- Os: *Oryza sativa*
- Pd: *Phoenix dactylifera*
- Sl: *Solanum lycopersicum*
- Sp: *Spirodela polyrhiza*
- Zm: *Zea mays*
- Zoma: *Zostera marina*

DCL2

DCL4

B

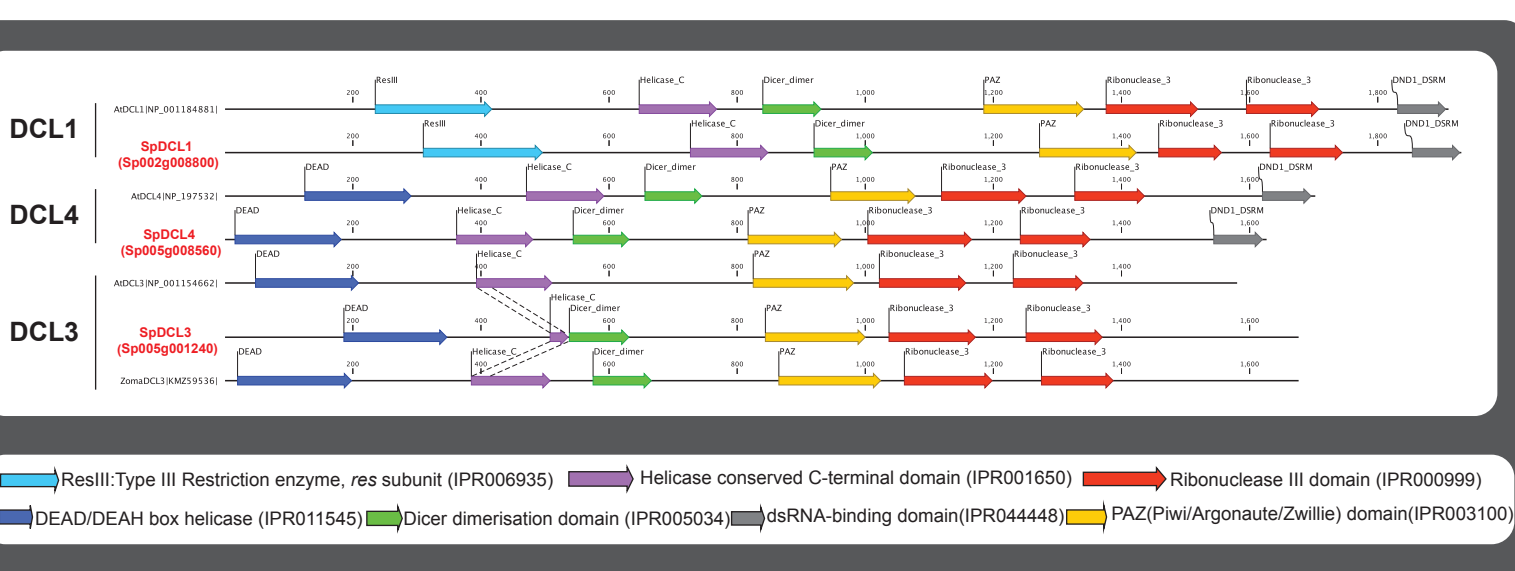
DCL1

DCL4

DCL3

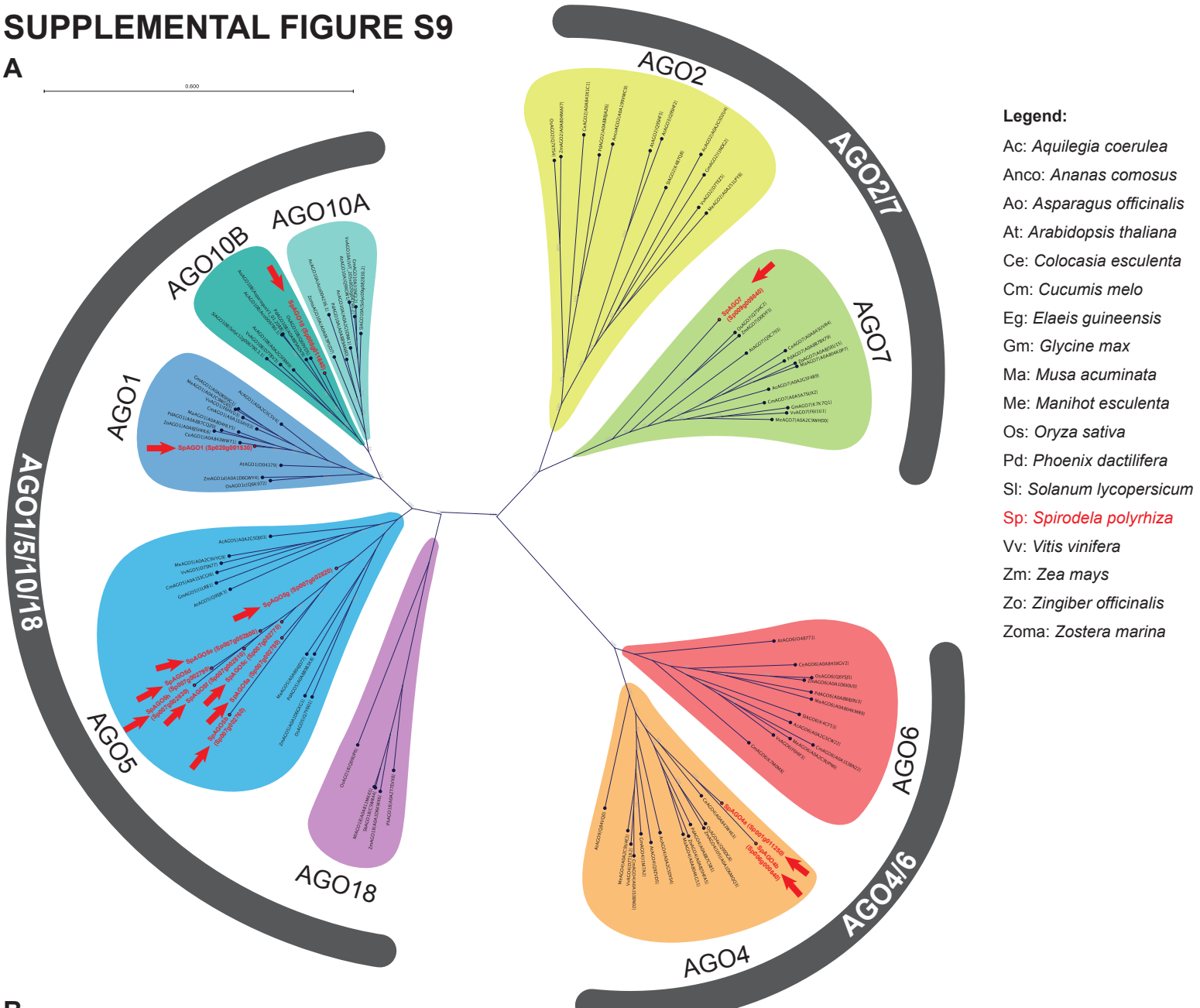
Supplemental Figure S8: Phylogenetic analysis of *Spirodela polyrhiza* DCL proteins.

(A) Unrooted phylogenetic tree of DCL proteins from several angiosperms including those identified in the *Spirodela polyrhiza* genome. The maximum likelihood tree was constructed with 1000 bootstrap replications. Protein families are highlighted in bubbles of different colors. Arrows point to *Spirodela* proteins. *Spirodela* proteins and annotations were named accordingly to their position in the tree. Uniprot entry codes appear next to the name of proteins in the tree. For *Spirodela*, the gene annotation ID is shown instead. The sequence of all proteins used to build the tree, their alignment and tree files can be found in the raw data files corresponding to this figure. (B) Domain annotation of *Spirodela* proteins in (A) along those of their orthologues in other plant species. Numbers along linear protein representations indicate positions in amino acids. Domain annotations were obtained using Interpro and Pfam databases, their integrated InterPro ID codes are display in the graphical legend. Filled arrows indicate significant domain predictions, empty arrows indicate non-significant predictions. For simplicity, Sp9509 gene identifiers have been shortened from Sp9509d(xxx)g(yyyyyy) to Sp(xxx)g(yyyyyy) (where (xxx) is chromosome number, and (yyyyyy) gene number).

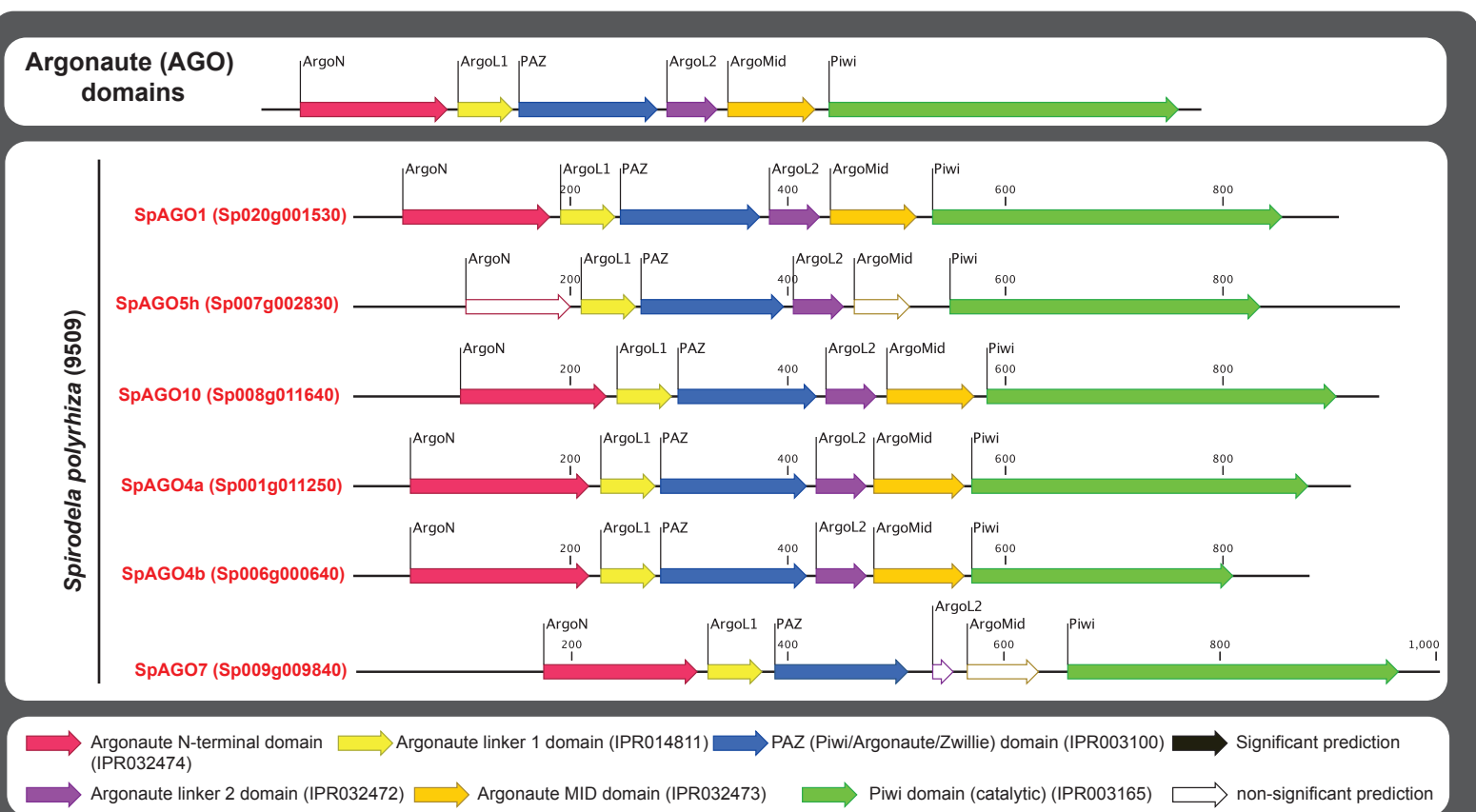


SUPPLEMENTAL FIGURE S9

A



B

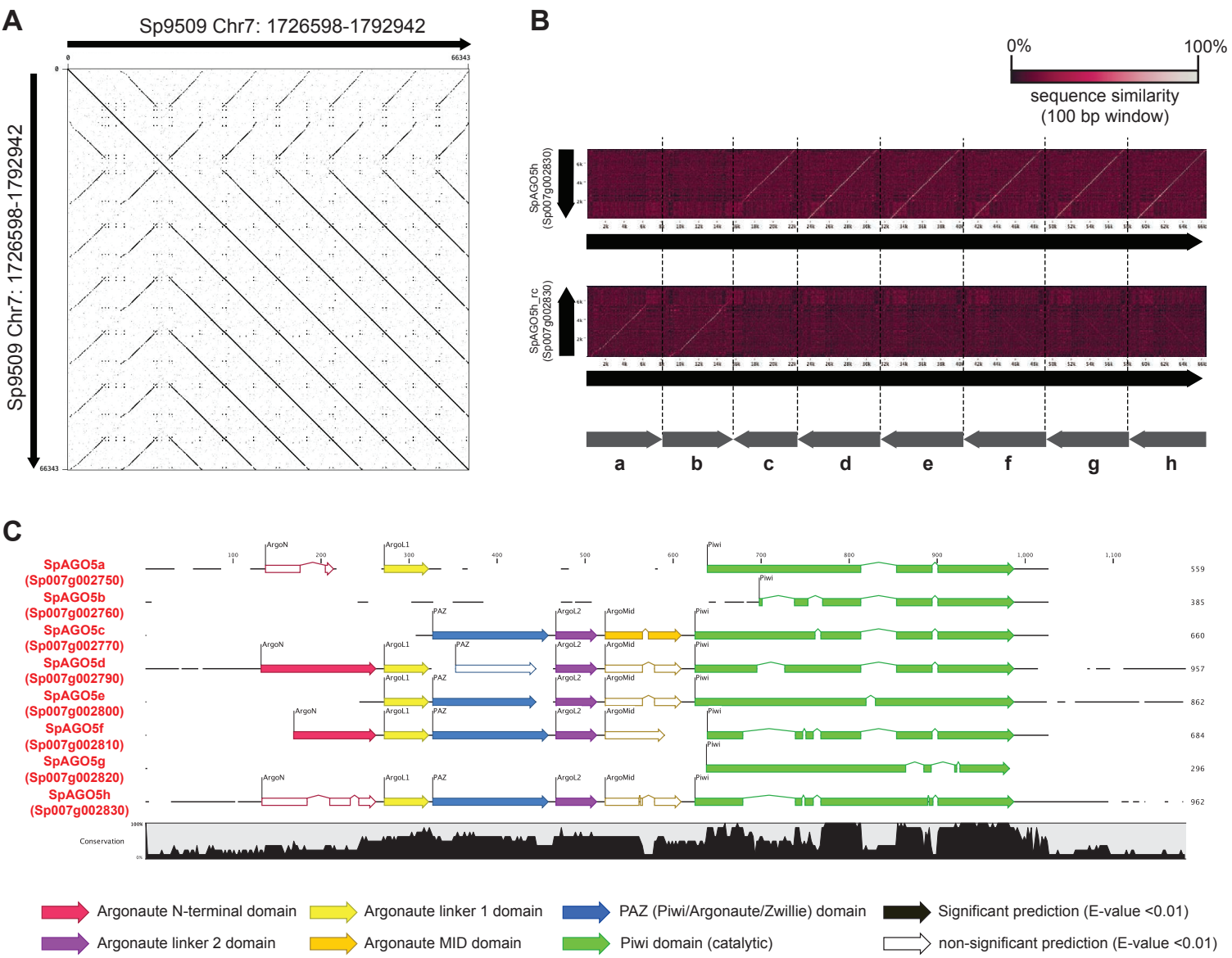


Legend on next page

Supplemental Figure S9: Phylogenetic analysis of *Spirodela polyrhiza* AGO proteins.

(A) Unrooted phylogenetic tree of AGO proteins from several angiosperms including those identified in the *Spirodela polyrhiza* genome. The maximum likelihood tree was constructed with 1000 bootstrap replications. Protein families are highlighted in bubbles of different colors. Arrows point to *Spirodela* proteins. *Spirodela* proteins and annotations were named accordingly to their position in the tree. Uniprot entry codes appear next to the name of proteins in the tree. For *Spirodela*, the gene annotation ID is shown instead. The sequence of all proteins used to build the tree, their alignment and tree files can be found in the raw data files corresponding to this figure. **(B)** Domain annotation of *Spirodela* proteins in (A) along those of their orthologues in other plant species. Numbers along linear protein representations indicate positions in amino acids. Domain annotations were obtained using Interpro and Pfam databases, their integrated InterPro ID codes are display in the graphical legend. Filled arrows indicate significant domain predictions, empty arrows indicate non-significant predictions. For simplicity, Sp9509 gene identifiers have been shortened from Sp9509d(xxx)g(yyyyyy) to Sp(xxx)g(yyyyyy) (where (xxx) is chromosome number, and (yyyyyy) gene number).

SUPPLEMENTAL FIGURE S10

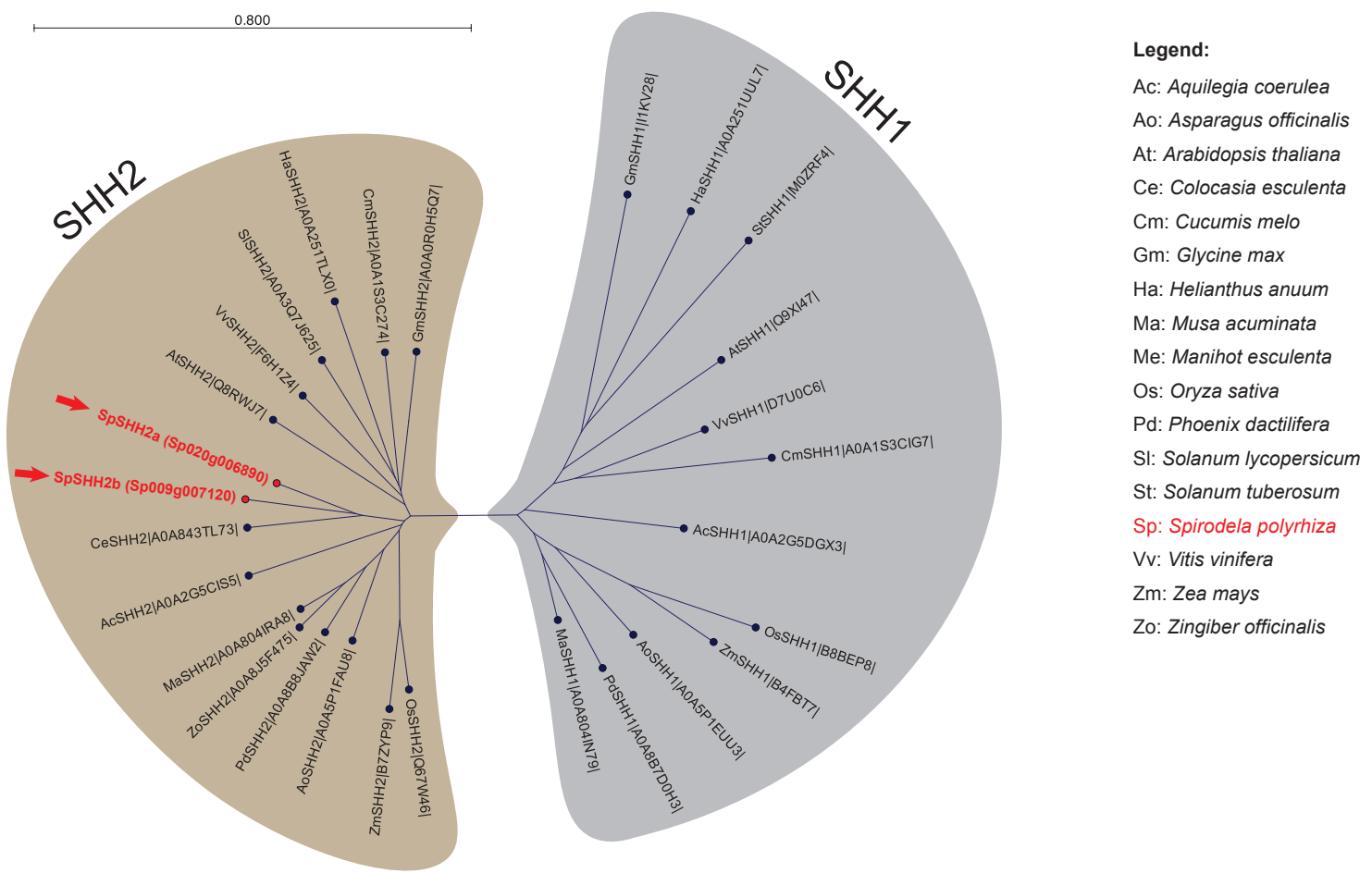


Supplemental Figure S10: *Spirodela* #9509 AGO5 cluster.

(A) Dot plot of the genomic region in Chromosome 7 containing the eight copies of AGO5 identified in the *Spirodela polyrhiza* #9509 genome (see Supplementary Figure S9). The dot plot was generated using Gepard 2.0 with 100 bp window as word size. The plot shows the presence of eight tandem duplications, two in sense and six in antisense. **(B)** Sequence similarity dot plot of the same genomic region as in (A) against the DNA sequence of the longest AGO5 copy (*SpAGO5h*) in both sense and antisense using a 100 bp sliding window. High sequence similarity regions were used to define an average 8 kbp region containing each of the identified AGO5 copies that has been duplicated. **(C)** Protein alignment of all eight AGO5 copies including domain prediction annotations suggesting that many of the AGO5 copies might not be functional. Domain annotation of *Spirodela* AGO5 proteins. Numbers along linear protein representations indicate positions in amino acids. Domain annotations were obtained using Interpro and Pfam databases. Filled arrows indicate significant domain predictions, empty arrows indicate non-significant predictions. For simplicity, Sp9509 gene identifiers have been shortened from Sp9509d(yyy)g(yyyyyy) to Sp(yyy)g(yyyyyy) (where (yyy) is chromosome number, and (yyyyyy) gene number).

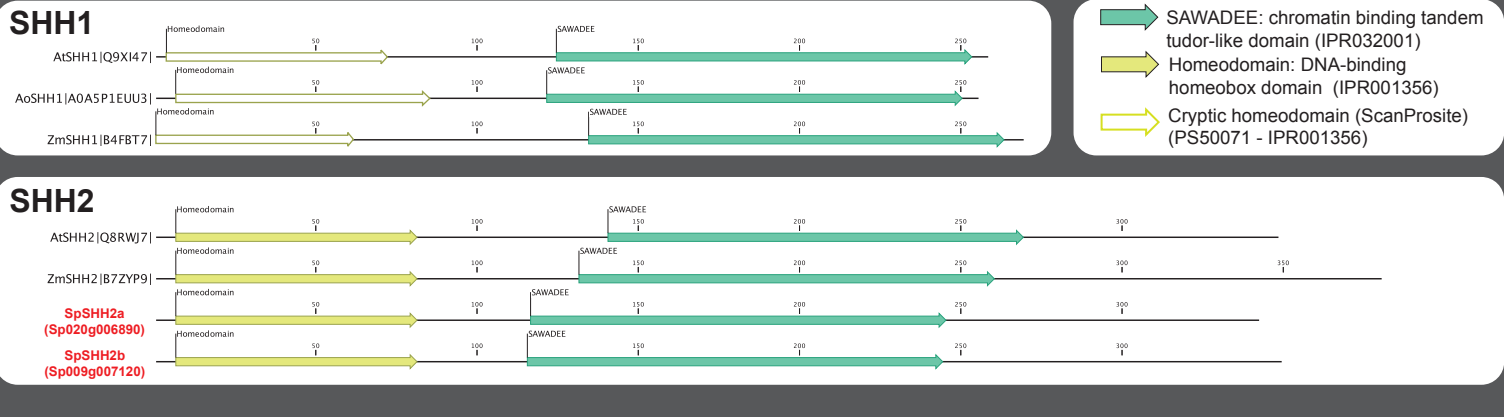
SUPPLEMENTAL FIGURE S11

A



B

SAWADEE homologues

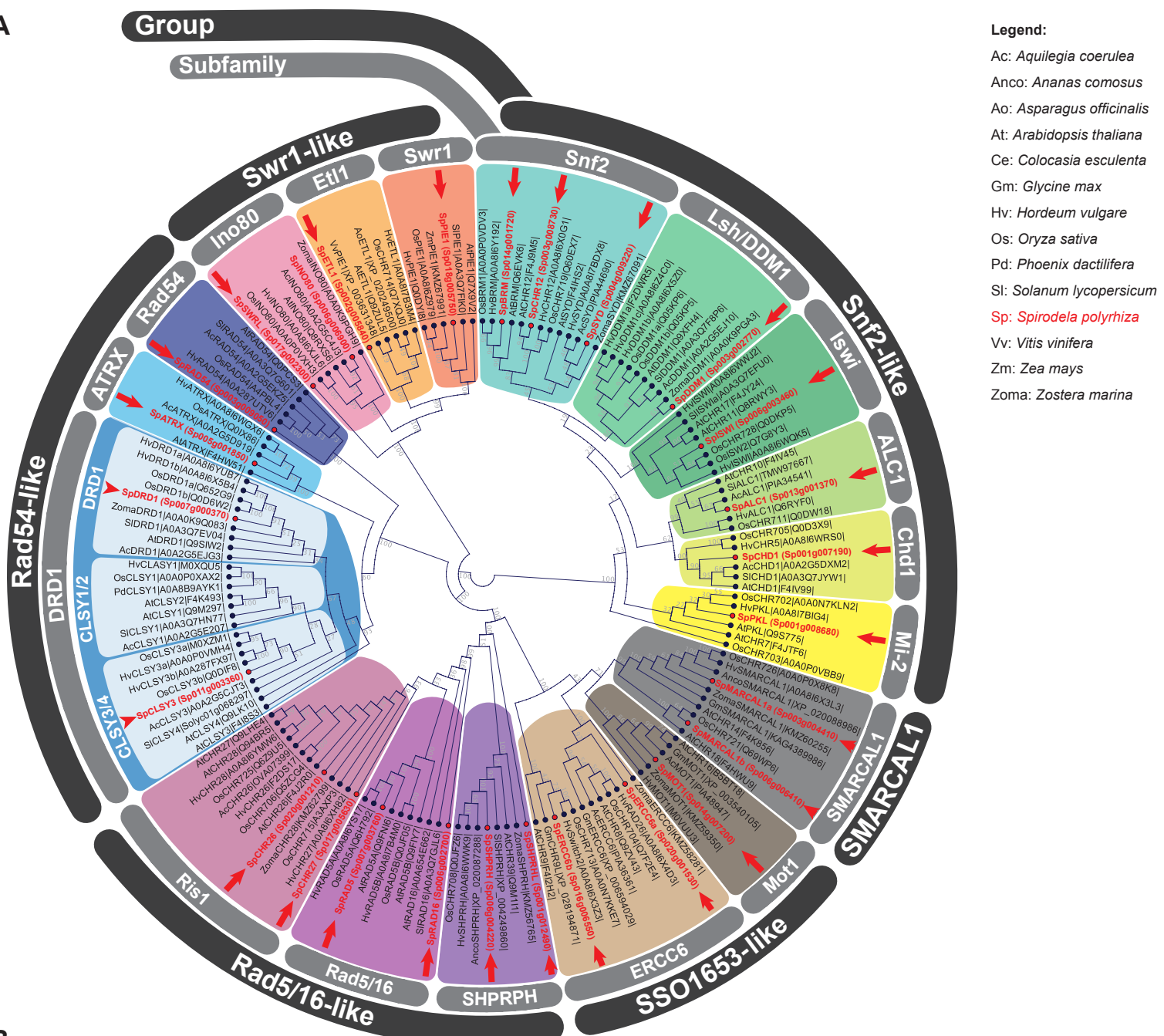


Supplemental Figure S11: Phylogenetic analysis of *Spirodela polyrhiza* SHH proteins.

(A) Unrooted phylogenetic tree of SHH proteins from several angiosperms including those identified in the *Spirodela polyrhiza* genome. The maximum likelihood tree was constructed with 1000 bootstrap replications. Protein families are highlighted in bubbles of different colors. Arrows point to *Spirodela* proteins. *Spirodela* proteins and annotations were named accordingly to their position in the tree. Uniprot entry codes appear next to the name of proteins in the tree. For *Spirodela*, the gene annotation ID is shown instead. The sequence of all proteins used to build the tree, their alignment and tree files can be found in the raw data files corresponding to this figure. (B) Domain annotation of *Spirodela* proteins in (A) along those of their orthologues in other plant species. Numbers along linear protein representations indicate positions in amino acids. Domain annotations were obtained using Interpro, Pfam and Prosite databases, their integrated InterPro ID codes are displayed in the graphical legend. The cryptic homeodomain found within SHH1 was only identified using ScanProsite. Filled arrows indicate significant domain predictions, empty arrows indicate non-significant predictions. For simplicity, Sp9509 gene identifiers have been shortened from Sp9509d(xxx)g(yyyyyy) to Sp(xxx)g(yyyyyy) (where (xxx) is chromosome number, and (yyyyyy) gene number).

SUPPLEMENTAL FIGURE S12

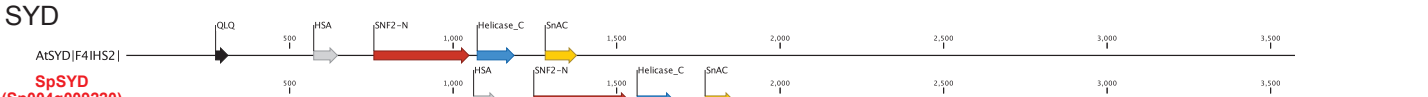
A



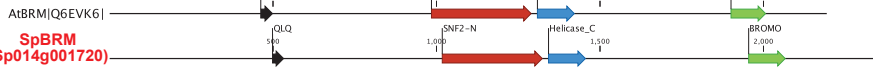
B

Snf2-like

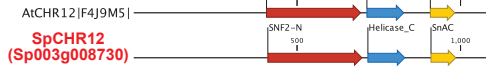
Snf2



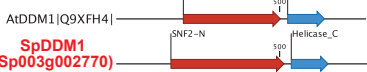
BRM



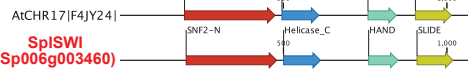
CHR12



Lsh/DDM1



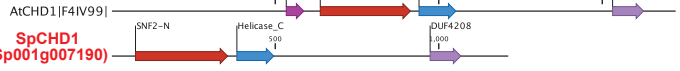
Iswi



ALC1



CHD1



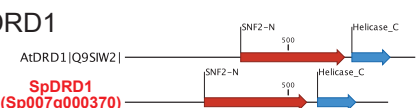
Mi-2



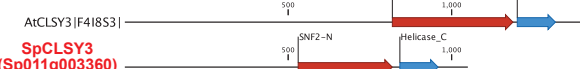
Continues on next page (incl. legend)

Rad52-like

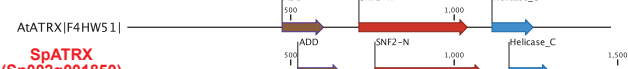
DRD1



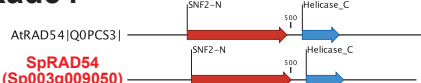
CLSY3



ATRX

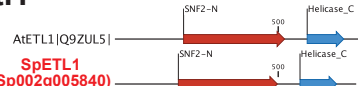


Rad54

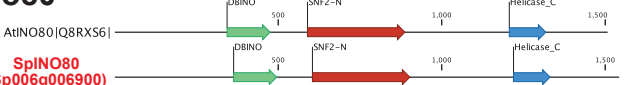


Swr1-like

Etl1



Ino80

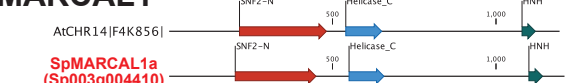


Swr1



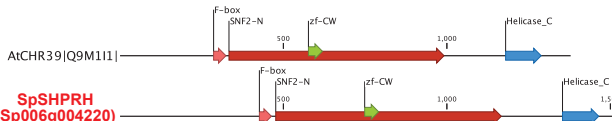
SMARCAL1

SMARCAL1

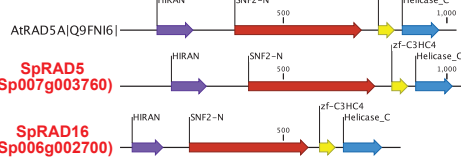


Rad5/16-like

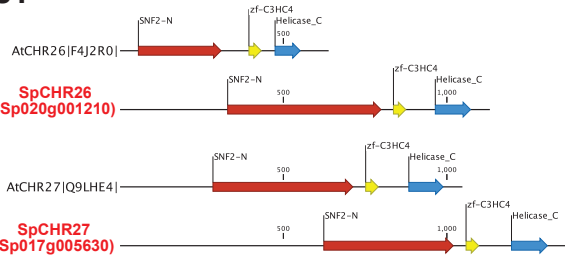
SHPRH



Rad5/16

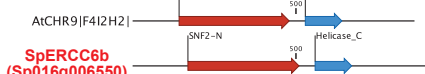
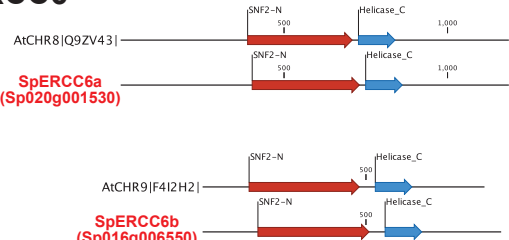


Ris1

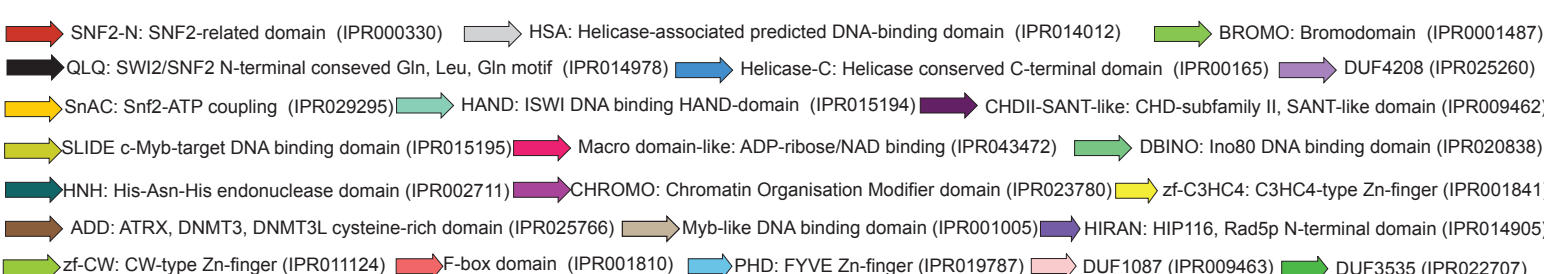
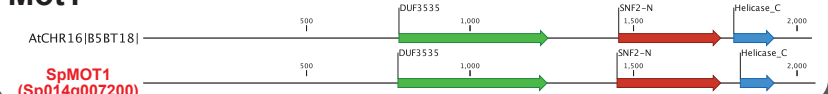


SSO1653-like

ERCC6



Mot1



Supplemental Figure S12: Phylogenetic analysis of *Spirodea polyrhiza* Snf2 chromatin remodelers.

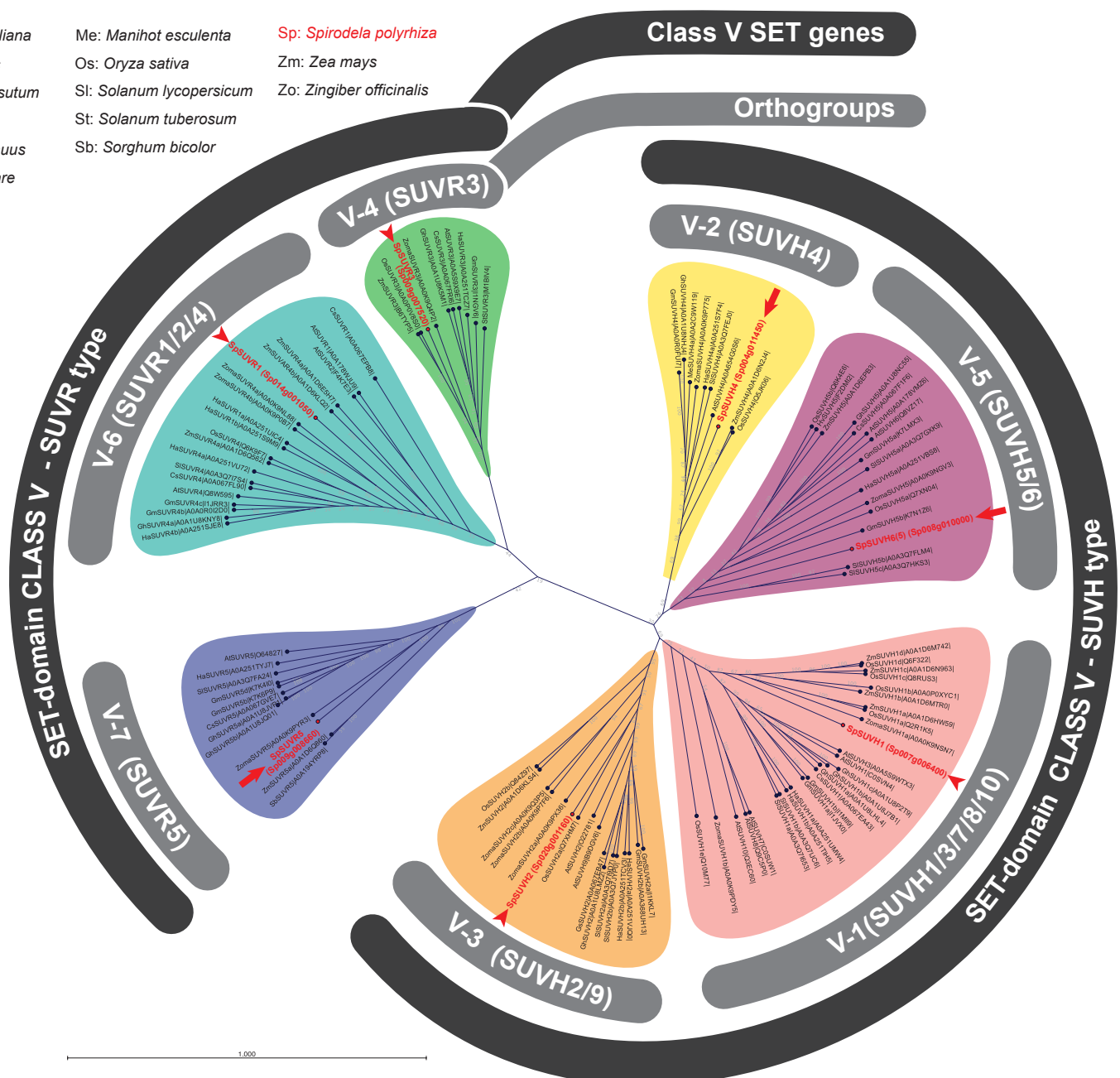
(A) Unrooted phylogenetic tree of angiosperm Snf2 ATP-dependent chromatin remodelers from several species including those identified in the *Spirodea polyrhiza* genome. The maximum likelihood tree was constructed with 1000 bootstrap replications. Protein subfamilies are highlighted in bubbles of different colors. *Spirodea* proteins and annotations were named accordingly to their position in the tree. Uniprot entry codes appear next to the name of proteins in the tree. For *Spirodea*, the gene annotation ID is shown instead. Arrows point to *Spirodea* proteins. The sequence of all proteins used to build the tree, their alignment and tree files can be found in the raw data files corresponding to this figure. **(B)** Domain annotation of *Spirodea* proteins in (A) along those of their orthologues in other plant species. Numbers along linear protein representations indicate positions in amino acids. Domain annotations were obtained using InterPro and Pfam databases, their integrated InterPro ID codes are displayed in the graphical legend. Filled arrows indicate significant domain predictions, empty arrows indicate non-significant predictions. For simplicity, Sp9509 gene identifiers have been shortened from Sp9509d(xxx)g(yyyyyy) to Sp(xxx)g(yyyyyy) (where (xxx) is chromosome number, and (yyyyyy) gene number).

SUPPLEMENTAL FIGURE S13

A

Legend:

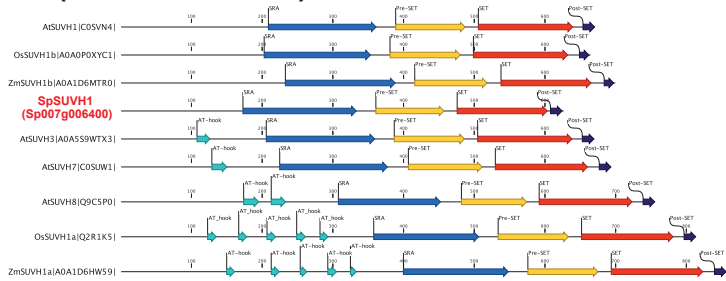
At: *Arabidopsis thaliana*
 Cs: *Citrus sinensis*
 Gh: *Gossypium hirsutum*
 Gm: *Glycine max*
 Ha: *Helianthus annuus*
 Hv: *Hordeum vulgare*
 Me: *Manihot esculenta*
 Os: *Oryza sativa*
 Sl: *Solanum lycopersicum*
 St: *Solanum tuberosum*
 Sb: *Sorghum bicolor*
 Sp: *Spirodela polyrhiza*
 Zm: *Zea mays*
 Zo: *Zingiber officinalis*



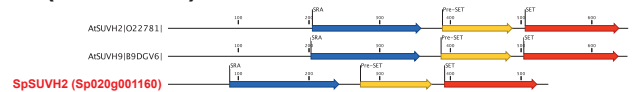
B

Class V SET genes - SUVH type

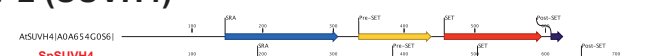
V-1 (SUVH1/3/7/8/10)



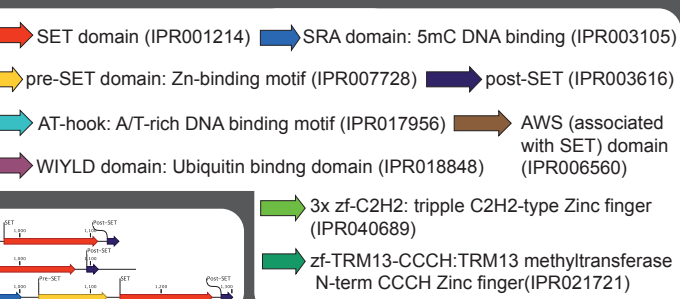
V-3 (SUVH2/9)



V-2 (SUVH4)



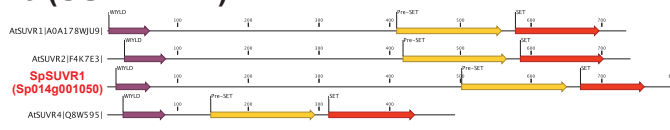
V-5 (SUVH5/6)



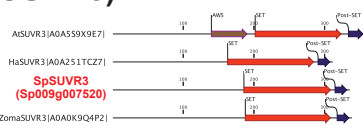
Continues on next page (incl. legend)

Class V SET genes - SUVR type

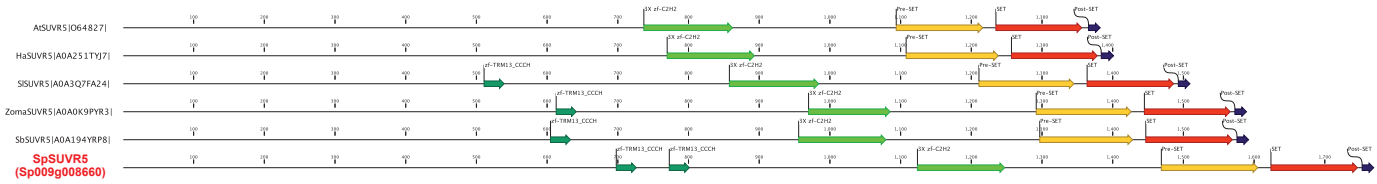
V-6 (SUVR1/2/4)



V-4 (SUVR3)



V-7 (SUVR5)



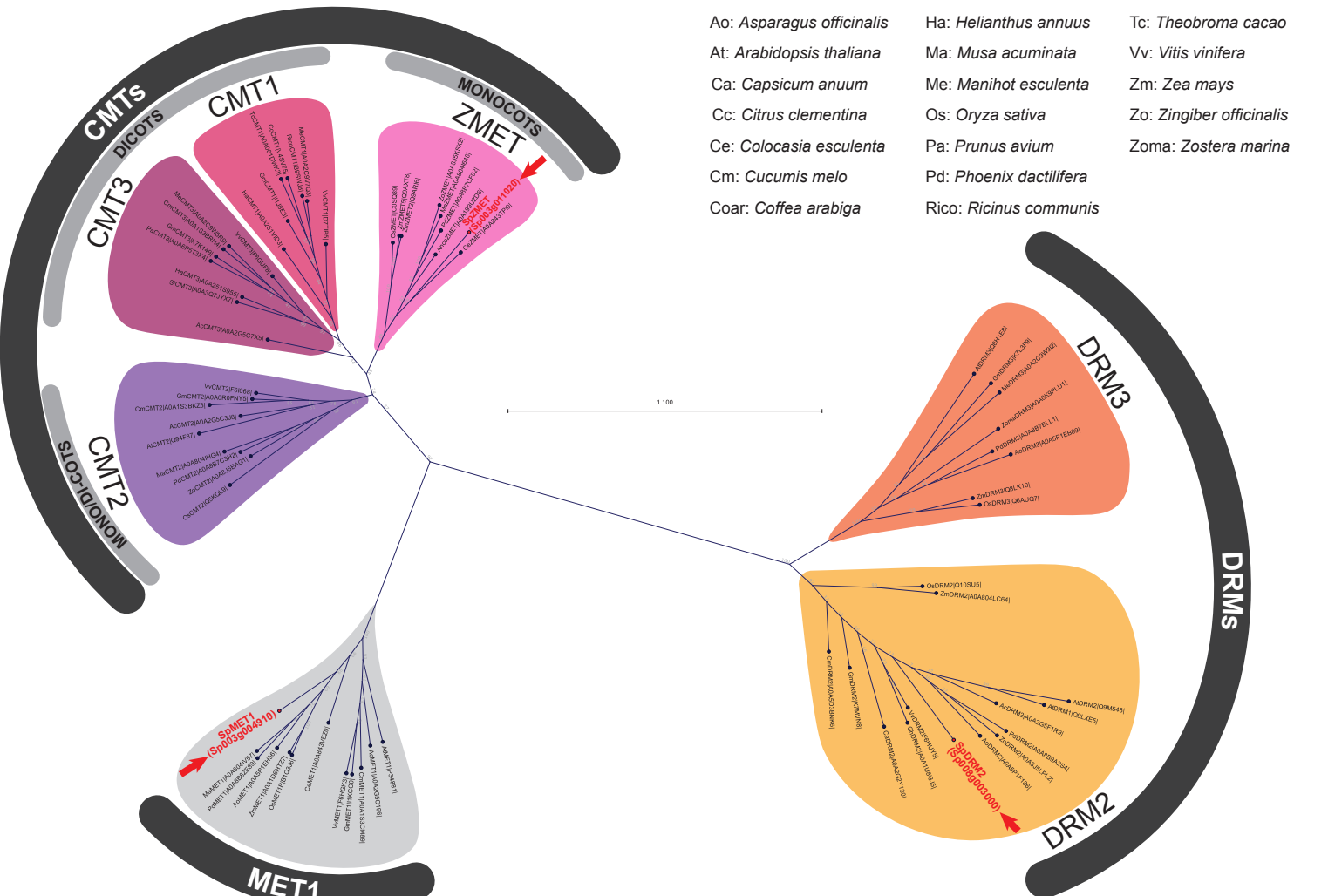
Supplemental Figure S13: Phylogenetic analysis of *Spirodea polyrhiza* SUVH and SUVR proteins.

(A) Unrooted phylogenetic tree of angiosperm Class V SET domain-containing proteins, Su(var)3-9 homologues and relatives (SUVH and SUVR), from several species including those identified in the *Spirodea polyrhiza* genome. The maximum likelihood tree was constructed with 1000 bootstrap replications. Protein families are highlighted in bubbles of different colors. *Spirodea* proteins and annotations were named accordingly to their position in the tree. Arrows point to *Spirodea* proteins. Uniprot entry codes appear next to the name of proteins in the tree. For *Spirodea*, the gene annotation ID is shown instead. The sequence of all proteins used to build the tree, their alignment and tree files can be found in the raw data files corresponding to this figure.

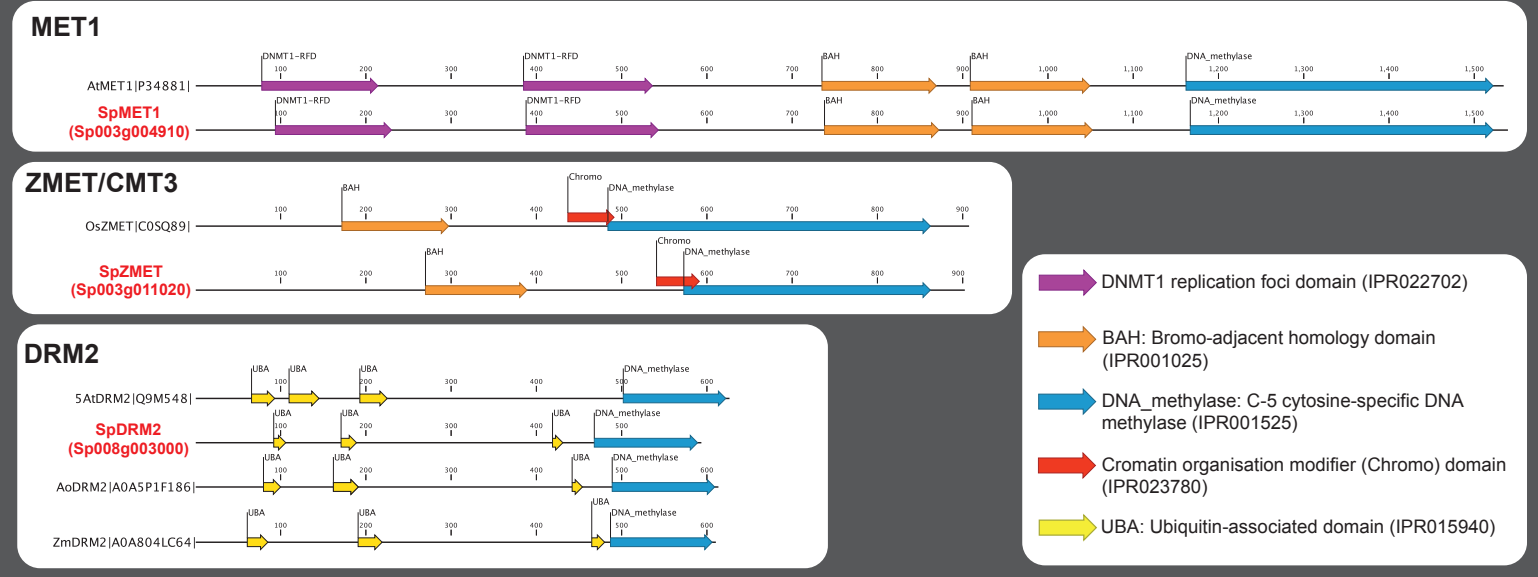
(B) Domain annotation of *Spirodea* proteins in (A) along those of their orthologues in other plant species. Numbers along linear protein representations indicate positions in amino acids. Domain annotations were obtained using Interpro and Pfam databases, their integrated InterPro ID codes are display in the graphical legend. Filled arrows indicate significant domain predictions, empty arrows indicate non-significant predictions. For simplicity, Sp9509 gene identifiers have been shortened from Sp9509d(xxx)g(yyyyyy) to Sp(xxx)g(yyyyyy) (where (xxx) is chromosome number, and (yyyyyy) gene number).

SUPPLEMENTAL FIGURE S14

A



B

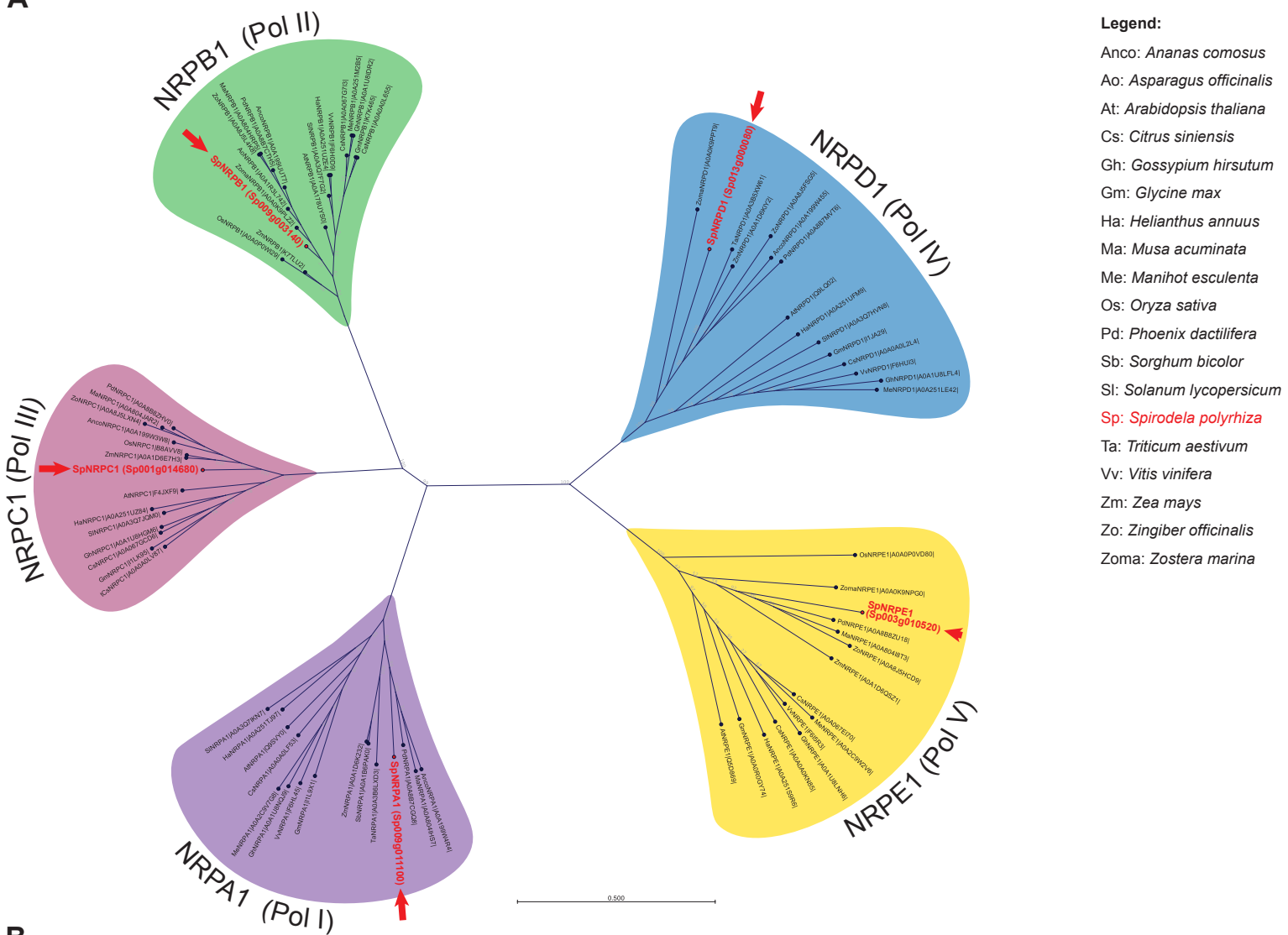


Supplemental Figure S14: Phylogenetic analysis of *Spirodeла polyrhiza* DNA methyltransferases.

(A) Unrooted phylogenetic tree of angiosperm DNA methyltransferase protein families: MET1, Chromomethylases (CMTs) and Domains Rearranged Methyltransferases (DRMs), from several species including those identified in the *Spirodeла polyrhiza* genome. The maximum likelihood tree was constructed with 1000 bootstrap replications (see Materials and Methods). Protein families are highlighted in bubbles of different colors. *Spirodeла* proteins and annotations were named accordingly to their position in the tree. Uniprot entry codes appear next to the name of proteins in the tree. Arrows point to *Spirodeла* proteins. For *Spirodeла*, the gene annotation ID is shown instead. The sequence of all proteins used to build the tree, their alignment and tree files can be found in the raw data files corresponding to this figure. (B) Domain annotation of *Spirodeла* proteins in (A) along those of their orthologues in other plant species. Numbers along linear protein representations indicate positions in amino acids. Domain annotations were obtained using Interpro and Pfam databases, their integrated InterPro ID codes are display in the graphical legend. Filled arrows indicate significant domain predictions, empty arrows indicate non-significant predictions. For simplicity, Sp9509 gene identifiers have been shortened from Sp9509d(xxx)g(yyyyyy) to Sp(xxx)g(yyyyyy) (where (xxx) is chromosome number, and (yyyyyy) gene number).

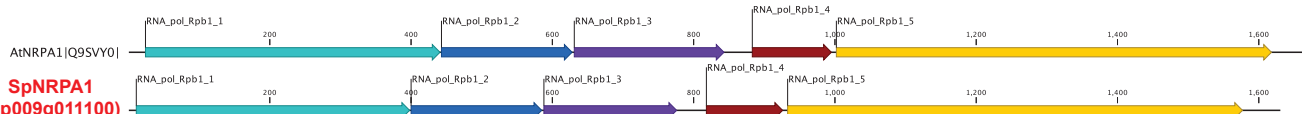
SUPPLEMENTAL FIGURE S15

A

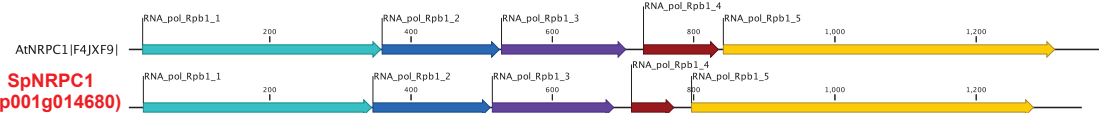


B

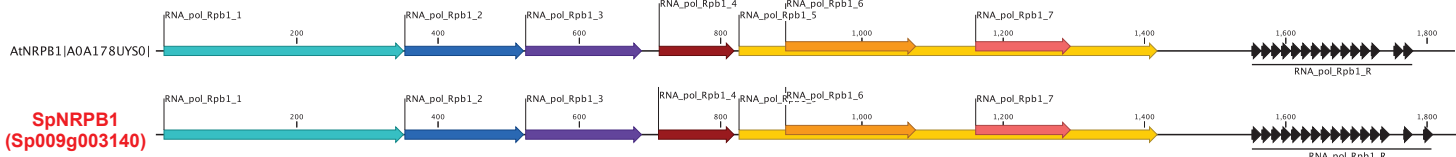
NRPA1 (RNA Pol I)



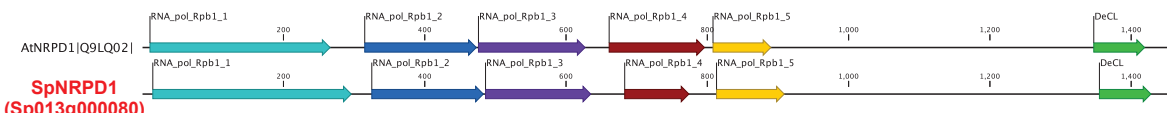
NRPC1 (RNA Pol III)



NRPB1 (RNA Pol II)



NRPD1 (RNA Pol IV)



Continues on next page (incl. legend)

NRPE1 (RNA Pol V)



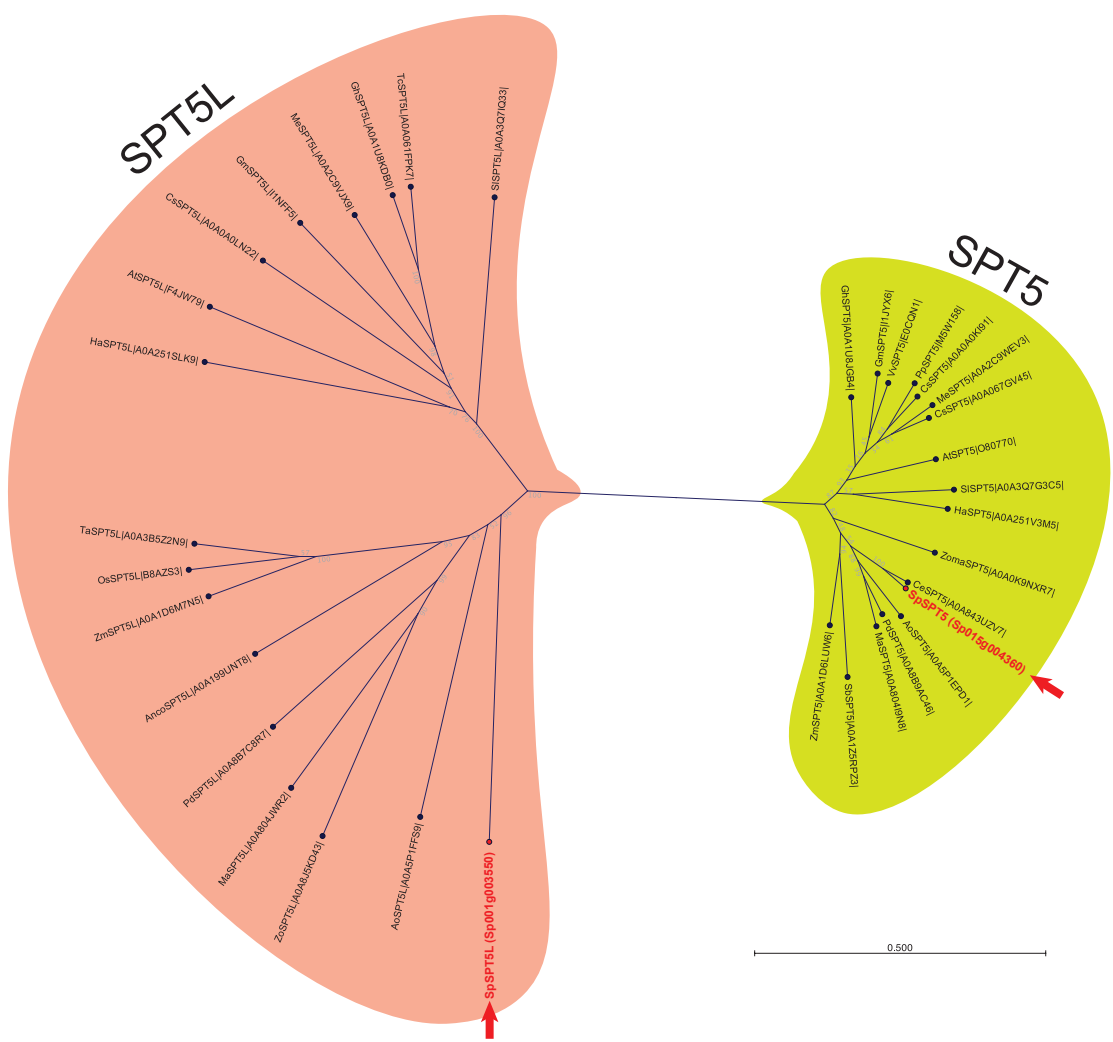
- RNA_pol_Rpb1_1: DNA-dependent RNA polymerase domain 1. Clamp domain: Maintenance of transcription bubble, DNA and RNA positioning (IPR007080)
- RNA_pol_Rpb1_2: DNA-dependent RNA polymerase domain 2. Active site (IPR000722)
- RNA_pol_Rpb1_3: DNA-dependent RNA polymerase domain 3. Pore domain: nucleotides access channel into the active site (IPR007066)
- RNA_pol_Rpb1_4: DNA-dependent RNA polymerase domain 4. Funnel domain: binding site for elongation factors (IPR007083)
- RNA_pol_Rpb1_5: DNA-dependent RNA polymerase domain 5. Discontinuous cleft domain: DNA binding (IPR007081)
- RNA_pol_Rpb1_6: DNA-dependent RNA polymerase domain 6. Shelf module domain (IPR007075)
- RNA_pol_Rpb1_7: DNA-dependent RNA polymerase domain 7. Part of the lobe domain (IPR007073)
- RNA_pol_Rpb1_R: Repetitive C-terminal domain (CTD) of RNA Pol II. Regulation of gene expression and Pol II activity dependent of its phosphorylation pattern (IPR000684)
- DeCL (DUF3232): RRP6L1 exoribonuclease interacting domain (PF11523 - Not integrated in InterPro)
- GW/WG repeats: Gly/Trp repeats involved in Argonaute (AGO) binding/recruitment.

Supplemental Figure S15: Phylogenetic analysis of *Spirodesla polyrhiza* RNA Polymerase large subunit (NRP) proteins.

(A) Unrooted phylogenetic tree of Nuclear RNA Polymerase (NRP) large subunit proteins from several angiosperms including those identified in the *Spirodesla polyrhiza* genome. The maximum likelihood tree was constructed with 1000 bootstrap replications. Protein families are highlighted in bubbles of different colors. Their cognate RNA Polymerase complex (Pol I-V) is indicated in brackets. *Spirodesla* proteins and annotations were named accordingly to their position in the tree. Arrows point to *Spirodesla* proteins. Uniprot entry codes appear next to the name of proteins in the tree. For *Spirodesla*, the gene annotation ID is shown instead. The sequence of all proteins used to build the tree, their alignment and tree files can be found in the raw data files corresponding to this figure. **(B)** Domain annotation of *Spirodesla* proteins in (A) along those of their orthologues in other plant species. Numbers along linear protein representations indicate positions in amino acids. Domain annotations were obtained using InterPro and Pfam databases, their integrated InterPro ID codes are display in the graphical legend. Filled arrows indicate significant domain predictions, empty arrows indicate non-significant predictions. Position of Gly/Trp (GW/WG) repeats (AGO-hooks) for NRPE1 are also indicated. For simplicity, Sp9509 gene identifiers have been shortened from Sp9509d(xxx)g(yyyyyy) to Sp(xxx)g(yyyyyy) (where (xxx) is chromosome number, and (yyyyyy) gene number).

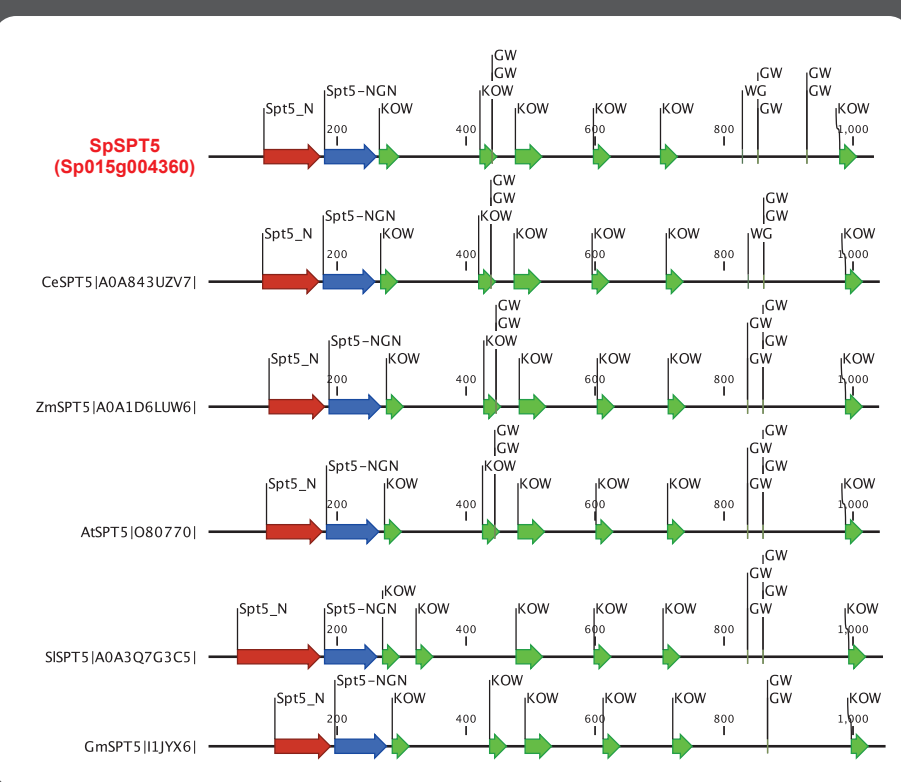
SUPPLEMENTAL FIGURE S16

A



B

SPT5 (RNA Pol II)



→ Spt5_N: acidic N-term of early transcription elongation factor Spt5 (IPR022581)

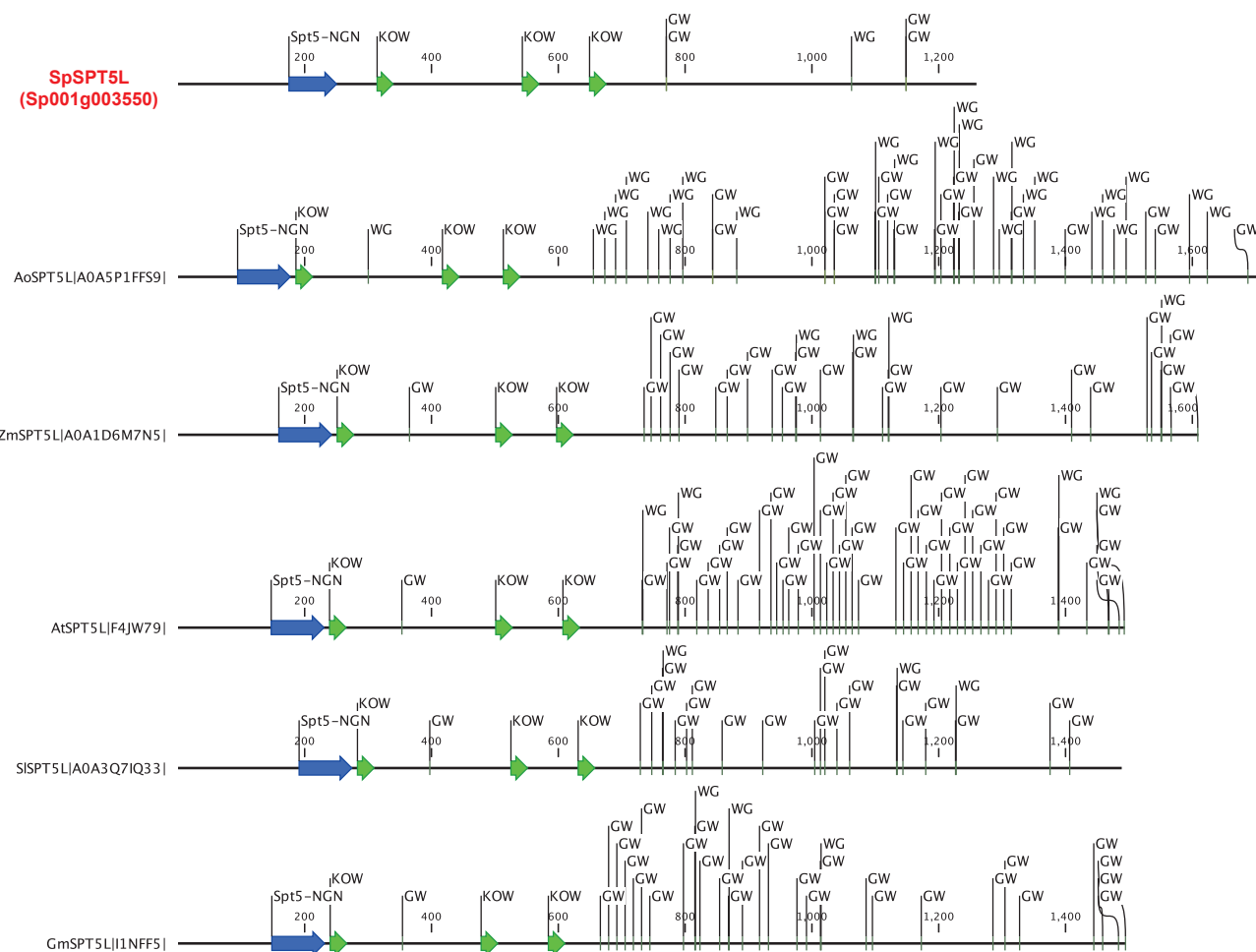
→ Spt5-NGN: Spt5-NusG N-terminal domain (IPR022581)

→ KOW: Kyrides, Ouzounis, Woese domain (IPR005824)

GW/GW repeats: Gly/Trp repeats involved in Argonaute (AGO) binding/recruitment.

Continues on next page (incl. legend)

SPT5-Like (RNA Pol V)



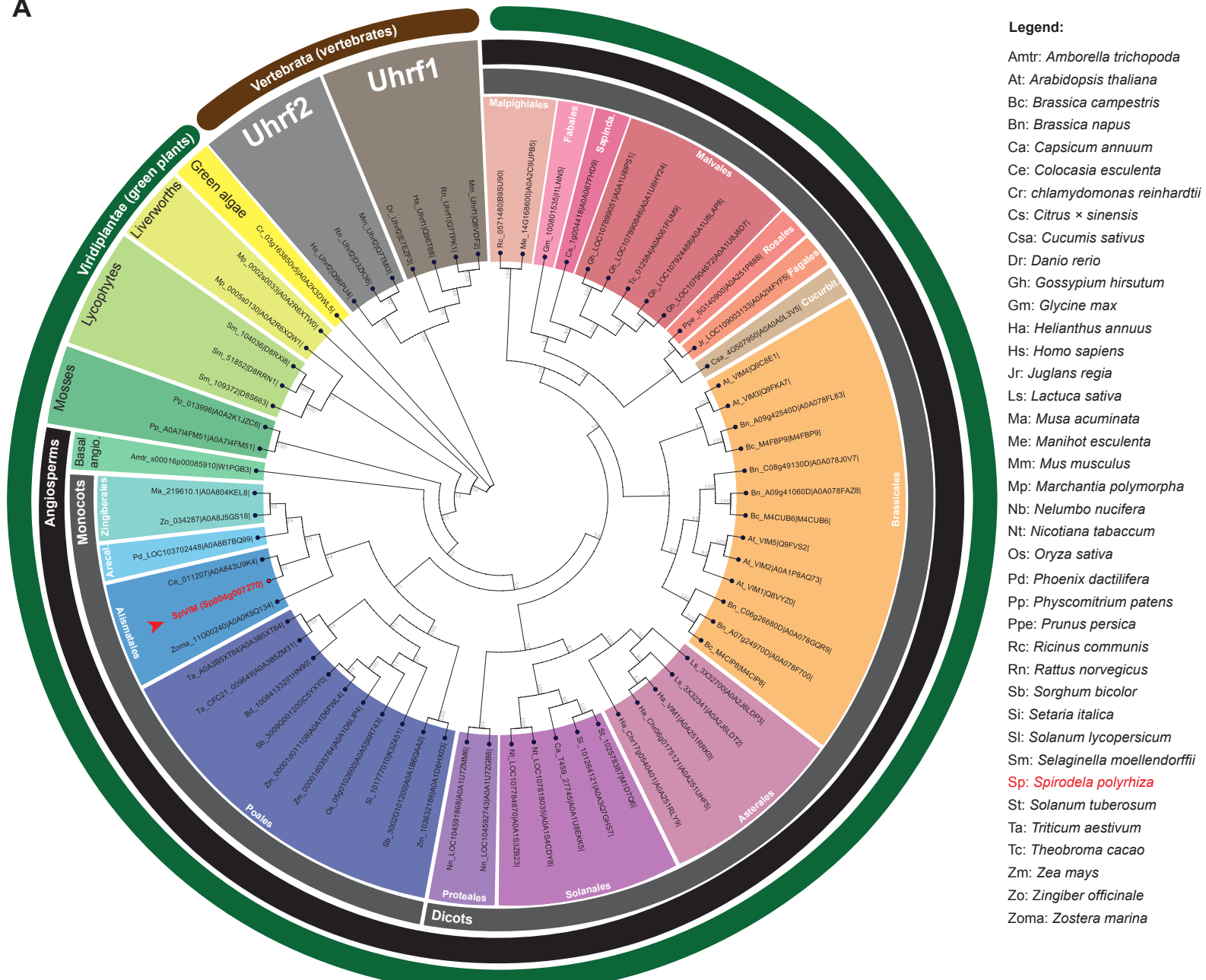
Supplemental Figure S16: Phylogenetic analysis of *Spirodesla polyrhiza* SPT5 and SPT5L proteins.

(A) Unrooted phylogenetic tree of the Pol II transcription elongation factor SPT5 and its parologue, the Pol V interactor, SPT5-like (SPT5L) proteins from several angiosperms including those identified in the *Spirodesla polyrhiza* genome. The maximum likelihood tree was constructed with 1000 bootstrap replications. *Spirodesla* proteins and annotations were named accordingly to their position in the tree. Arrows point to *Spirodesla* proteins. Uniprot entry codes appear next to the name of proteins in the tree. For *Spirodesla*, the gene annotation ID is shown instead. The sequence of all proteins used to build the tree, their alignment and tree files can be found in the raw data files corresponding to this figure.

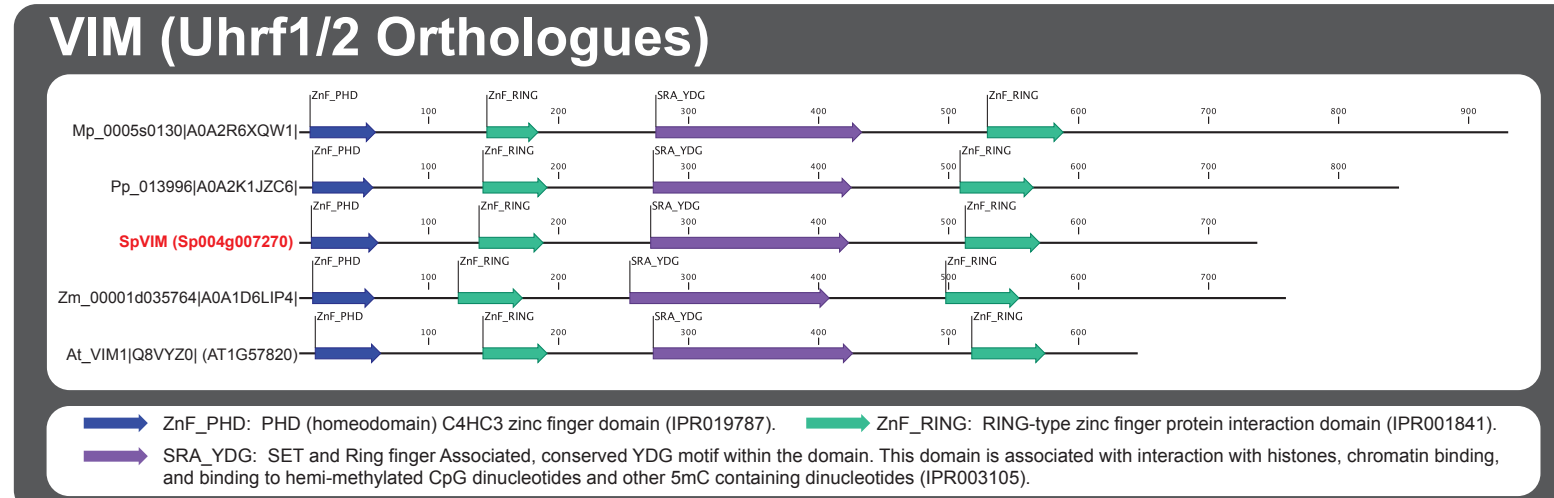
(B) Domain annotation of *Spirodesla* proteins in (A) along those of their orthologues in other plant species. Numbers along linear protein representations indicate positions in amino acids. Domain annotations were obtained using InterPro and Pfam databases, their integrated InterPro ID codes are displayed in the graphical legend. Filled arrows indicate significant domain predictions, empty arrows indicate non-significant predictions. Position of Gly/Trp (GW/WG) repeats (AGO-hooks) are also indicated. For simplicity, Sp9509 gene identifiers have been shortened from Sp9509d (xxx)g(yyyyyy) to Sp(xxx)g(yyyyyy) (where (xxx) is chromosome number, and (yyyyyy) gene number).

SUPPLEMENTAL FIGURE S17

A



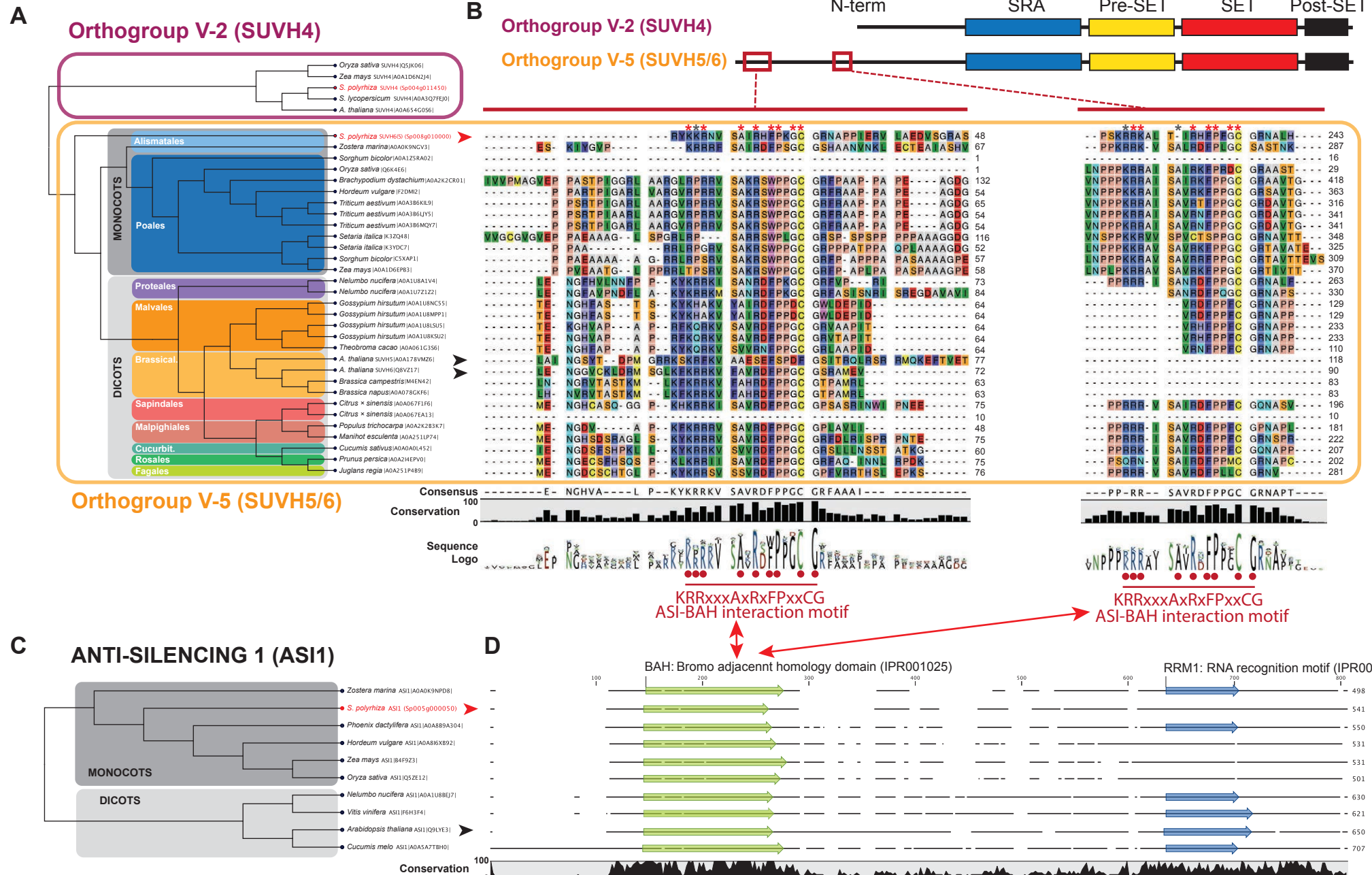
B



Supplemental Figure S17: Phylogenetic analysis of *Spirodela polyrhiza* VIM proteins.

(A) Unrooted phylogenetic tree of animal and plant Uhrf1/2 orthologues, VIM, from several species including that identified in the *Spirodela polyrhiza* genome. The maximum likelihood tree was constructed with 1000 bootstrap replications. Gene ID ad UniProt entry codes appear next to the name of proteins in the tree. For *Spirodela*, the gene annotation ID is shown instead. Arrows point to *Spirodela* proteins. The sequence of all proteins used to build the tree, their alignment and tree files can be found in the raw data files corresponding to this figure. **(B)** Domain annotation of *Spirodela* proteins in (A) along those of their orthologues in other species. Numbers along linear protein representations indicate positions in amino acids. Domain annotations were obtained using the InterPro database, their ID codes are display in the graphical legend. For simplicity, Sp9509 gene identifiers have been shortened from Sp9509d(xxx)g(yyyyyy) to Sp(xxx)g(yyyyyy) (where (xxx) is chromosome number, and (yyyyyy) gene number).

SUPPLEMENTAL FIGURE S18

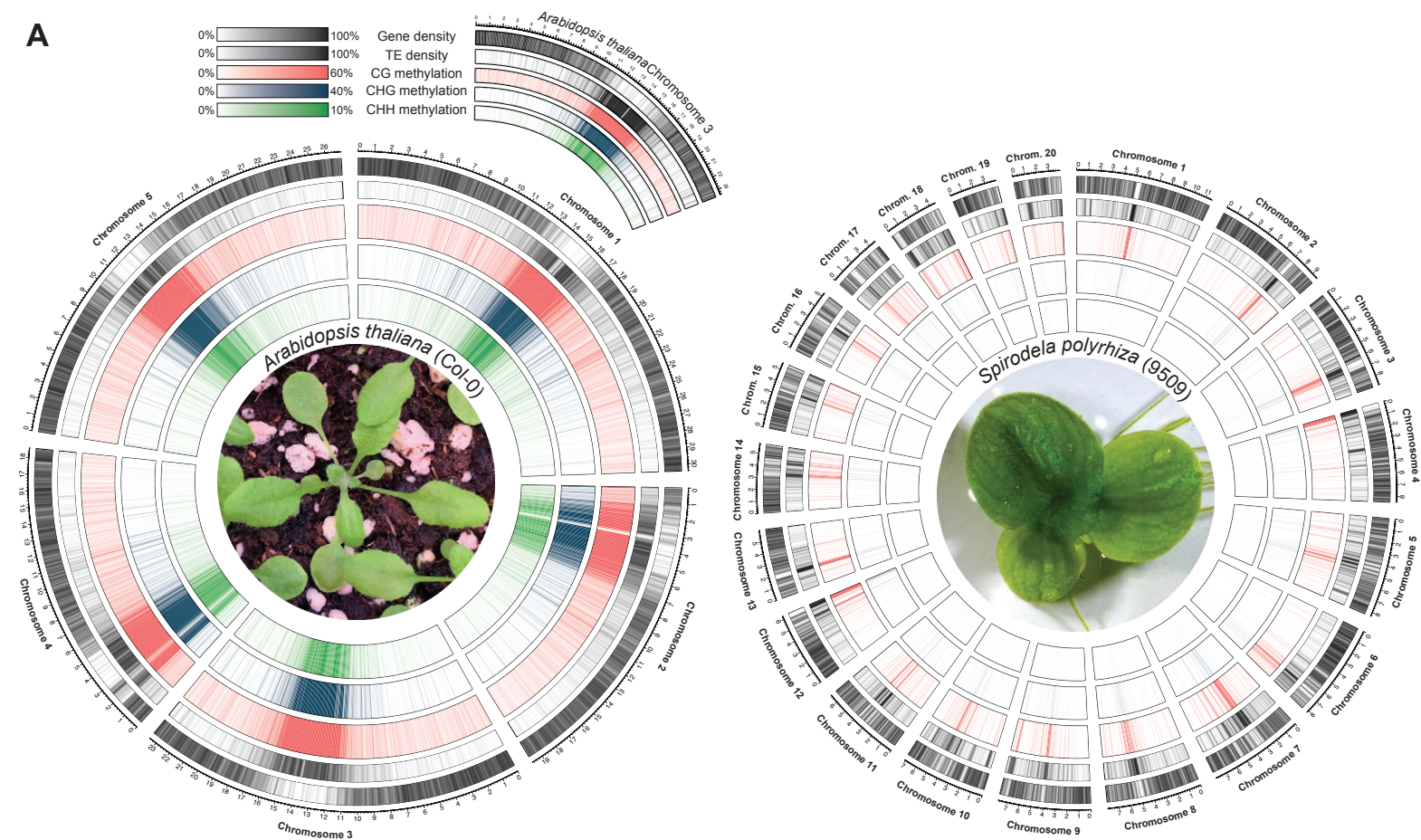


Supplemental Figure S18: Phylogenetic analysis of *Spirodela polyrhiza* SET-domain Class V orthogroup V-5 (SUVH5/6) and ASI1 proteins.

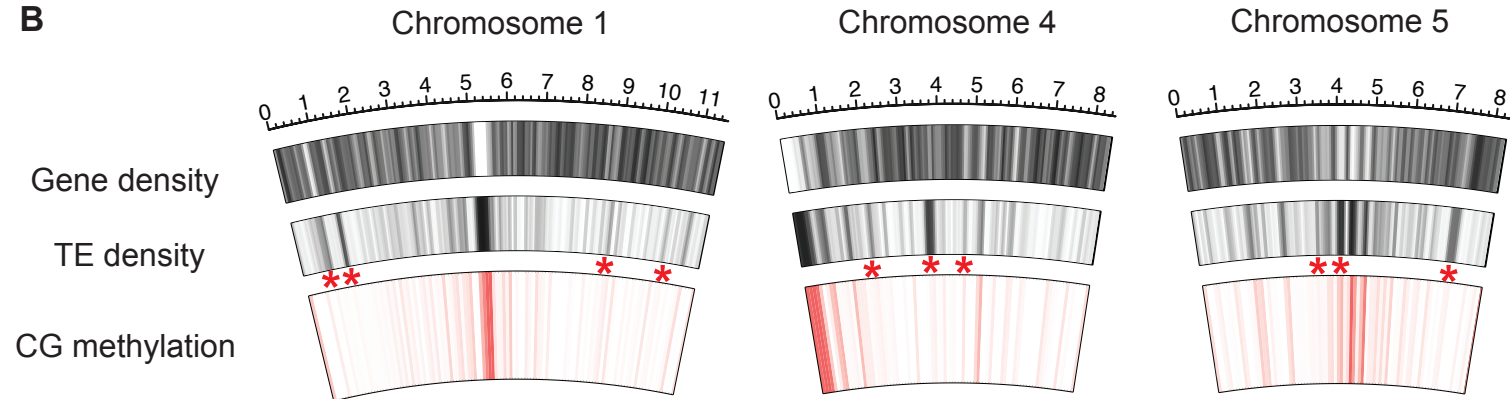
(A) Unrooted phylogenetic tree of angiosperm Class V SET Orthogroup V-5 proteins (SUVH5/6) from several species including those identified in the *Spirodela polyrhiza* genome. SUVH4 (orthogroup V2) proteins were added as outgroup. The maximum likelihood tree was constructed with 1000 bootstrap replications. Arrows point to *Spirodela* (red) and *Arabidopsis* (black) proteins. Uniprot entry codes appear next to the name of proteins in the tree. For *Spirodela*, the gene annotation ID is shown instead. (B) Schematic representation of SUVH4/5/6 domain structure along their protein sequence and multiple protein sequence alignment of SUVH5/6 proteins from A. Only N-terminal regions from SUVH5/6 containing the conserved ASI-BAH interaction motif are shown along their consensus sequence, sequence logo and conservation. The ASI-BAH interaction motif, as described in Zhang et al., 2023, is indicated below. Red dots mark the conserved aa's identified in Zhang et al., 2023. Asterisks above *Spirodela* SUVH6(5) mark, in red, conserved or, in grey, non-conserved or missing aa from the motif. (C) Same as A but for ASI1 orthologues. (D) Multiple protein sequence alignment of ASI1 proteins from C along their conservation. Domain annotations were obtained using Interpro and Pfam databases, their integrated InterPro ID codes are displayed. For simplicity, Sp9509d(xxx)g(yyyyy) to Sp(xxx)g(yyyyy) (where (xxx) is chromosome number, and (yyyyy) gene number). The sequence of all proteins used to build the tree, their alignment and tree files can be found in the raw data files corresponding to this figure.

SUPPLEMENTAL FIGURE S19

A



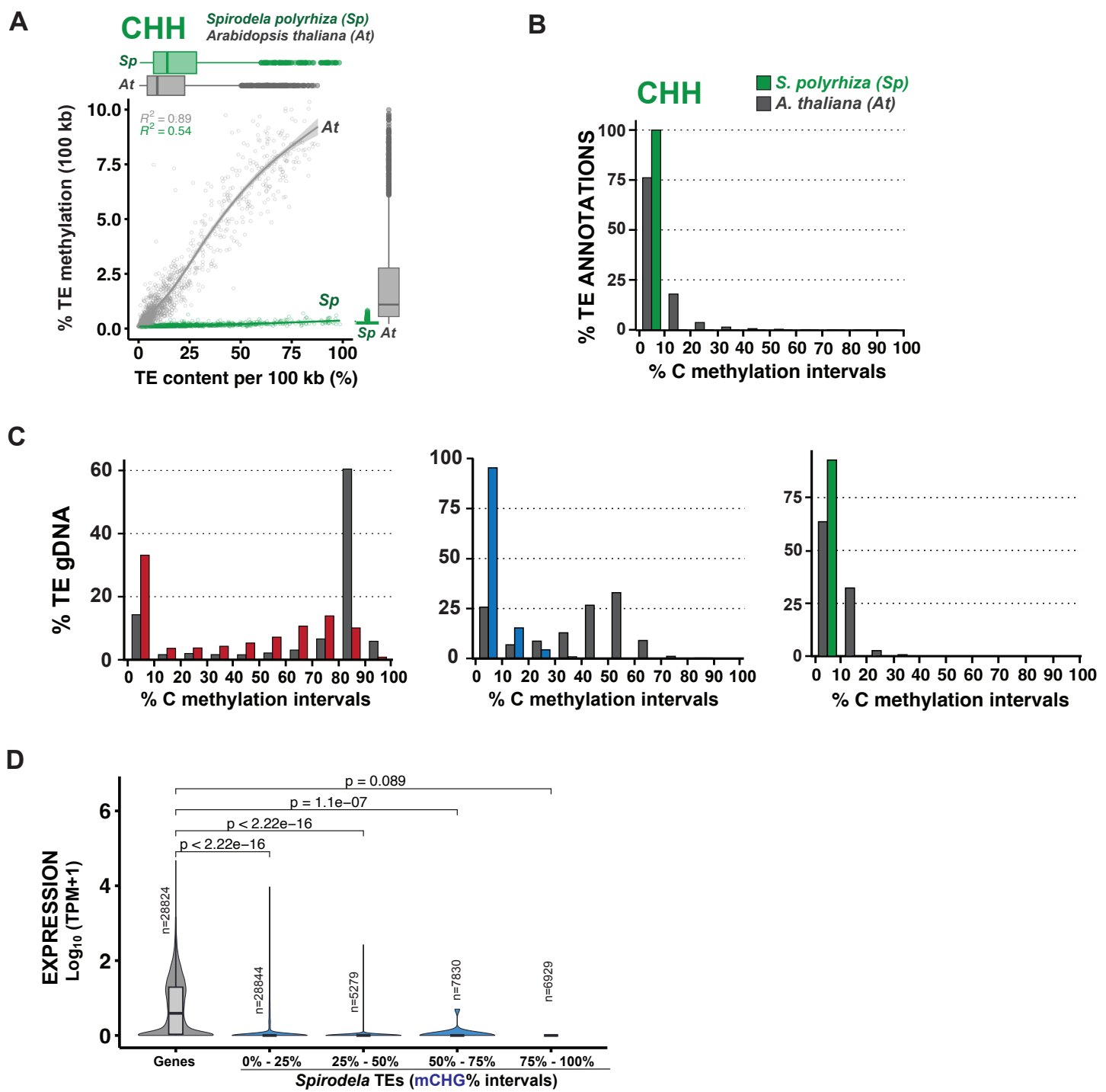
B



Supplemental Figure S19: Genome-wide distribution of DNA methylation in *Spirodela polyrhiza*.

A Circos plot of genome-wide distribution of DNA methylation densities by chromosome in *Spirodela* and *Arabidopsis*. From outside to inside: gene density, TE density, CG, CHG and CHH methylation. Mean DNA methylation, gene and TE densities values within the indicated ranges are displayed for 100 kbp intervals in 50 kbp sliding windows. **B** Detail of three *Spirodela* chromosomes from (A) showing gene, TEs and CG methylation densities. Asterisks mark high TE density regions with low CG methylation levels.

SUPPLEMENTAL FIGURE S20



Supplemental Figure S20: Distribution of CHH DNA methylation in *Spirodelta polyrhiza*.

(A) Scatter plot and best fit line of average TE CHH DNA methylation against TE content per 100 kb genomic bins in *Arabidopsis* and *Spirodelta*. **(B)** Bar plot of the percentage of TE-occupied genomic space displaying a given DNA methylation level within 10% incremental intervals of CG, CHG and CHH methylation in *Arabidopsis* and *Spirodelta*. **(C)** Bar plot of the distribution (%) of TE annotations (≥ 100 bp) within 10% incremental intervals of CHH methylation in *Arabidopsis* and *Spirodelta*. **(D)** Analysis of *Spirodelta* TE expression within 25% incremental intervals of CHG methylation. Global gene expression values are shown for comparison. Wilcoxon rank sum test was used to compare expression level between genes and each TE intervals. In all boxplots: median is indicated by solid bar; the boxes extend from the first to the third quartile and whiskers stretch to the furthest value within 1.5 times the interquartile range.

SUPPLEMENTAL FIGURE S21

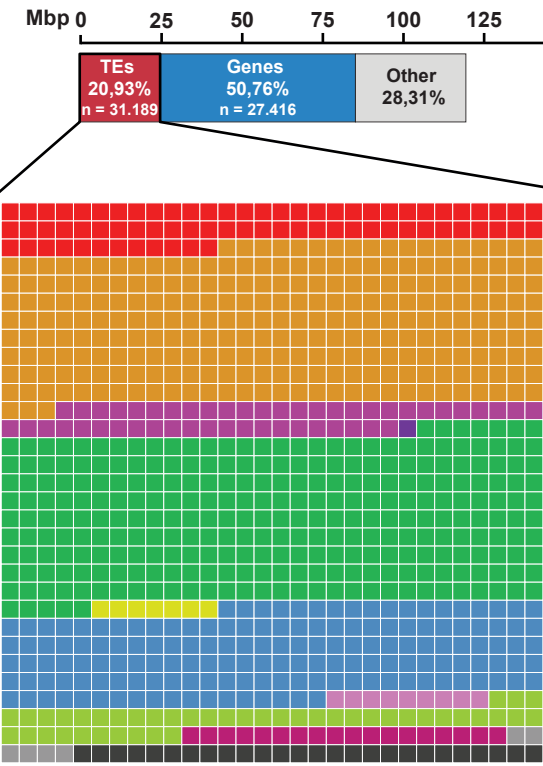
CLASS	ORDER	SUPERFAMILY	CODE
(R)	Long Terminal Repeat (LTR) (L)	<i>Ty1/Copia</i> (C)	RLC
	non-LTR LINE (I)	<i>Ty3/Gypsy</i> (G)	RLG
	non-LTR SINE (S)	<i>Unknown</i> (X)	RLX
	<i>Unknown</i> (X)	<i>LINE</i> (L)	RIL
	<i>Unknown</i> (X)	<i>Other/Unknown</i> (X)	RIX
(D)	Terminal Inverted Repeat (TIR) (T)	<i>tRNA</i> (T)	RST
	non-TIR (H)	<i>7SL</i> (L)	RSL
	<i>Unknown</i> (X)	<i>5S</i> (S)	RSS
	<i>Unknown</i> (X)	<i>Unknown</i> (X)	RSX
	<i>Unknown</i> (X)	<i>Unknown</i> (X)	RXX
Unknown (X)	Terminal Inverted Repeat (TIR) (T)	<i>Tc1/Mariner</i> (T)	DTT
	non-TIR (H)	<i>Mutator</i> (M)	DTM
	<i>Unknown</i> (X)	<i>PIF-Harbinger</i> (H)	DTH
	<i>Unknown</i> (X)	<i>CACTA</i> (C)	DTC
	<i>Unknown</i> (X)	<i>hAT</i> (A)	DTA
Unknown (X)	non-TIR (H)	<i>Unknown</i> (X)	DTX
	<i>Unknown</i> (X)	<i>Helitron</i> (H)	DHH
	<i>Unknown</i> (X)	<i>Unknown</i> (X)	DHX
	<i>Unknown</i> (X)	<i>Unknown</i> (X)	DXX
	<i>Unknown</i> (X)	<i>Unknown</i> (X)	XXX

Supplemental Figure S21: Transposon classification, nomenclature and codes used in this study.

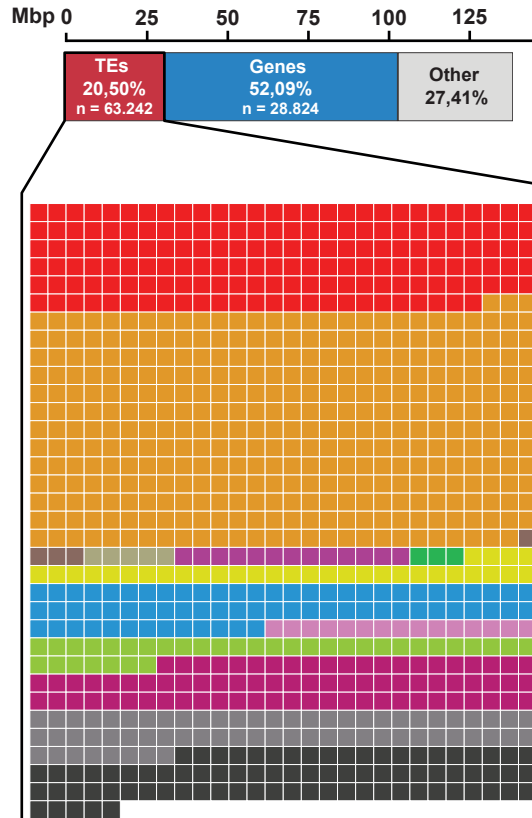
SUPPLEMENTAL FIGURE S22

A

A. thaliana (Col-0): 119,15 Mbp



S. polyrhiza (9509): 138,55 Mbp



- CLASS I
 - RLC: Ty1/Copia
 - RLG: Ty3/Gypsy
 - RLX: LTR Unk
 - RI(L/X): LINE
 - RS(T/L/S): SINE
 - RXX: RTE Unk
- CLASS II
 - DHH: RC/Helitron
 - DTT: Tc1/Mariner
 - DTM: Mutator
 - DTH: Harbinger
 - DTC: CACTA
 - DTA: hAT
 - DXX: DTE Unk
 - XXX: Unknown

B

Arabidopsis thaliana (Col-0)

Spirodela polyrhiza (9509)

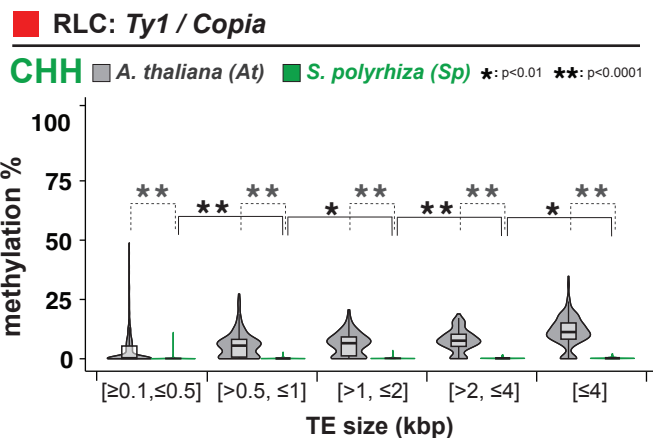
Superfamily	DNA (kbp)	% gDNA	% TE gDNA	DNA (kbp)	% gDNA	% TE gDNA
CLASS I						
RLC	1920,719	1,612 %	7,694 %	5415,233	3,908 %	17,512 %
RLG	6978,646	5,857 %	27,956 %	12123,494	8,750 %	39,206 %
RLX	-	-	-	200,412	0,145 %	0,648 %
RI(L/X)	1276,831	1,072 %	5,115 %	411,652	0,297 %	1,331 %
RS(T/L/X)	32,105	0,027 %	0,129 %	23,336	0,017 %	0,075 %
RXX	-	-	-	155,536	0,112 %	0,503 %
CLASS II						
DHH	7560,501	6,346 %	30,287 %	103,235	0,075 %	0,334 %
DTT	190,03	0,159 %	0,761 %	1140,593	0,823 %	3,689 %
DTM	4148,023	3,481 %	1,662 %	2259,622	1,631 %	7,307 %
DTH	248,765	0,209 %	0,997 %	478,383	0,345 %	1,547 %
DTC	1178,414	0,989 %	4,721 %	1214,221	0,876 %	3,927 %
DTA	462,131	0,388 %	1,851 %	2521,626	1,820 %	8,155 %
DXX	689,039	0,578 %	2,760 %	2691,772	1,943 %	8,705 %
Unk	55,341	0,046 %	0,222 %	2183,405	1,576 %	7,061 %

Supplemental Figure S22: Transposon composition of *Arabidopsis thaliana* (Col-0) and *Spirodela polyrhiza* (9509) genomes

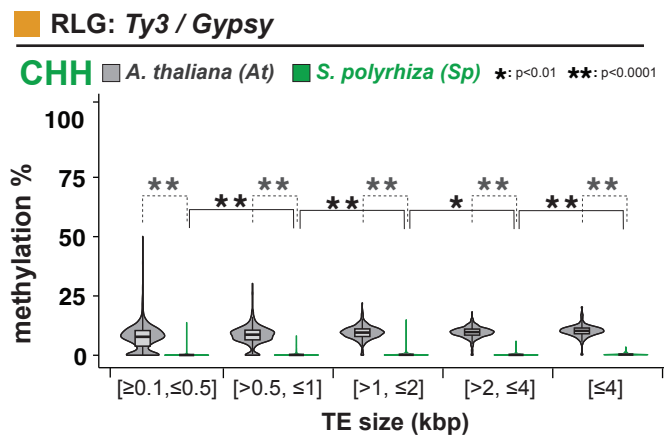
(A) Waffle chart of the relative contribution of different TE superfamilies over the total genomic space occupied by TEs in *Arabidopsis* and *Spirodela*. (B) Table with TE superfamily content as total amount of DNA (in kbp), relative to genome size (% gDNA) and the portion of the genome occupied by TEs (%TE gDNA) in both species.

SUPPLEMENTAL FIGURE S23

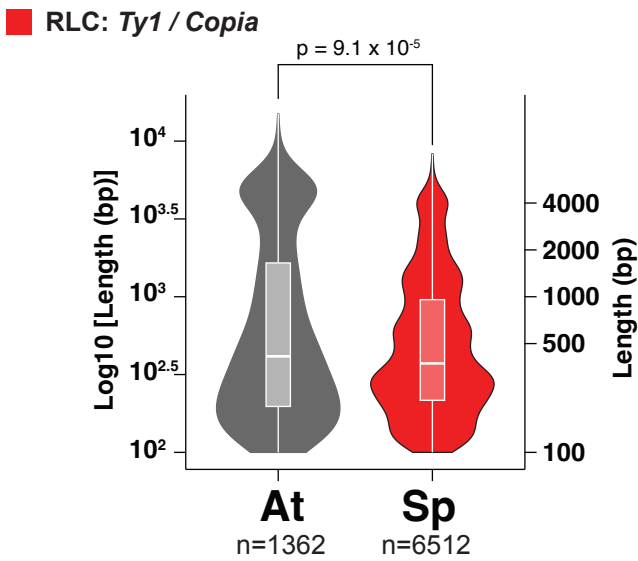
A



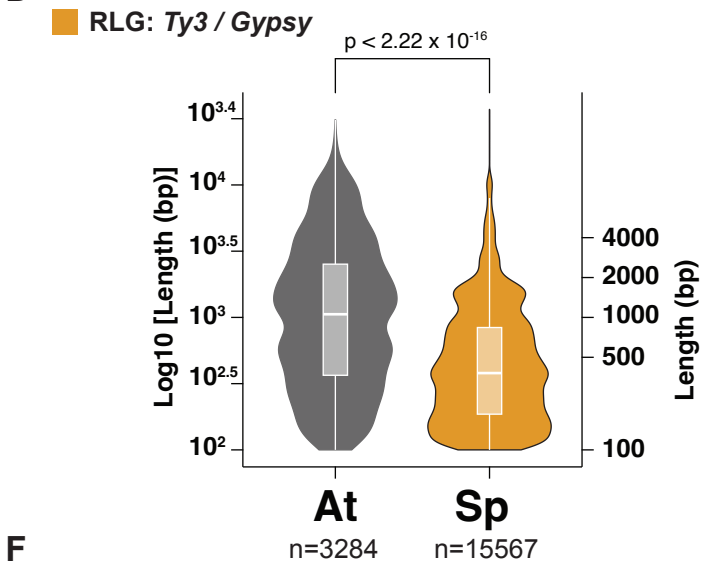
B



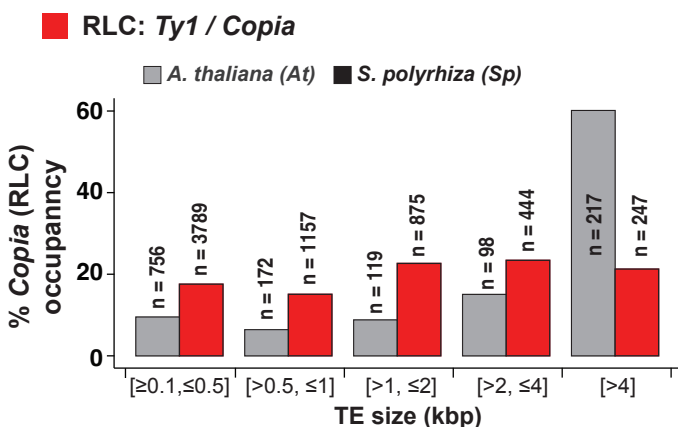
C



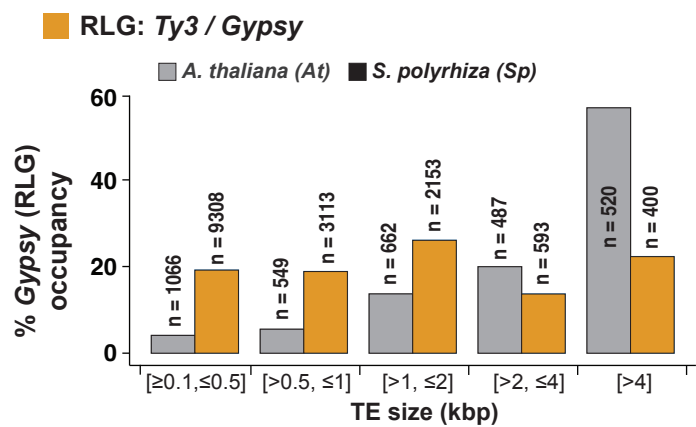
D



E



F



Supplemental Figure S23: mCHH levels across TE sizes and RLC and RLG length distribution in *Arabidopsis* and *Spirodela* genomes.

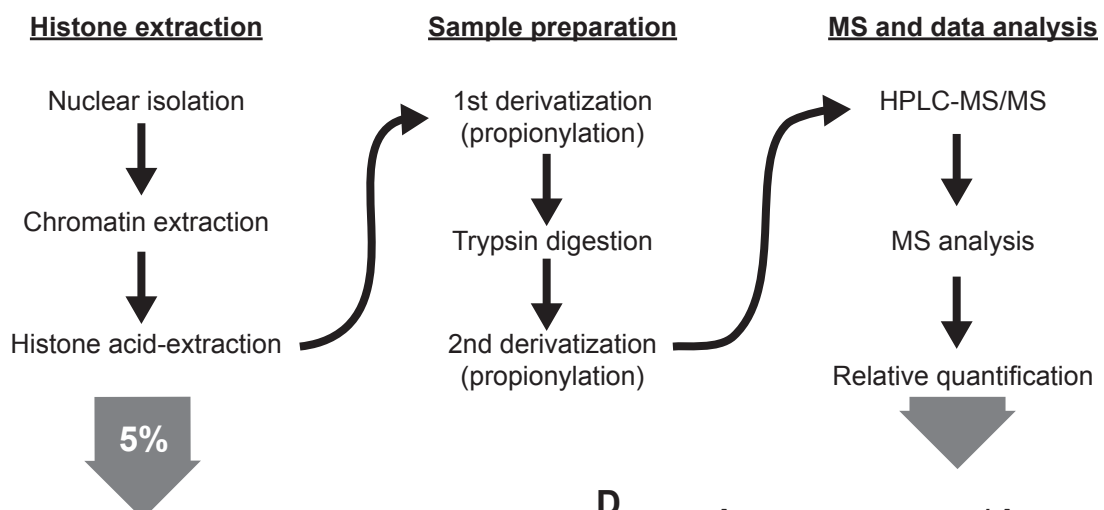
(A-B) Analysis of CHH methylation levels (%) between different length range groups for RLC: Ty1/Copia (a) and RLG: Ty3/Gypsy (b) in *Arabidopsis* and *Spirodela*. n values are indicated in panels E and F **(C-D)** Length distribution of RLC (C) and RLG (D) TE annotations in *Arabidopsis* and *Spirodela* genomes. **(E-F)** Number of TE annotations and relative contribution to their superfamily genomic occupancy at each size bin for RLC (E) and RLG (F). (*) indicates p-value <0.01 (**) indicates p-value <0.0001 (Wilcoxon rank sum test) In all boxplots: median is indicated by solid bar; the boxes extend from the first to the third quartile and whiskers stretch to the furthest value within 1.5 times the interquartile range. At: *Arabidopsis*, Sp: *Spirodela*.

SUPPLEMENTAL FIGURE S24

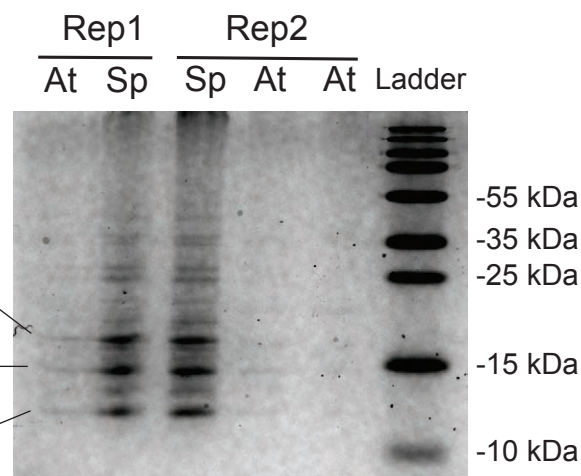
A

At-H3 *N*-ARTKQTARKKSTGGKAPRKQLATKAARKSAP(A/T)TGGVKKPHR-C
 Sp-H3 *N*-ARTKQTARKKSTGGKAPRKQLATKAARKSAP(A/T)TGGVKKPHR-C

B

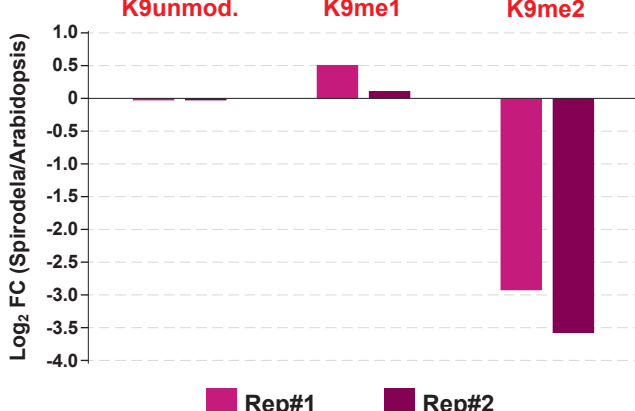


C



D

A [$K_{9(mod)}$ STGGKAPR] / **A** [KSTGGKAPR]

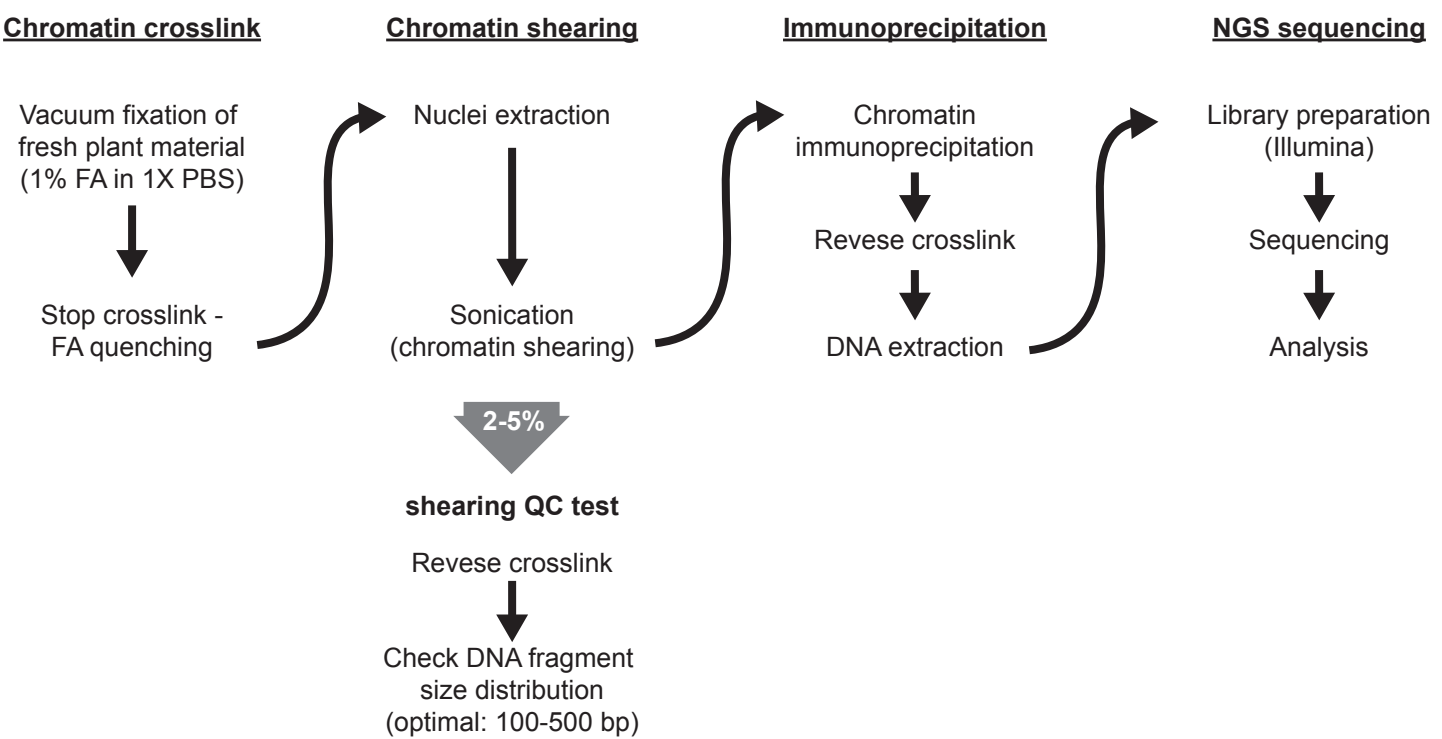


Supplemental Figure S24: Mass spectrometry (MS) quantification of H3K9me1/2 abundance in *Spirodesla*.

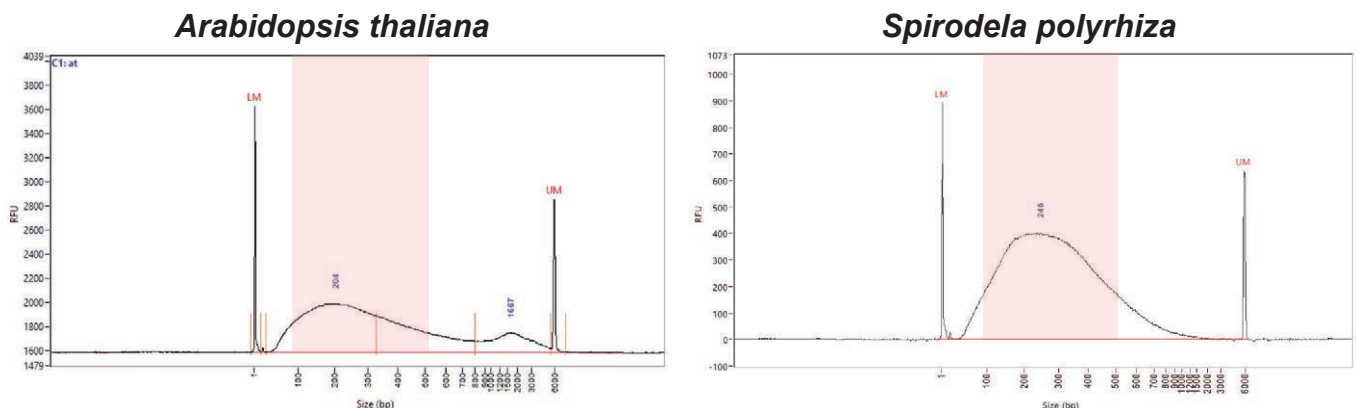
(A) Sequence of the 40 first aa of *Spirodesla* and *Arabidopsis* Histone 3 N-term. Lysine 9 (K9) and the associated peptide in the MS data is indicated and underlined. (B) Simplified workflow scheme of the steps from sample preparation to MS used. (C) Coomassie staining of denaturing SDS-PAGE gel of histones after acid extraction for quantity and quality control prior to sample preparation for MS. (D) Relative abundance of unmodified H3K9, H3K9me1 and H3K9me2 in *Spirodesla* compared to *Arabidopsis*. Abundance of each modification was calculated in each species by the ratio between the area of each modified peptide to the sum area of the peptide containing H3K9 independently of the modifications present.

SUPPLEMENTAL FIGURE S25

A



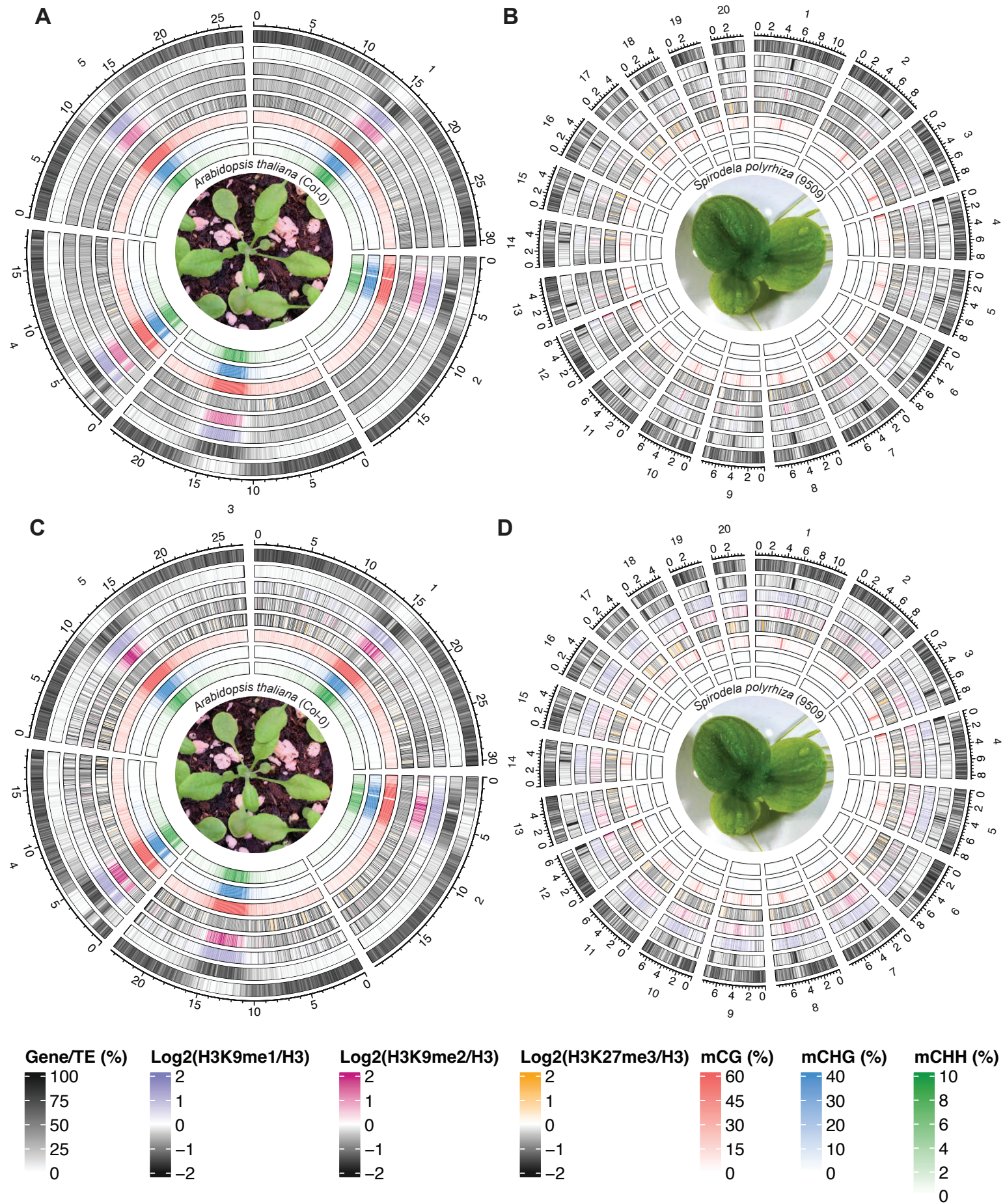
B



Supplemental Figure S25: Chromatin immunoprecipitation (ChIP) workflow and quality control in *Spirodesla*.

(A) Simplified workflow scheme of the ChIP and control steps. **(B)** Size distribution of DNA fragments after chromatin shearing and sample preparation quality control prior to IP (by investigating DNA fragment length distribution in a fragment analyser). The 100 to 500 bp size range is shadowed. LM and UM, lower and upper marker from Agilent Fragment Analyser respectively.

SUPPLEMENTAL FIGURE S26



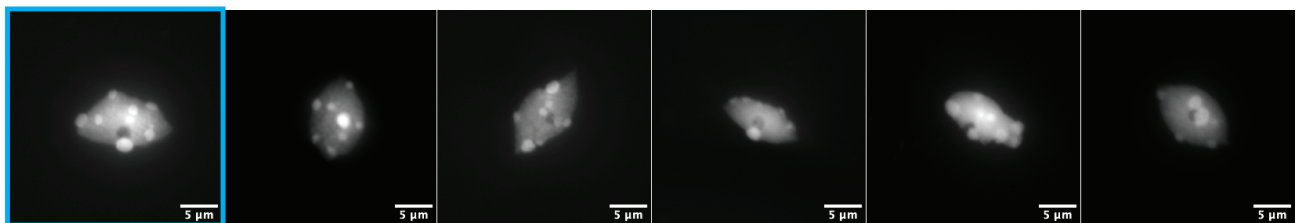
Supplemental Figure S26: Genome-wide distribution of H3K9me1, H3K9me2 and H3K27me3 in *Spirodela polyrhiza*.

(A-B) Circos plot of genome-wide distribution of H3K9me1, H3K9me2 and H3K27me3 enrichment densities by chromosome in *Spirodela* and *Arabidopsis*. From outside to inside: gene density, TE density, H3K9me1, H3K9me2, H3K27me3, CG, CHG and CHH methylation. Mean values within the indicated ranges are displayed for 100 kbp intervals in 50 kbp sliding windows. (C-D) Same as (A-B) but mean values were calculated only considering TE annotations (≥ 100 bp) for 100 kbp intervals in 50 kbp sliding windows.

SUPPLEMENTAL FIGURE S27

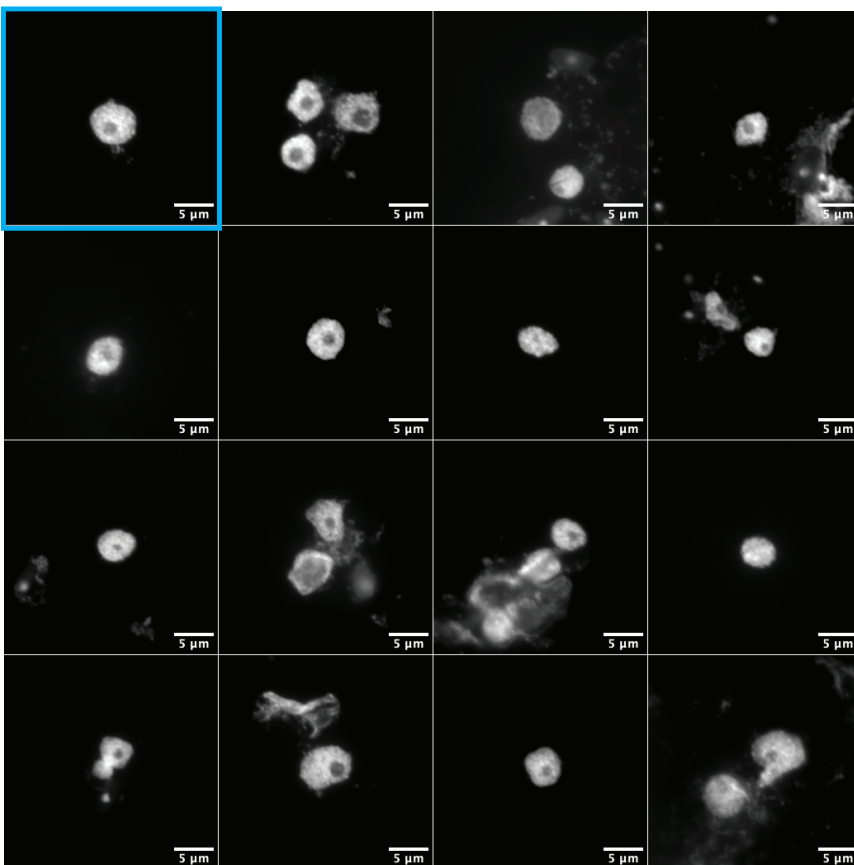
A

Arabidopsis thaliana (Col-0)



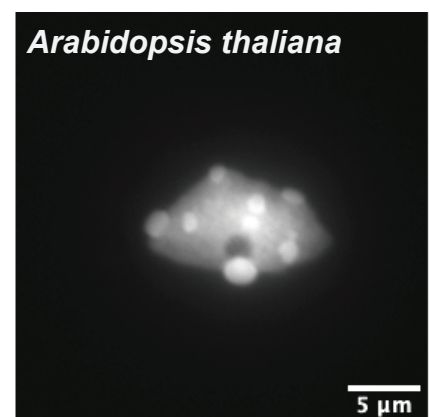
B

Spirodelia polyrhiza (9509)

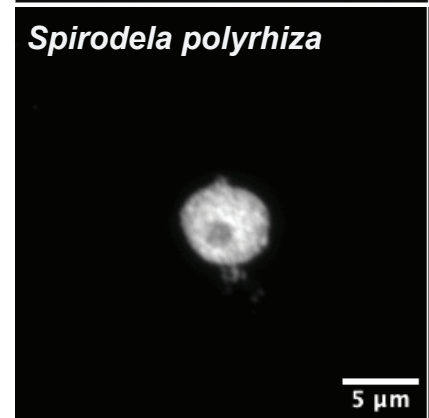


C

Arabidopsis thaliana



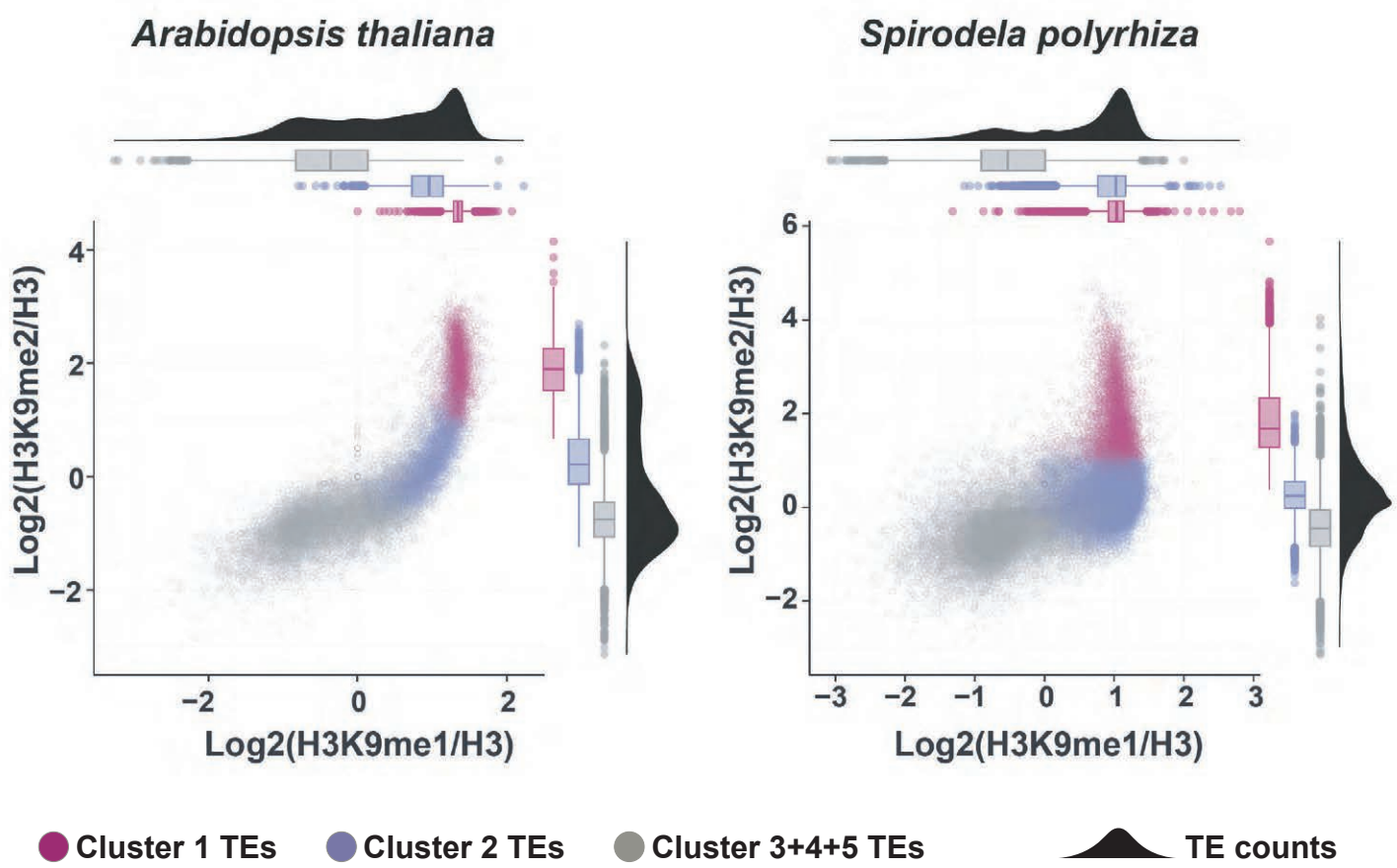
Spirodelia polyrhiza



Supplemental Figure S27: *Spirodelia* chromatin organization in interphase nuclei.

(A-B) Gray-scale fluorescent images of DAPI-stained interphase nuclei of *Arabidopsis* (A) and *Spirodelia* (B). C Enlargement of representative nuclei from both species (framed in blue in A and B). Scale bars = 5 μm.

SUPPLEMENTAL FIGURE S28

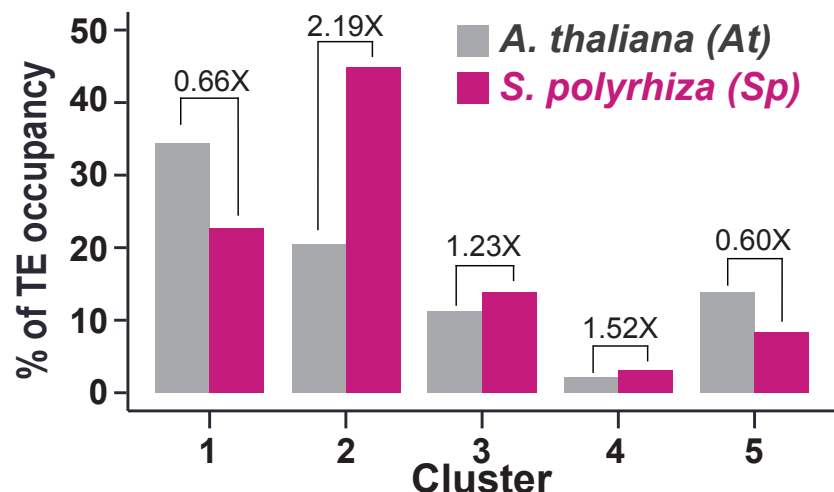


Supplemental Figure S28: Distribution of H3K9me1/2 in *Spirodea* TEs.

Scatterplots of H3K9me1 and H3K9me2 enrichment at *Spirodea* and *Arabidopsis* TEs colored by cluster (as defined in Figure 5).

SUPPLEMENTAL FIGURE S29

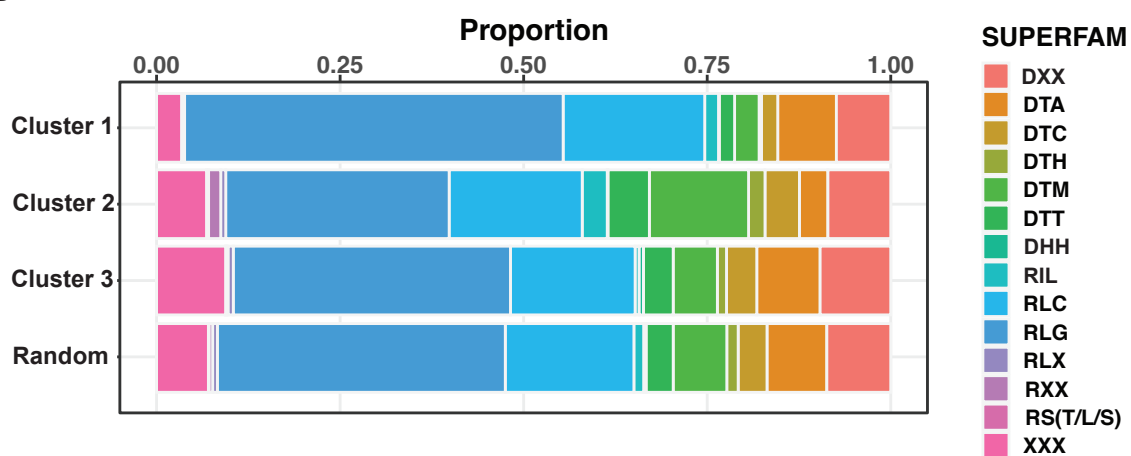
A



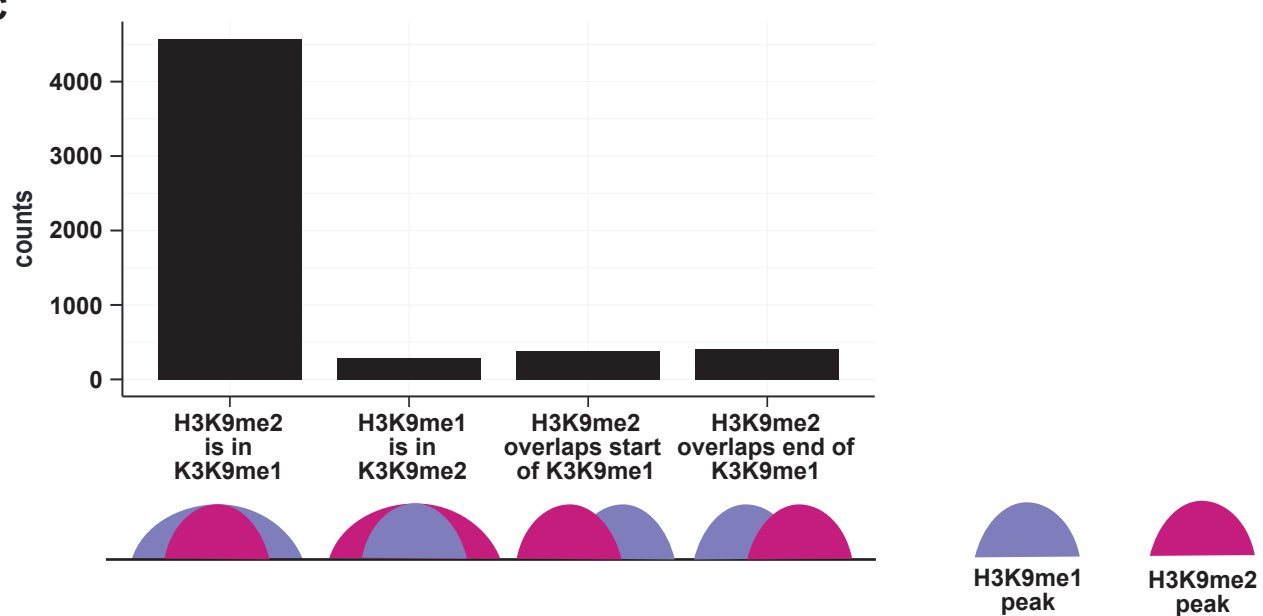
Supplemental Figure S29: Relative TE occupancy for each ChIP cluster, position and TE composition of H3K9me1 and H3K9me2 peaks to each other in *Spirodea*.

(A) Relative (%) occupancy of TE genomic space of each of the TE clusters defined in Figure 5 in *Arabidopsis* (grey) and *Spirodea* (colored). (B) TE superfamily composition (as proportion) of clusters 1, 2, 3 and a random subsampling. See Supplemental Fig. S21 for a description of TE superfamily codes. (C) Bar plot of overlapping H3K9me1 and H3K9me2 broad peaks, defined using MACS2 (version 2.2.5). Overlaps between the 2 marks were identified using `findOverlapsOfPeaks` (`maxgap = 1000`) from `ChIPpeakAnno` (version 3.6.5). Scheme illustrating the possible relationships between overlapping broad peaks.

B

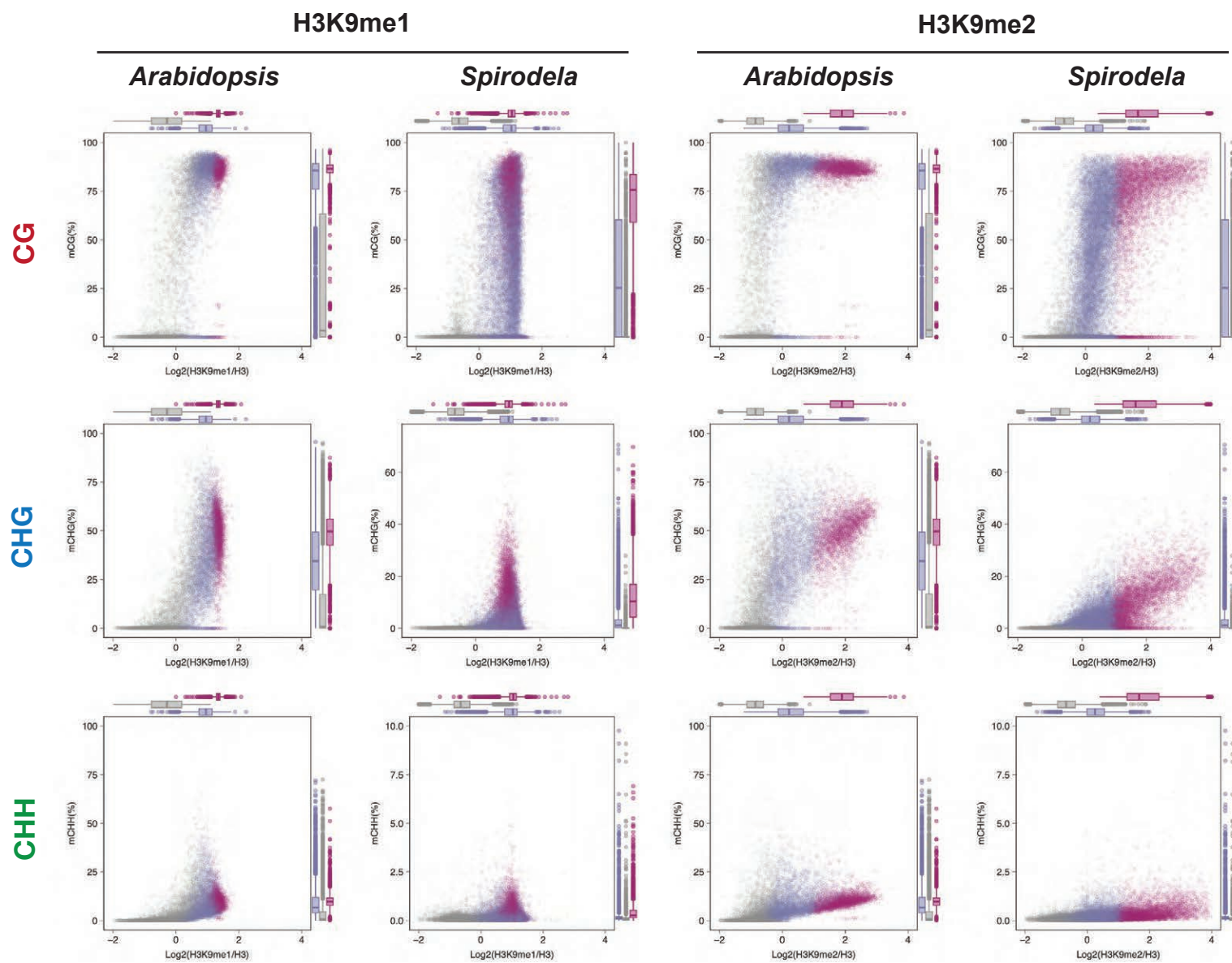


C



SUPPLEMENTAL FIGURE S30

● Cluster 1 TEs ● Cluster 2 TEs ● Cluster 3+4+5 TEs

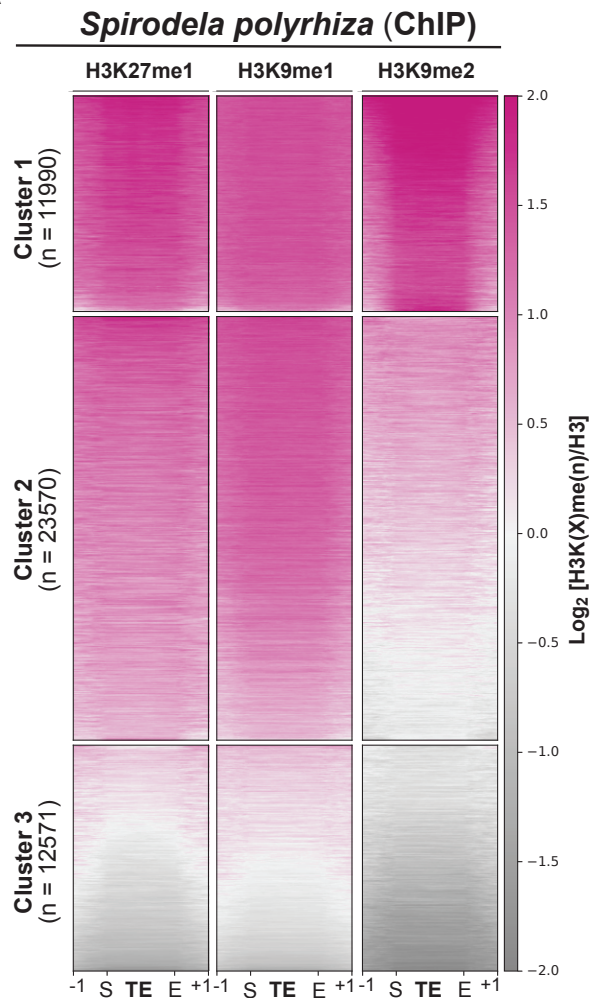


Supplemental Figure S30: Analysis of H3K9me1/2 association to DNA methylation in *Arabidopsis* and *Spirodelia*.

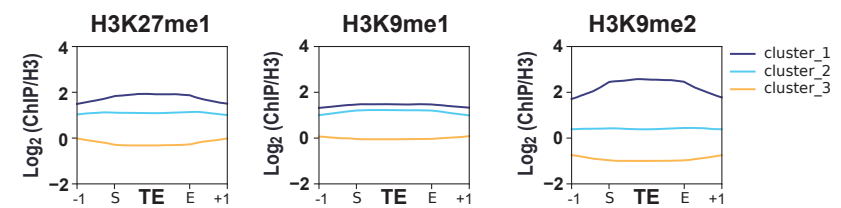
Scatter plots of DNA methylation in all three contexts against H3K9me1 and H3K9me2 enrichments of TEs in Cluster 1, 2 and 3/4/5 combined (as defined in Figure 5) in *Spirodelia* and *Arabidopsis*.

SUPPLEMENTAL FIGURE S31

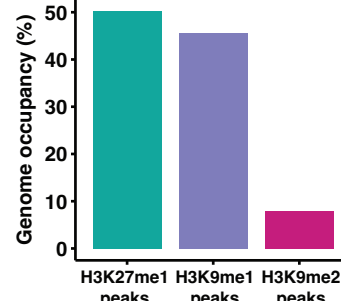
A



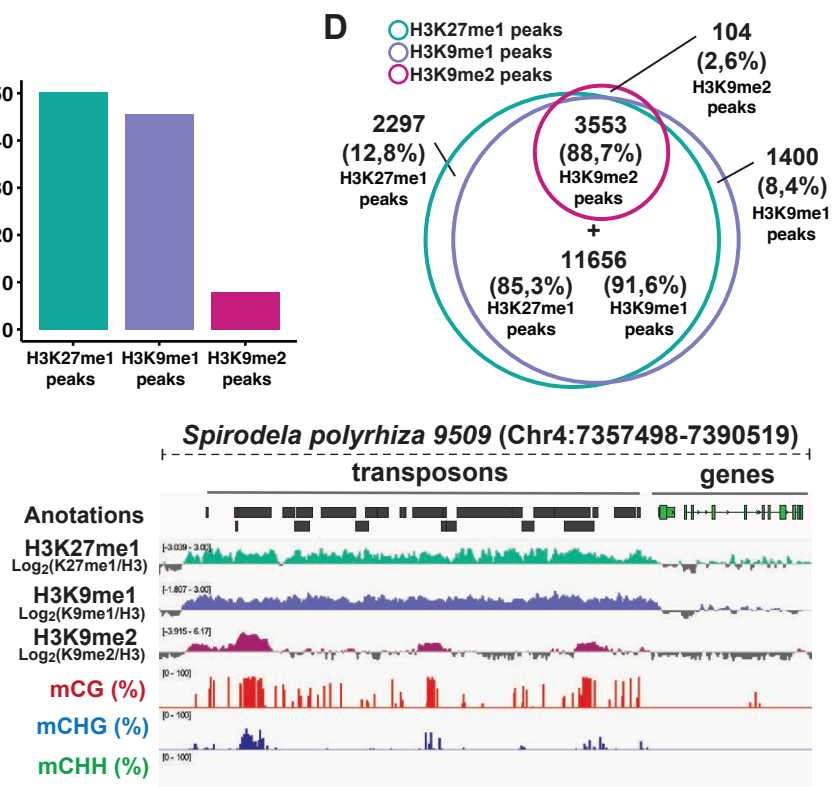
B



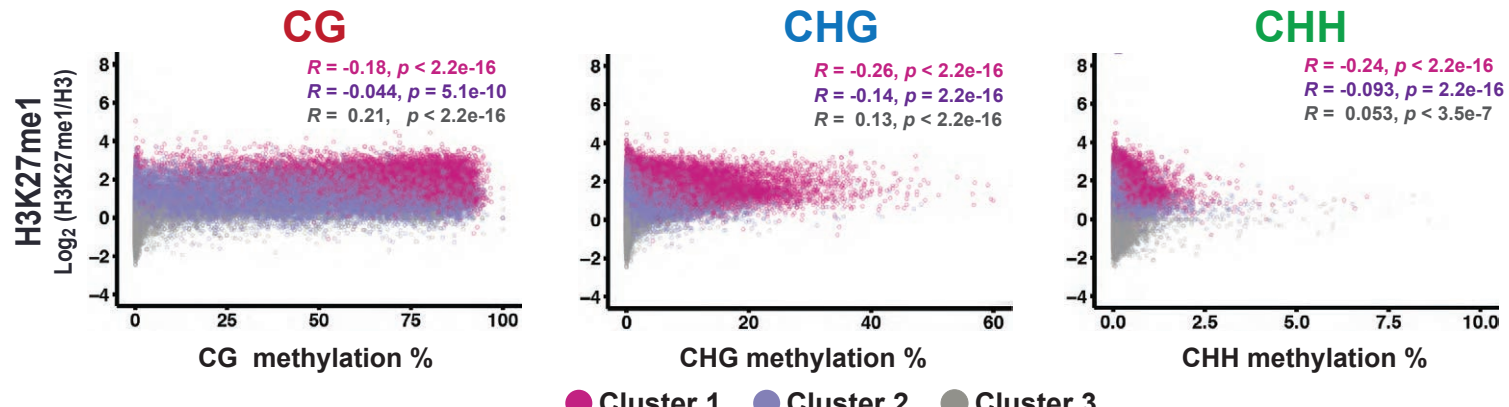
C



E



F

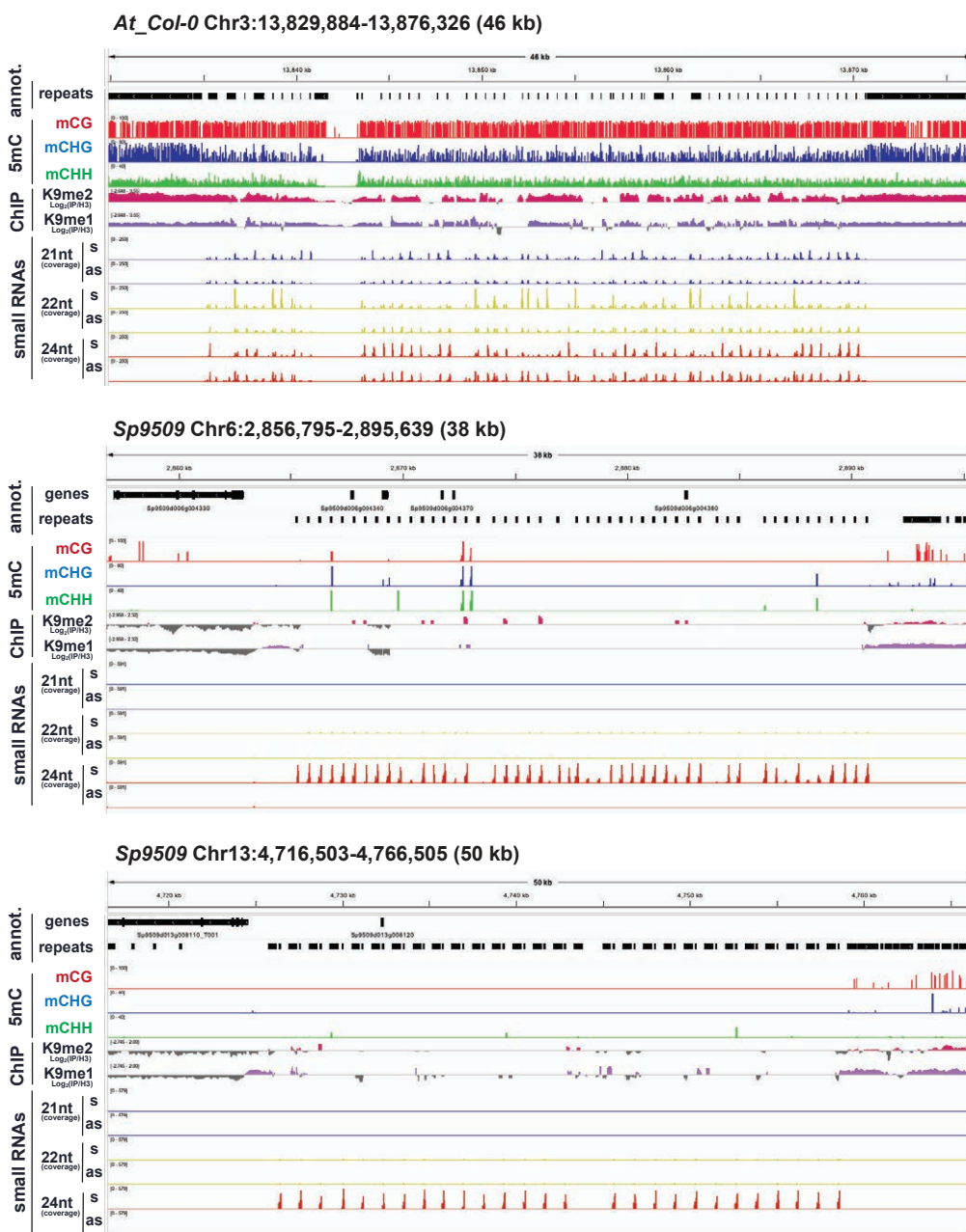


Supplemental Figure S31: Patterns of H3K27me1 and H3K9me1/2 distribution in *Spirodesa polyrhiza* transposons.

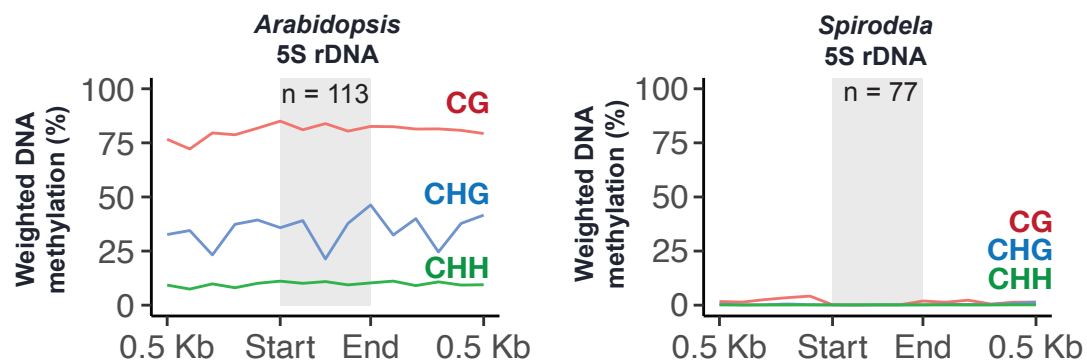
(A) Heatmap of k -means clustering of transposons in *Spirodesa* using H3K27me1, H3K9me1 and H3K9me2 enrichment over H3, presented as $\text{log}_2[\text{ChIP}(X)/\text{ChIP}(H3)]$. Enrichment is represented by color, while depletion is shown in gray. Each row corresponds to a length-normalized TE annotation ± 1 kb. Transposons are grouped into clusters 1 to 3 based on the abundance of examined marks. **(B)** Metaplots of average weighted H3K27me1, H3K9me1 and H3K9me2 enrichments over H3 at Cluster 1, 2 and 3 transposons ± 1 kb in *Spirodesa*. **(C)** Genome occupancy (%) of H3K27me1, H3K9me1 and H3K9me2 in the *Spirodesa* genome. **(D)** Venn diagram of the overlap between H3K27me1, H3K9me1 and H3K9me2 peaks along *Spirodesa* genome. **(E)** Genome browser capture of the distribution of H3K27me1, H3K9me1 and H3K9me2 enrichments, together with DNA methylation, along genes and transposons in *Spirodesa*. **(F)** Scatter plots of DNA methylation in all three contexts against H3K27me1 enrichment of TEs in *Spirodesa*. R and p indicate Pearson correlation coefficients and p -values.

SUPPLEMENTAL FIGURE S32

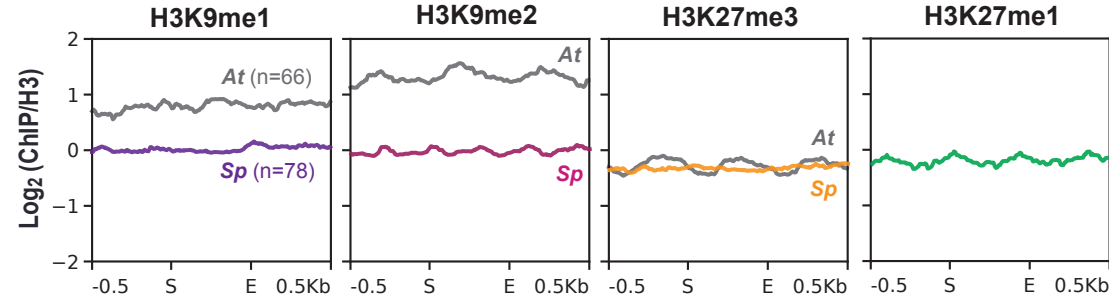
A



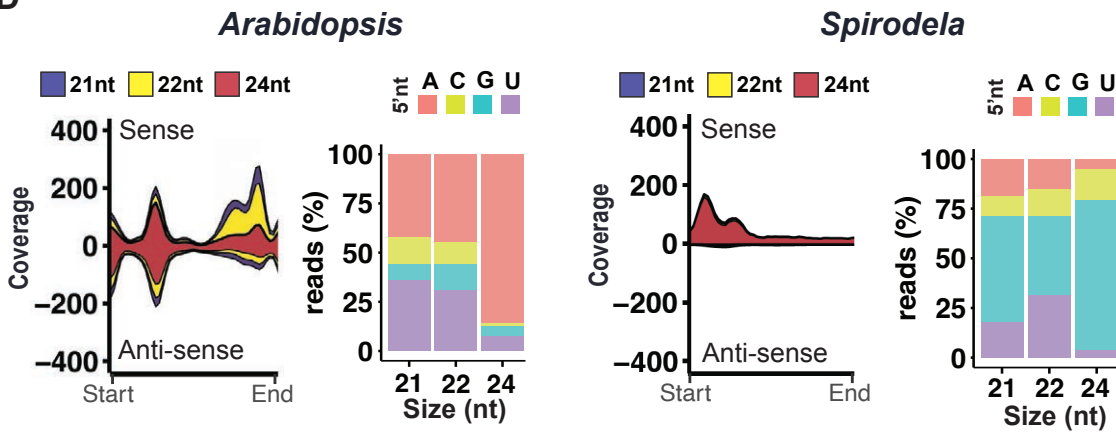
B



C



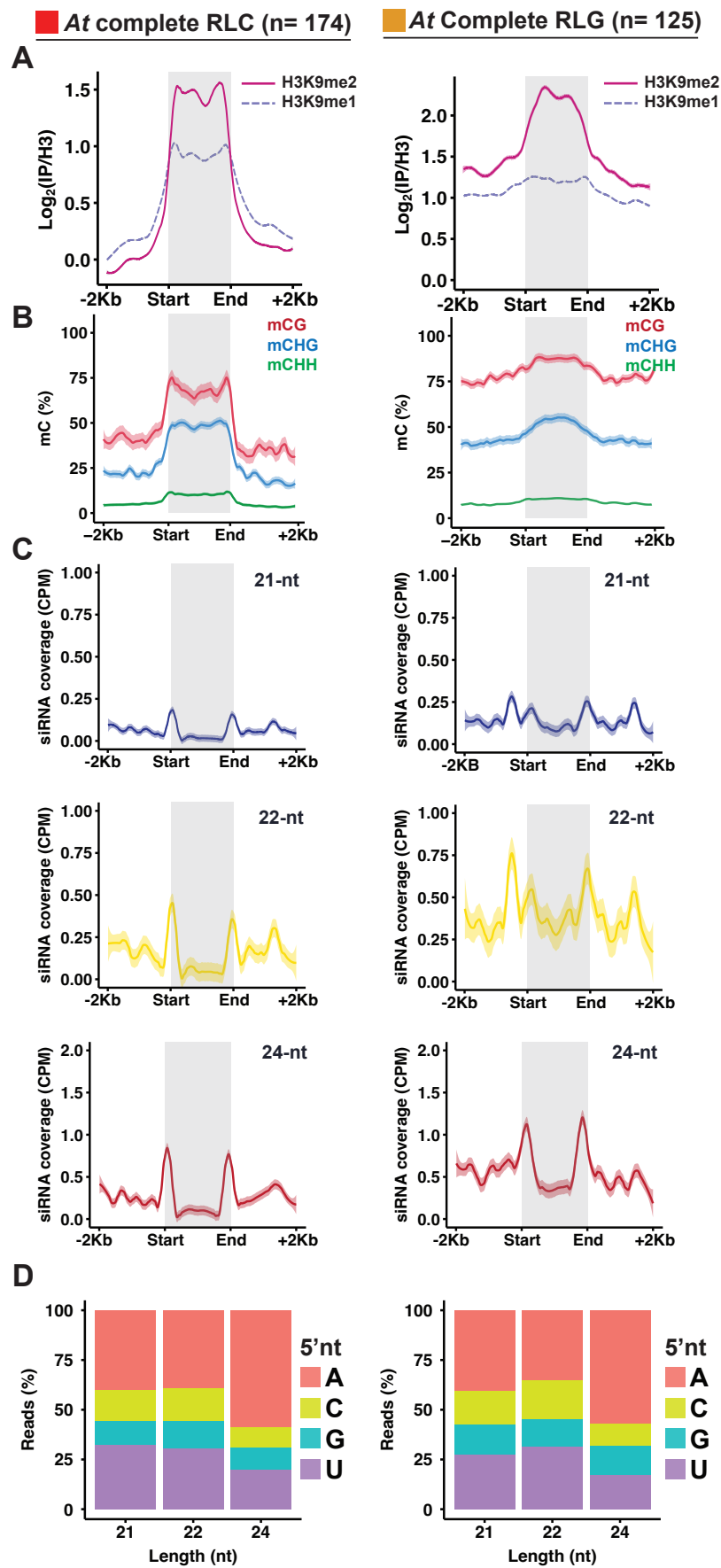
D



Supplemental Figure S32: Analysis of the epigenetic and small RNA landscape of 5S rRNA repeats in *Spirodea*.

(A) Genome browser captures of *Arabidopsis* Col-0 5S rDNA array in Chromosome 3 and the two *Spirodea* 9509 5S rDNA arrays in Chromosomes 6 and 13. From top to bottom tracks display: gene and TE annotations, mCG, mCHG and mCHH methylation; H3K9me2 and H3K9me1 enrichment profiles; sense and anti-sense (relative to the 5S rDNA annotations) 21-, 22- and 24-nt siRNAs. (B) Metaplots of averaged weighted DNA methylation in all three contexts over 5S rDNA annotations \pm 0.5 kb flanking regions in *Arabidopsis* and *Spirodea*. n indicates the number of 5S rDNA loci for which enough information (coverage) was available for analysis. (C) Metaplots of average weighted H3K9me1, H3K9me2, H3K27me3 and H3K27me1 (only for *Spirodea*) enrichments over H3 at 5S rDNA annotations \pm 0.5 kb in *Arabidopsis* (grey line) and *Spirodea* (colored line). n indicates the number of 5S rDNA loci for which enough H3 ChIP coverage (> 5 reads) was available for analysis. (D) Stacked distribution of 21-22-24-nt siRNAs and their 5'-nucleotide composition mapping to 5S rDNA in *Arabidopsis* and *Spirodea*.

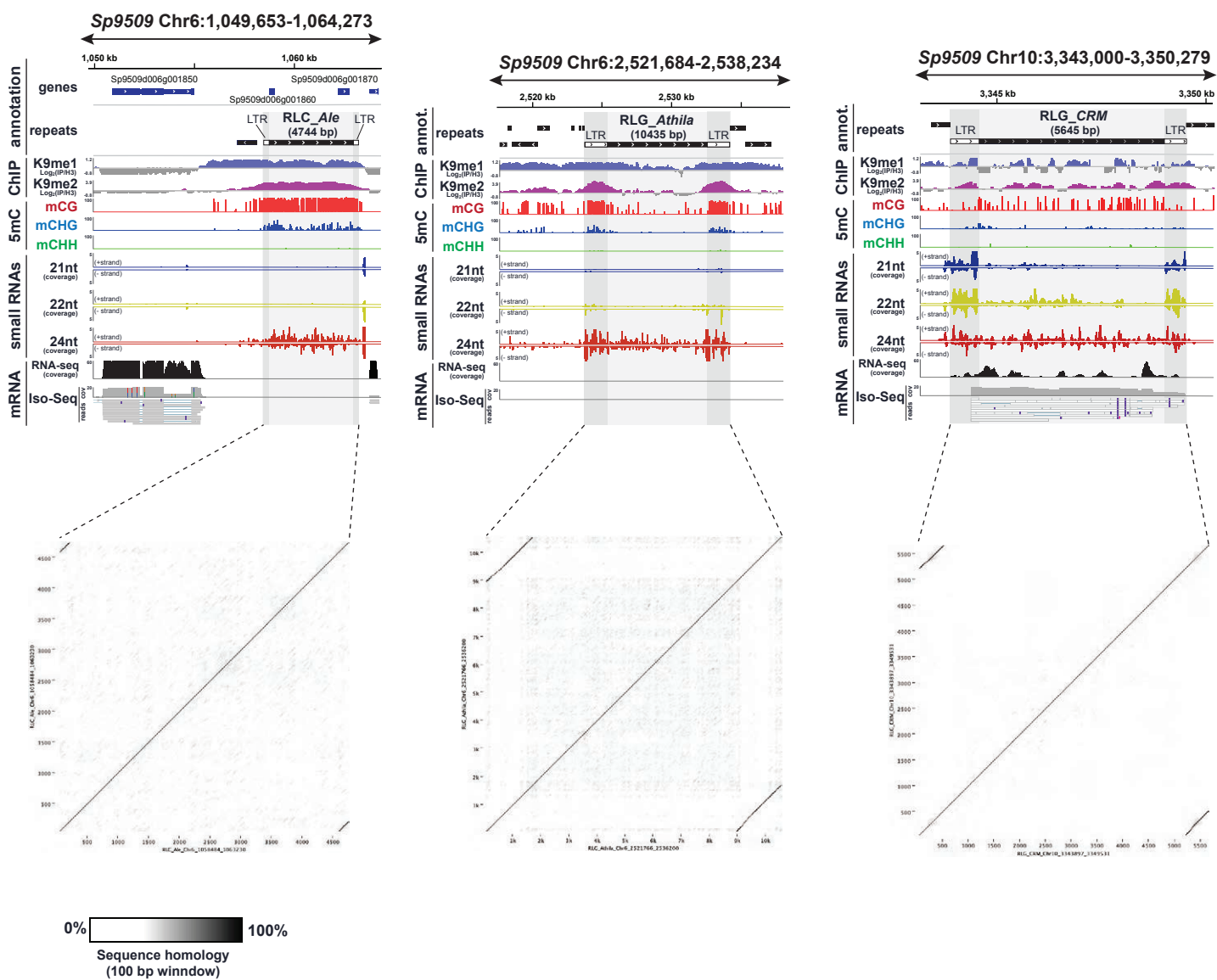
SUPPLEMENTAL FIGURE S33



Supplemental Figure S33: Distribution of silencing epigenetic marks and small RNAs in *Arabidopsis* RLC and RLG complete TEs.

(A) Metaplots of average weighted H3K9me1 (solid line) and H3K9me2 (dashed line) enrichments over H3 at complete RLC (left) and RLG (right) transposon annotations \pm 2 kb in *Arabidopsis*. Complete TEs were defined as those for which all RLC and RLG protein domains were identified. n indicates number of complete elements in each superfamily. **(B)** Metaplots of averaged weighted DNA methylation in all three contexts over RLC and RLG transposons \pm 2 kb flanking regions in *Arabidopsis*. **(C)** Metaplots of averaged weighted 21-, 22- and 24-nt small RNA abundance over complete RLC and RLG \pm 2 kb flanking regions in *Arabidopsis*. In all metaplots (A-D), solid lines represent the mean and colored shadows the standard deviation of the mean. **(D)** 5'-nucleotide (5'nt) composition distribution (as % of reads) of 21-, 22- and 24-nt siRNAs mapping to intact RLC and RLG \pm 2 kb flanking regions in *Arabidopsis*. d 5'-nucleotide (5'nt) composition distribution (as % of reads) of 21-, 22- and 24-nt siRNAs mapping to intact RLC and RLG \pm 2 kb flanking regions in *Arabidopsis*.

SUPPLEMENTARY FIGURE S34

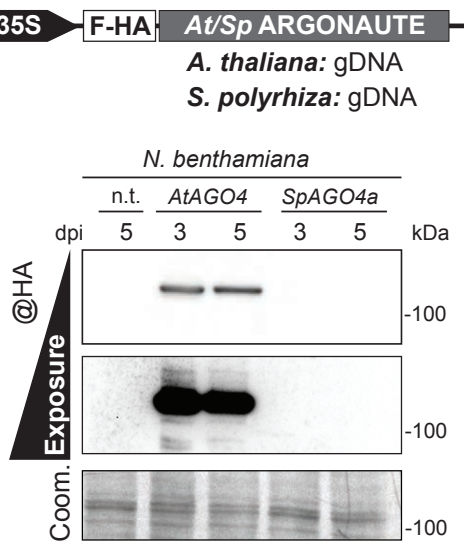


Supplementary Figure S34: LTR identification for complete TEs in Figure 6.

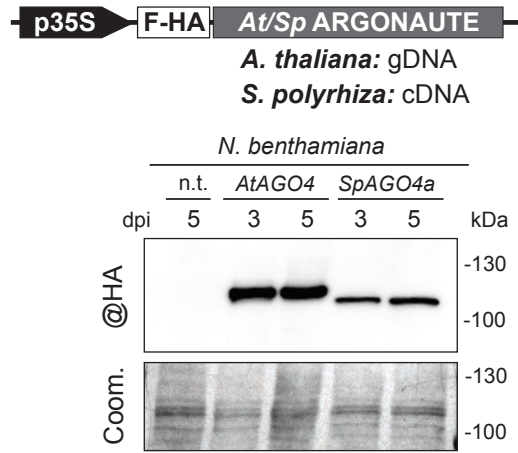
To identify LTRs of complete TEs, dot plots of their sequences against themselves were generated to identify the direct repeats. Dot plots were generated using a 100 bp window sliding at single bp intervals.

SUPPLEMENTAL FIGURE S35

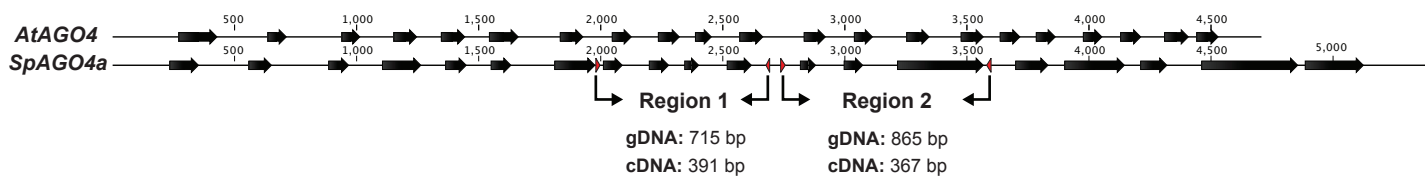
A



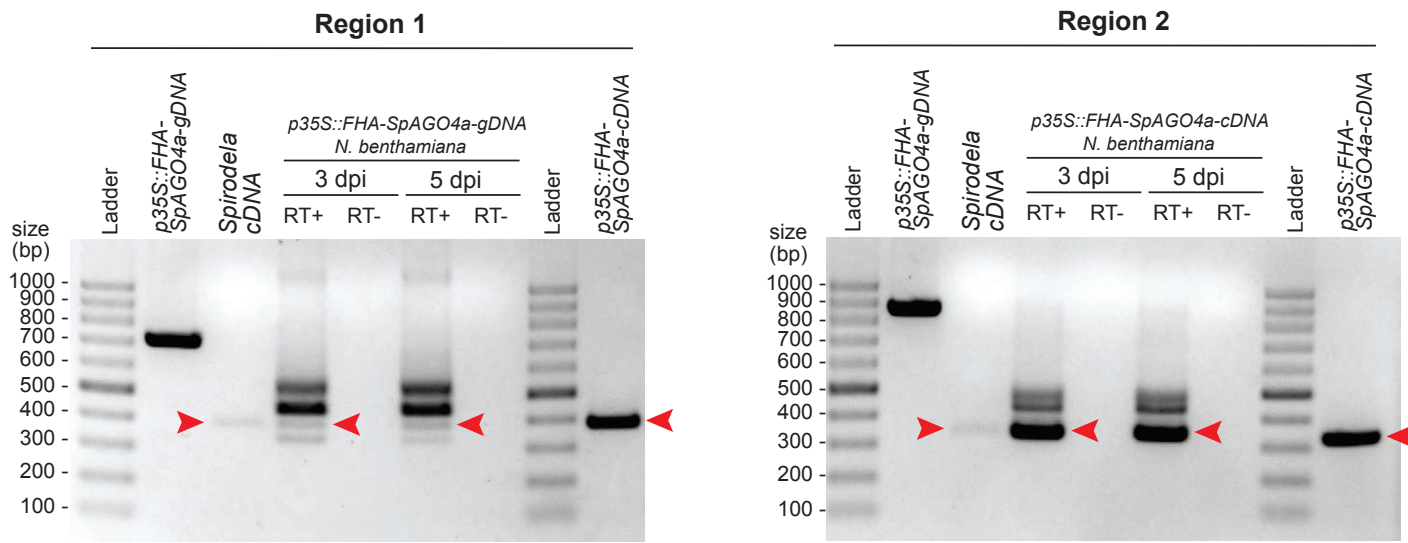
D



B



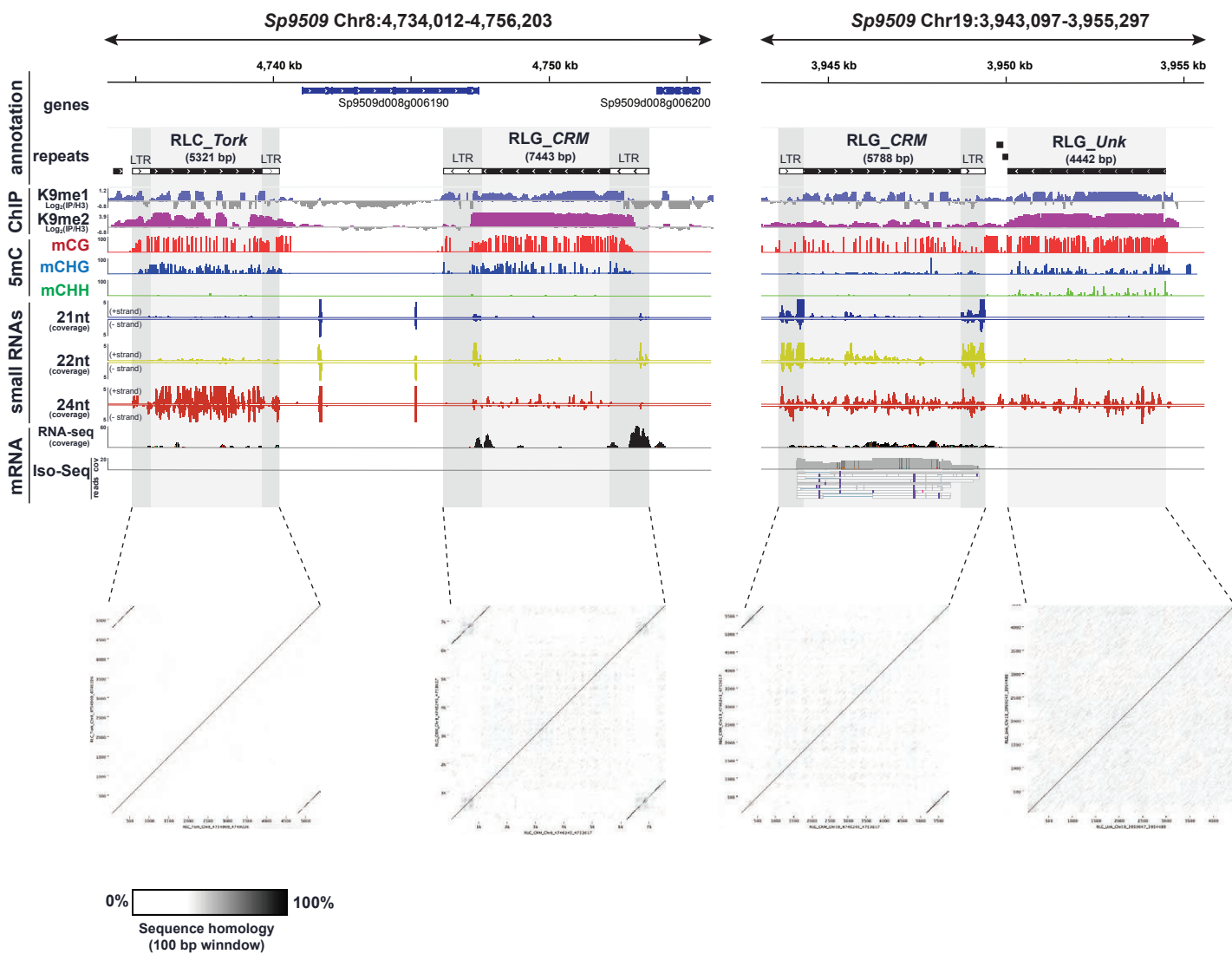
C



Supplemental Figure S35: Defects in SpAGO4a splicing in *N. benthamiana* prevent its transient expression from gDNA.

(A) Protein blot analysis of *Arabidopsis* and *Spirodesla* AGO4 (AtAGO4 and SpAGO4a) gDNA transient expression in *N. benthamiana* at 3 and 5 days post infiltration (dpi). n.i.: non-infiltrated. Coomassie (Coom.) staining of blot is shown as loading. Scheme of constructs infiltrated in *N. benthamiana* leaves for transient expression is shown above. p35S: CaMV 35S promoter; F-HA: in-frame N-term Flag and HA peptide tags. Genomic (gDNA) or cDNA origin of the AGO4 sequences is indicated. **(B)** Schematic representation of AtAGO4 and SpAGO4a loci. Introns are represented by arrows. Position of PCR primers used to determine efficiency and completion of splicing across indicated regions are indicated by red triangles. Expected amplicon sizes in each case is indicated below **(C)** Agarose gel electrophoresis of RT-PCRs of regions in (B) of SpAGO4a transient expression in *N. benthamiana*. Arrowheads indicated the expected size of properly spliced mRNA as expected from in silico predictions and validated by RT-PCR in *Spirodesla* cDNA. Plasmid DNA containing SpAGO4a gDNA is used as control for unspliced PCR, *Spirodesla* total cDNA and plasmid containing SpAGO4a cDNA are used as positive controls for properly spliced mRNA size. **(D)** Protein blot analysis of AtAGO4 gDNA and SpAGO4a cDNA transient expression in *N. benthamiana* at 3 and 5 days post infiltration (dpi). n.i.: non-infiltrated. Coomassie (Coom.) staining of blot is shown as loading. Scheme of constructs infiltrated in *N. benthamiana* leaves for transient expression is shown above. p35S: CaMV 35S promoter; F-HA: in-frame N-term Flag and HA peptide tags. Genomic (gDNA) or cDNA origin of the AGO4 sequences is indicated.

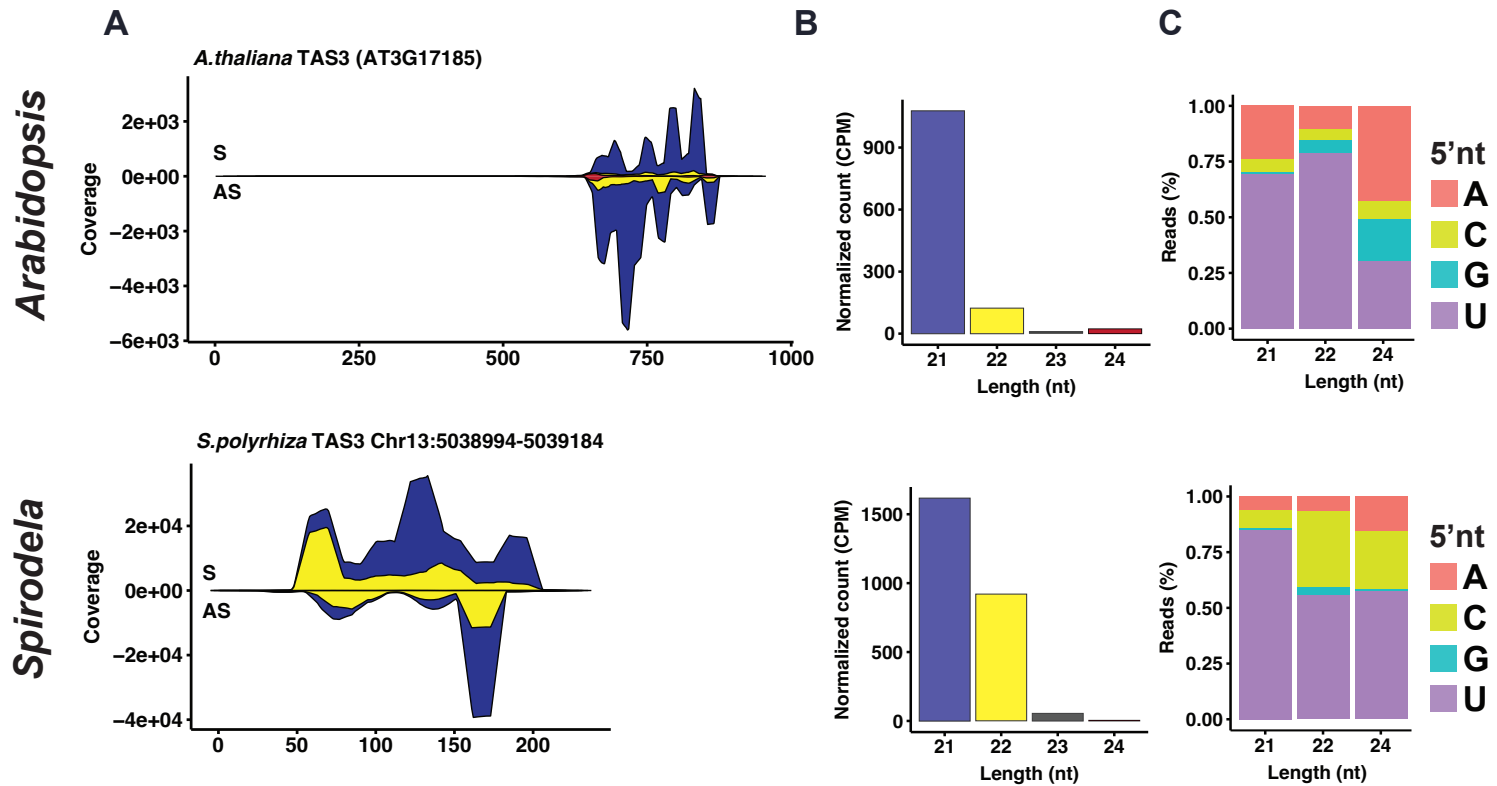
SUPPLEMENTAL FIGURE S36



Supplemental Figure S36: Additional examples of siRNA producing TEs in *Spirodea*.

Genome browser captures of selected complete TEs in *Spirodea*. From top to bottom tracks display: gene and TE annotations, H3K9me1 and H3K9me2 enrichment profiles; mCG, mCHG and mCHH methylation; 21-, 22- and 24-nt siRNA mapping to Watson (+) and Crick (-) DNA strands; RNA expression by short (illumina) and long reads (Iso-Seq). Superfamily, clade and length (in bp) of TEs is indicated above their annotation. Light and dark gray shadow delimit TEs and LTRs respectively across all tracks. Dot plots of their sequences against themselves were generated to identify the direct repeats using a 100 bp window sliding at single bp intervals.

SUPPLEMENTAL FIGURE S37

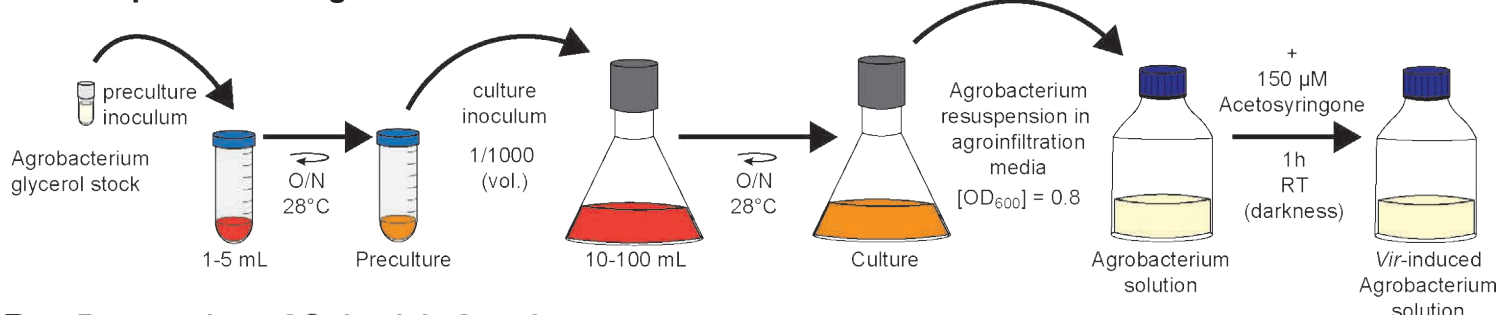


Supplemental Figure S37: TAS3 tasiRNAs in *Spirodea*.

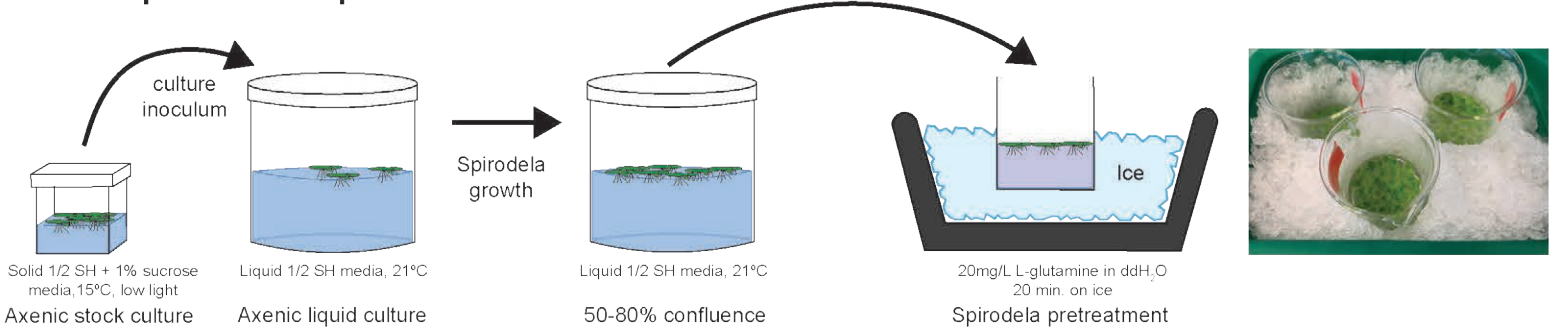
(A) Stacked distribution of sense (S) and antisense (AS) TAS3 tasiRNA in *Arabidopsis* and *Spirodea*. **(B)** Size distribution and abundance of TAS3 tasiRNA in *Spirodea* and *Arabidopsis*. **(C)** 5'-nucleotide (5'nt) composition distribution of 21-, 22- and 24-nt siRNAs mapping TAS3 in *Spirodea* and *Arabidopsis*.

SUPPLEMENTAL FIGURE S38

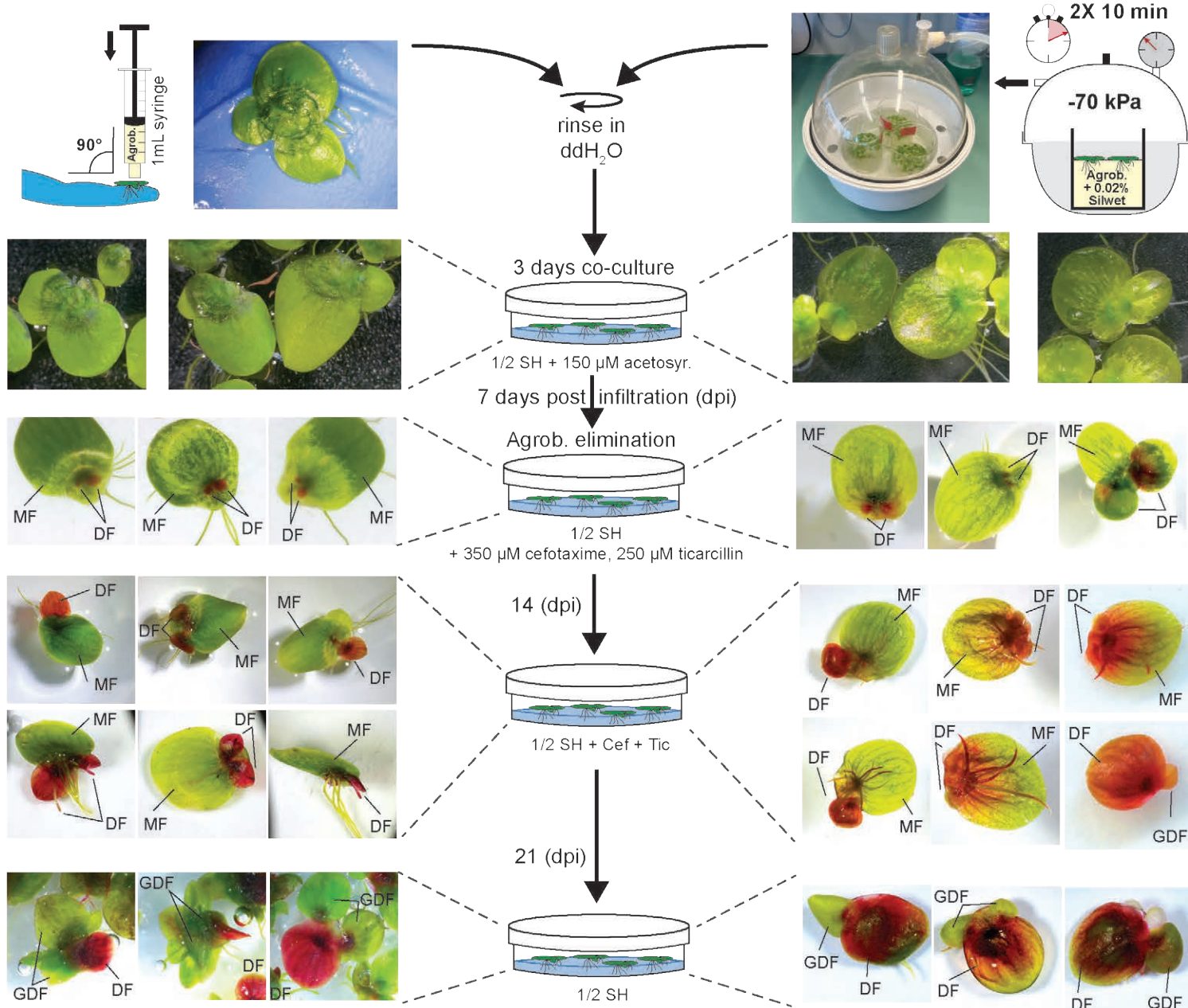
A Preparation of Agrobacterium cells



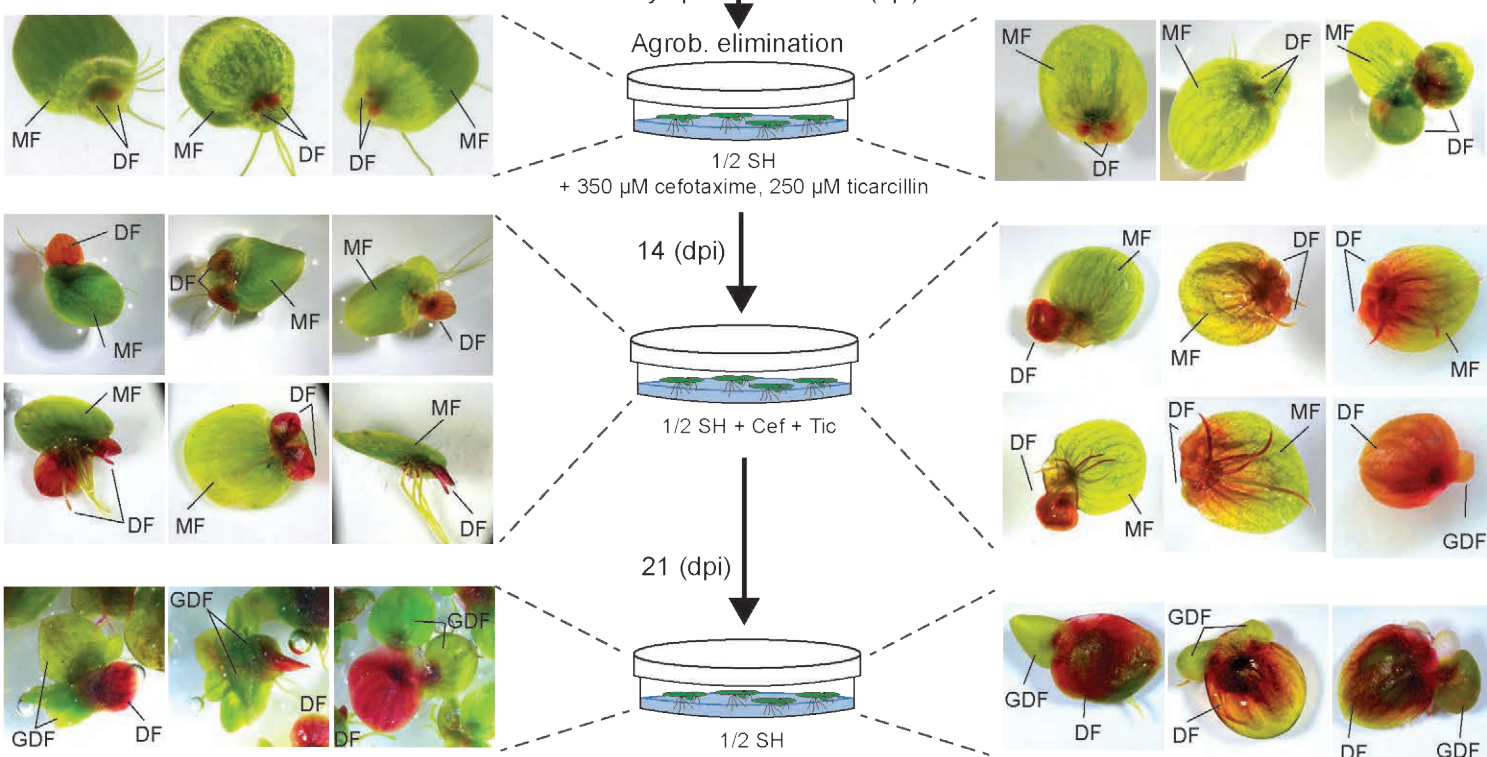
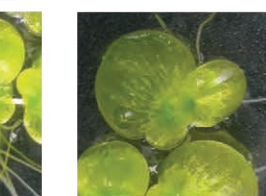
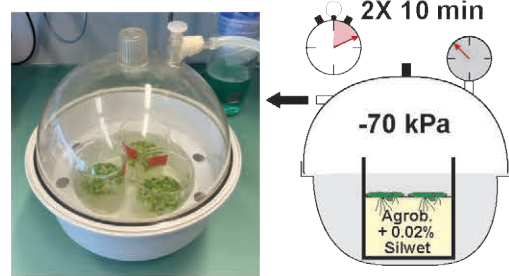
B Preparation of Spirodesla fronds



C Manual agroinfiltration



D Vacuum agroinfiltration



Legend in next page

Supplemental Figure S38: Transient expression procedure in *Spirodela*.

(A) For *Agrobacterium*-mediated transient expression in *Spirodela* standard procedures for the preparation and induction of *Agrobacterium* cells carrying plant binary vectors with the desired construct were followed. **(B)** *Spirodela* cultures are started from axenic stock cultures and grown to 50-80% confluence as saturated cultures are more recalcitrant to the procedure. Prior agroinfiltration, fronds are pretreated in a cold solution of 20mg/L of L-glutamine on ice for 20 min. Induced *Agrobacterium* cultures can then be infiltrated into *Spirodela* fronds manually **(C)** or applying vacuum **(D)**. **(C)** Procedure for manual agroinfiltration. Bacterial solutions are infiltrated locally above the budding pockets. **(D)** Procedure for vacuum infiltration. *Spirodela* cultures are placed on bacteria solutions in a vacuum bell and vacuum is applied twice. In both procedures, excess of *Agrobacterium* is eliminated before plants are co-cultured with the bacteria. Then *Agrobacterium* is eliminated from media with antibiotics and plants are cultured normally. While manual infiltration yields a more uniform transient expression in developing fronds at the infiltrated area **(C)**, it is more tedious and less plants can be processed. Vacuum infiltration on the other hand allows for the infiltration of a greater number of plants, however the resulting expression is less homogeneous. In both cases daughter fronds appear to express uniformly transgenic reporters, their progeny does not express it, hence we considered the system to be transient .MF: mother frond; DF: daughter frond; GDF: grand-daughter frond.

SUPPLEMENTAL FIGURE S39

Name	Sequence 5'->3'	Use	Note
FLAG F	GAAACGACAATCTGATCCAAGCTCAAGCTAAGCTTGGAGCTCAACTTGATAG	FLAG Gibson cloning	
FLAG R	GTAGGATCCGCCACCTCCCTGTCTATCGTACCTTGTAAATCCATGAAGCCTGCTTTTGACAAACTTGCTG	FLAG Gibson cloning	
HA F	GGCGGATCCTACCCATACGATGTTCCAGATTACGCTGGAGGcGGTCTAGATACCAGCTTCTTGACAAAGTGG	HA cloning	
HA R	CAGACCCGGGAGGTCACTGGATTTGGTTAGG	HA cloning	
AtAGO4_gDNA F	<i>CATA CGAT GTTCCAGATTACGCTGGAGGC GG TGATTCAACAAATGGTAACGGAGC</i>	AtAGO4_gDNA Gibson cloning	Homologous sequence to backbone for Gibson assembly in italics. In bold AtAGO4 sequence.
AtAGO4_gDNA R	<i>CACCACTTGACAAGAAAGCTGGGTATCTAGTTAACAGAAGAACATGGAGTTGGC</i>	AtAGO4_gDNA Gibson cloning	Homologous sequence to backbone for Gibson assembly in italics. In bold AtAGO4 sequence.
SpAGO4_gDNA F	<i>GCAACTAGTGGAAAAACAGAGGGGGAAAGAACAG</i>	SpAGO4_gDNA Bcul cloning	Bcul RE site italics. In bold SpAGO4 sequence.
SpAGO4_gDNA R	<i>GCAACTAGTTCAGCAGAAGAACATGGAAC TGCTC</i>	SpAGO4_gDNA Bcul cloning	Bcul RE site italics. In bold SpAGO4 sequence.
SpAGO4_cDNA F	<i>GCAACTAGTGC CCATGAAAAGACCAGGAACGGAA</i>	SpAGO4_cDNA Bcul cloning	Bcul RE site italics. In bold SpAGO4 sequence. Primer match both SpAGO4 in Spirodela
SpAGO4_cDNA R	<i>GCAACTAGTT CAGCAGAAGAACATGGAGCTGCTC</i>	SpAGO4_cDNA Bcul cloning	Bcul RE site italics. In bold SpAGO4 sequence. Primer match both SpAGO4 in Spirodela
SpAGO4a r1 F	TCCCCAAGAGAGGATGAGAG	RT-PCR	See Supplemental_Fig_S35
SpAGO4a r1 R	GTCCACCC TAACATTGG	RT-PCR	See Supplemental_Fig_S35
SpAGO4a r2 F	CGCTTCTCTGTATCTTC	RT-PCR	See Supplemental_Fig_S35
SpAGO4a r2 R	GAGATATTGAAGGCCACTGCC	RT-PCR	See Supplemental_Fig_S35
Scarlet probe F	ATGGTGAGCAAGGGTGAAGCCG	Northern probe	
Scarlet probe R	TTACTTGAGAGTTCGTCCATAC	Northern probe	
RUBY probe F	CAACACCATCGAAGTAGTGC	Northern probe	
RUBY probe R	TACCACATCCTCCACATTG	Northern probe	
miR159a probe	TAGAGCTCCCTCAATCCAAA	Northern probe	

Supplemental Figure S39: Oligos used in this study.

Supplemental Methods

Plant material description and growth conditions:

***Spirodes polystachya* sterilization and stocks.** Upon arrival, the initial culture was amplified and further sterilized to obtain axenic cultures. In brief, 50 fronds of *Spirodes* were incubated in 10 ml of a 0.5% DanKlorix® solution (Colgate-Palmolive; commercial detergent containing 2.8% Na-Hypochlorite) for 1 minute under agitation. Subsequently, the sterilizing solution was removed, and the fronds were washed three times with sterile water before being transferred to individual wells in 6-well plates containing 6 ml of sterile ½ SH + 2% sucrose media. After one week, fronds in wells with no visible growth of microorganisms were transferred to plates with solid (2% Gelrite™, Duchefa Biochemie, #G1101) ½ SH medium + 10% sucrose for further confirmation of absence of contamination. For long term storage, fronds were grown on solid ½ SH medium + 10% sucrose in Magenta™ GA-7 containers, in a plant growth cabinet (SEQI-P4, Percival) in long day conditions (16h light /8h dark) at 15°C, with low light (intensity of 19.5 $\mu\text{M m}^{-2} \text{s}^{-1}$). Axenic stocks were sub-cultured every 6 months.

***Arabidopsis*:** *Arabidopsis thaliana* ecotype *Columbia-0* (Col-0, salk_CS60000) was used as WT. The PolIV mutant, *nrpd1a-4* (salk_083051) was previously described (Kanno et al. 2005). These lines were provided by The Nottingham *Arabidopsis* Stock Centre (NASC) (<http://arabidopsis.info/>). For all experiment with *Arabidopsis*, seeds were surface sterilized and sown in half-strength Murashige and Skoog (1/2 MS) media, (Duchefa Biochemie, #M0231) solid medium plates, stratified in the dark at 4°C for 3 days, and transferred to a growth chamber with long-day conditions (16h light /8h dark) at 21°C with a LED light intensity of 85 $\mu\text{M m}^{-2} \text{s}^{-1}$. Seedlings were then harvested and flash-frozen. When needed, seedlings were transferred to soil and grown under long-day conditions (16h light /8h dark) at 21°C, 60% humidity with a LED light intensity of 89 $\mu\text{M m}^{-2} \text{s}^{-1}$.

***Nicotiana benthamiana*:** After 7 days at 4°C in the dark, *Nicotiana* seeds were sown in soil, germinated, and grown under long-day conditions (16h light /8h dark) at 21°C, 60% humidity with a LED light intensity of 89 $\mu\text{M m}^{-2} \text{s}^{-1}$. They were used for agroinfiltration experiments once they have developed 4-6 true leaves. WT and *rdr6i* mutant lines seeds were previously described (Schwach et al. 2005).

Plant imaging:

Pictures of plants were taken with a Canon EOS 80D camera or with an Andonstar AD409 digital microscope. Scans of *N. benthamiana* leaves and *Spirodela* cultures in dishes were performed with an Epson Perfection V600 photo scanner.

Phylogenetic analysis and protein domain annotation:

To identify *Spirodela* orthologues and paralogues, DNA and protein sequences from *Arabidopsis* genes involved in silencing were retrieved from TAIR10 and blasted against *Spirodela* protein database (BLAST+(Camacho et al. 2009) version 2.8.1, blastp -qcov_hsp_perc 60 or 30) or against the *Spirodela* genome (BLAST+ version 2.8.1, tblastn with default parameters) to retrieve as many putative orthologues as possible. Candidate genes and proteins were sorted based on the presence of known domains and orthogroups formed based on known orthologues from other angiosperms. Protein sequences from several angiosperms were obtained from the EBI-EMBL Uniprot database (Consortium et al. 2022) (<https://www.uniprot.org>) based on blast searches against known proteins of each family and orthogroup. Protein alignments were performed using CLC Main Workbench 20 (QIAGEN) with Gap open cost = 10; Gap extension cost = 1 parameters. Using the same software, alignments were then used to generate unrooted trees with the Neighbor Joining method and Jukes-Cantor substitution model for protein distance. Maximum likelihood trees were constructed with 1000 bootstrap replicates. Domain annotations were carried as well in CLC with the Pfam-A v35 database (Mistry et al. 2020) and further validated and expanded by independent annotation using predictions with the Interpro database (Paysan-Lafosse et al. 2022).

Protein extraction and western blot:

Protein extraction: For protein extraction from *Arabidopsis* and *Spirodela*, plant material was flash-frozen upon harvesting and ground with a Silamat S6 as described in the RNA extraction section. For *N. benthamiana*, leaf tissue was ground in liquid nitrogen using mortar and pestle. 100mg of ground tissue was mixed and homogenized for 5 min. with 500µl of extraction buffer (0.7 M sucrose, 0.5 M Tris-HCl, pH 8, 5 mM EDTA, pH 8, 0.1 M NaCl, 2% b-mercaptoethanol) and cOmpleteTM mini EDTA-free protease inhibitor cocktail (Roche, #04693159001) following

manufacturer's instructions. 1 volume of TRIS-buffered phenol (pH 8) was added and incubated with agitation for 5 minutes. The upper phenolic phase was recovered after centrifugation (12000g for 10 min at 4°C) and proteins precipitated with 5 volumes of 0.1 M ammonium acetate dissolved in methanol at -20°C overnight. Following centrifugation (5000g for 15 min at 4°C), the resulting protein pellet obtained was washed twice with 0.1 M ammonium acetate dissolved in methanol and resuspended in 50-100 µL of resuspension buffer (3% SDS, 62.3 mM Tris-HCl, pH 8, 10% glycerol).

Protein blots: Western blot was carried following standard denaturing SDS-PAGE and blotting procedures ([Sambrook and Russell 2001](#)). Unless otherwise specified, 150µg of protein were resolved on SDS-polyacrilamide gels, transferred onto Inmobilon-P PVDF membrane (Millipore, # IPVH00010) and incubated with the appropriate antibodies (see below) in PBS with 0.1% Tween-20 and 5% non-fat dried milk. The primary antibody was incubated overnight at 4°C, and the HRP-conjugated secondary antibody for 1 hour at room temperature. Detection was performed using Clarity Max™ Western ECL Substrate (Biorad, #1705062), and imaged with the ChemiDoc Imaging system (Bio-rad). Following detection, loading was verified by coomassie staining of membranes.

Primary antibodies used for western blot: monoclonal (mouse) anti-HA tag [12CA5] (Abcam, #ab1424), dilution 1:10000. Polyclonal (rabbit) anti-H3 (Abcam #ab1791), dilution 1:10000. Polyclonal (rabbit) anti-H3K9me1 (Abcam #ab8896), dilution 1:2000. Monoclonal (mouse) anti-H3K9me2 (Abcam #ab1220), dilution 1:2000.

Secondary antibodies used for western blot: Polyclonal (goat) anti-mouse HRP-conjugated (ThermoFisher, #62-6520), dilution 1:10000. Polyclonal (goat) anti-rabbit HRP-conjugated (ThermoFisher, #65-6120), dilution 1:10000.

Histone PTM analysis by mass spectrometry:

Sample preparation: Nuclear isolation and acid-extraction of histones was performed from 2gr of *Arabidopsis* 12 days-old seedlings and *Spirodela* fronds following the protocol described in ([Scheid et al. 2022](#)). To check for quality of the samples, an aliquot corresponding to 5% of the extracted protein samples were run on a denaturing 15% SDS-PAGE stained with coomassie for visualization of bands. Protein samples were brought to 40µL using a vacuum concentrator and 20 µL of each histone sample was supplemented with 2 µL of 1 M triethylammonium bicarbonate (TEAB). Propionic anhydride (Sigma-Aldrich, Nr 240311) was freshly diluted in a ratio of 1:100 with

molecular-grade H₂O, and 2 μ l of the dilution were added to each sample and incubated at room temperature for 2 min. The reaction was quenched by adding 2 μ l of 80 mM hydroxylamine (Thermo Scientific, #90115) and incubation at 37°C for 20 min. Histones were digested by adding 250 ng trypsin (Trypsin Gold, Promega #V5280) and incubating at 37°C overnight. For the second propionylation on peptide level, 6 μ l of a fresh Propionic anhydride 1:100 dilution was added to the sample which was again incubated for 2min at room temperature before being quenched with 3 μ l of 80 mM hydroxylamine as described above. Samples were acidified by adding 50 μ L of 5% formic acid and desalted on C18 (Empore, #2215-C18) StageTips as in ([Rappsilber et al. 2007](#)).

nanoLC-MS/MS Analysis: The nano HPLC system (UltiMate 3000 RSLC nano system, ThermoFisher Scientific) was coupled to a Q Exactive HF-X or an Orbitrap Exploris 480 mass spectrometer equipped with a Nanospray Flex ion source (all parts ThermoFisher Scientific). Peptides were loaded onto a trap column (PepMap Acclaim C18, 5 mm \times 300 μ m ID, 5 μ m particles, 100 \AA pore size, ThermoFisher Scientific) at a flow rate of 25 μ l/min using 0.1% TFA as mobile phase. After loading, the trap column was switched in line with the analytical column (PepMap Acclaim C18, 500 mm \times 75 μ m ID, 2 μ m, 100 \AA , ThermoFisher Scientific). Peptides were eluted using a flow rate of 230 nl/min, starting with the mobile phases 98% A (0.1% formic acid in water) and 2% B (80% acetonitrile, 0.1% formic acid) and linearly increasing to 45% B over the next 120 min. This was followed by a steep gradient to 95% B in 5 min, stayed there for 5 min and ramped down in 2 min to the starting conditions of 98% A and 2% B for equilibration at 30°C. The Q Exactive HF-X mass spectrometer was operated in data-dependent mode, using a full scan (m/z range 380-1500, nominal resolution of 60,000, target value 1e6) followed by MS/MS scans of the 10 most abundant ions. MS/MS spectra were acquired using normalized collision energy of 28, isolation width of 1.0 m/z, resolution of 30.000, a target value of 1e5 and maximum fill time of 105 ms. Precursor ions selected for fragmentation (exclude charge state 1, 7, 8, >8) were put on a dynamic exclusion list for 20s. Additionally, the minimum AGC target was set to 5e3 and intensity threshold was calculated to be 4.8e4. The peptide match feature was set to preferred and the exclude isotopes feature was enabled. The Orbitrap Exploris 480 mass spectrometer was operated in data-dependent mode 'Cycle Time', performing a full scan (m/z range 350-1200, resolution 60,000, normalized AGC target 100%, compensation voltage CV of -45V), followed by MS/MS scans of the most

abundant ions for a cycle time of 2.0 seconds. MS/MS spectra were acquired using an isolation width of 1.2 m/z, normalized AGC target 200%, HCD collision energy of 30, orbitrap resolution of 30,000, maximum injection time of 100 ms and minimum intensity set to 50,000. Precursor ions selected for fragmentation (include charge state 2-6) were excluded for 20 s. The monoisotopic precursor selection (MIPS) mode was set to Peptide and the exclude isotopes feature was enabled.

Peptide identification and data analysis: For peptide identification, the RAW-files were loaded into Proteome Discoverer (version 2.5.0.400, Thermo Scientific). All hereby created MS/MS spectra were searched using MS Amanda v2.0.0.19924 ([Dorfer et al. 2014](#)). For the protein-identification-set, the peptide and fragment mass tolerance was set to ± 10 ppm, the maximum number of missed cleavages was set to 2, using tryptic enzymatic specificity without proline restriction. Peptide and protein identification was performed in two steps. For an initial search the RAW-files were searched against the *Arabidopsis* database called TAIR10 (32,785 sequences; 14,482,855 residues) or the database called Spirodela_polyrhiza_3_9509 (28,688 sequences; 8,725,633 residues), supplemented with common contaminants and sequences of proteins of interest. The result was filtered to 1 % FDR on protein level using the Percolator algorithm ([Käll et al. 2007](#)) integrated in Thermo Proteome Discoverer. A sub-database was generated for further processing. For the second search, the RAW-files were searched against the created sub-database using the same settings as above, but considering 5 missed cleavages and the following additional variable modifications: oxidation on methionine, deamidation on asparagine and glutamine, acetylation on lysine, phosphorylation on serine, threonine and tyrosine, methylation on lysine and arginine, di-methylation on lysine and arginine, tri-methylation on lysine, propionyl on lysine, propionyl on peptide N-terminal, glutamine to pyro-glutamate conversion at peptide N-terminal glutamine and acetylation on protein N-terminus. The localization of the post-translational modification sites within the peptides was performed with the tool ptmRS, based on the tool phosphoRS ([Taus et al. 2011](#)). Identifications were filtered again to 1 % FDR on protein and PSM level, additionally an Amanda score cut-off of at least 150 was applied. Proteins were filtered to be identified by a minimum of 2 PSMs in at least 1 sample. Peptides were subjected to label-free quantification using IMP-apQuant ([Doblmann et al. 2019](#)). Protein areas have been computed by summing up all peptides. Resulting protein areas were normalised using iBAQ ([Schwanhäusser et al. 2011](#)). For relative quantification of H3K9

modifications, the area of the peptides carrying each modification was normalized by the sum of the areas of the same peptide.

The mass spectrometry proteomics data have been deposited to the ProteomeXchange Consortium via the PRIDE partner repository with the dataset identifier PXD050443([Perez-Riverol et al. 2021](#)).

Chromatin immunoprecipitation (ChIP):

Chromatin immunoprecipitation (ChIP) was conducted on *Arabidopsis* 10-day-old seedlings (WT Col-0) and *Spirodela polyrhiza* #9509 fronds. Tissues (2g each) were fixed with 1% formaldehyde in PBS for 10 minutes at -70 kPa, and the cross-linking reaction was halted with 125 mM glycine. For nuclei isolation, the crosslinked tissues were frozen, ground into a fine powder in liquid nitrogen, and subsequently resuspended in M1 buffer (10 mM sodium phosphate pH 7.0, 100 mM NaCl, 1 M hexylene glycol, 10 mM 2-mercaptoethanol, and cOmpleteTM mini EDTA-free protease inhibitor cocktail (Roche, #04693159001)). The suspension was filtered through a double layered miracloth (Merck, #475855-1r), prior nuclei precipitation by centrifugation for 5 min, 2,000g at 4°C, followed by 5 rounds of washing using M2 buffer (10 mM sodium phosphate pH 7.0, 100 mM NaCl, 1 M hexylene glycol, 10 mM MgCl₂, 0.5% Triton X-100, 10 mM 2-mercaptoethanol, and cOmpleteTM) and a final washing round with M3 buffer (10 mM sodium phosphate pH 7.0, 100 mM NaCl, 10 mM 2-mercaptoethanol, and cOmpleteTM). Washed nuclei were resuspended in sonication buffer (10 mM Tris-HCl pH 8.0, 1 mM EDTA, 0.1% SDS, and protease inhibitor). Chromatin was sheared using a Covaris E220 High Performance Focused Ultrasonicator for 12 min at 4 °C (Duty factor 5.0; PIP 140.0; Cycles per Burst: 200) in 1 ml Covaris milliTUBE (Covaris, #520128), and debris was removed by centrifugation for 5 min, 12,000g at 4°C. The quality of the shearing step was assessed by controlling the length distribution of the DNA after sonication by reverse cross-linking DNA (as described below) on an aliquot of the sample (5%). DNA size distributions were analyzed on a 5200 Fragment Analyser System (Agilent, #M5310AA). A good shearing should yield DNA fragment of 150 to 300bp (Supplementary Figure 23). With the remaining sample, chromatin fragments were diluted 3X by adding 2 vol. of ChIP dilution buffer (16.7 mM Tris-HCl pH 8.0, 167 mM NaCl, 1.2 mM EDTA, 1.1% Triton X-100, 0.01% SDS, and cOmpleteTM). Protein A/G magnetic beads (ThermoFisher, #10002D and 10004D) (50mL of slurry per gr of tissue) were added to the sheared

chromatin depending on the antibody used (protein A beads for rabbit polyclonal antibodies and protein G for mouse monoclonal ones, see below) , followed by incubation (at 4 °C for 1 hr with rotation). Pre-cleared samples were then incubated overnight at 4°C overnight under rotation with 5 µg of specific antibodies: anti-H3 (rabbit polyclonal, Abcam, #ab1791), anti-H3K27me3 (rabbit polyclonal, Millipore, #07–449), anti-H3K4me3 (rabbit polyclonal, Abcam, #ab8580), anti-H3K9me1 (rabbit polyclonal, Abcam, 3ab8896), anti-H3K9me2 (mouse monoclonal, Abcam, #ab1220) or or anti-H3K27me1 (rabbit polyclonal, Merck-Millipore, #17–643). The following day, the samples were mixed and incubated with 30 µl of protein A/G magnetic beads (at 4 °C for 3 hr. with rotation), followed by several rounds of washing as follows: 2 rounds of low salt buffer (20 mM Tris-HCl pH 8.0, 150 mM NaCl, 2 mM EDTA, 1% Triton X-100, and 0.1% SDS), one of high salt buffer (20 mM Tris-HCl pH 8.0, 500 mM NaCl, 2 mM EDTA, 1% Triton X-100, and 0.1% SDS), one of LiCl buffer (10 mM Tris-HCl pH 8.0, 1 mM EDTA, 0.25 M LiCl, 1% IGEPAL CA-630, and 0.1% deoxycholic acid), and one final of TE buffer (10 mM Tris-HCl pH 8.0 and 1 mM EDTA). Immunoprecipitated DNA was eluted by adding 500 µl of elution buffer (1% SDS and 0.1 M NaHCO₃), followed by an incubation at 65°C for 15 minutes. Reverse crosslink was carried using 51 µl of reverse crosslink buffer (40 mM Tris-HCl pH 8.0, 0.2 M NaCl, 10 mM EDTA, 0.04 mg/ml proteinase K (ThermoFisher, #EO0491), incubated for 3 hr at 45°C followed by 16 hr at 65°C. Reverse crosslinked DNA was treated with 10 µg of RNaseA (ThermoFisher #EN0531) for 30min at RT , and purified with a MinElute PCR purification kit (Qiagen, #28004).

Staining of nuclei:

Arabidopsis tissue was obtained from the second youngest leaf of a 3-week-old rosette grown in soil. The leaf was cut and placed on a previously chilled (4°C) sterile wet gauze and immediately processed. *Spirodea* fronds were obtained from cultures as described above. Tissue was processed according to ([Galbraith et al. 1983](#)) using a sharp razor blade (AstraTM superior platinum double edge, P&G) in 500µl of modified Otto's buffer I: 0.1M citric acid (PanReac AppliChem, #131808.121), 0.5% Triton-x-100 (PanReac AppliChem, #A1388.1000), pH 1.5 ([Otto et al. 1981](#)). After filtering through a 35µm cell strainer (FalconTM, #352235), 10µl of the nuclei solution were spread onto a glass slide, let dry and mounted with 10µl of DAPI-containing

Vectashield Antifade Mounting Medium (Vector Laboratories, #H-1200). Images of the DAPI-stained nuclei were taken using a Zeiss Axio Imager.Z2 with a sCMOS camera.

AGO4 cloning:

Genomic DNA from *Spirodesla* and *Arabidopsis* was purified using Dneasy® Plant mini kit (Qiagen, #69104) following the manufacturer's instructions and RNA isolated using TRIzol™ (ThermoFisher, #15596018) as described elsewhere. For cDNA cloning, 1µg of total RNA was treated with DNase I (Themofisher, #EN0521) and cDNA was synthesized using Maxima® First Strand cDNA Synthesis Kit (Thermo Scientific, #K1641) according to manufacturer's instructions. Amplification of all fragments was performed using 100ng of genomic DNA or cDNA as template with Phusion™ High-Fidelity DNA Polymerase (Thermo Scientific, #531S) and the primers described in Supplemental material.

A plasmid for the expression in plants of proteins tagged at the N-terminus with Flag and HA under the CaMV35s promoter was produced (35spromoter-Flag-HA-35sTerm). First by introducing a DNA fragment with the Flag sequence into a binary vector plasmid containing the 35S promoter used as backbone (Addgene #167122) through BamHI and HindIII (Thermo Scientific, #FD0054 and #FD0505) digestion and assembled using Gibson Assembly® Master Mix (NewEngland Biolabs, #E2611). The resulting plasmid (CaMV35Sp-Flag) and a DNA fragment containing the HA tag and CaMV35s terminator separated by XbaI sites, were further combined using BamHI and SmaI (Thermo Scientific, #FD0054 and #FD0663) and ligated with T4 DNA ligase (Thermo Scientific, #EL0021). The XbaI sites were introduced by PCR in AtAGO4 gDNA and SpAGO4a gDNA, cloned into the plasmid described above (35spromoter-Flag-HA-35sTerm), through XbaI (Thermo Scientific, #FD0685) digestion sites using Gibson Assembly. The PCR-amplified SpAgo4a cDNA was cloned into the same plasmid by digesting the PCR fragment with introduced BcuI sites in the extremities (Thermo Scientific, #FD1254), compatible with XbaI sites present in the plasmid, through T4 DNA ligase. All primers used for cloning can be found within **Supplemental Fig. S39**. All plasmids were transformed into chemically competent *E.coli* (DH5 α), confirmed by SANGER sequencing, and deposit in Addgene with the following numbers: p35S:FHA-AtAGO4_gDNA (#216838), p35S:FHA-SpAGO4a_gDNA (216841), p35S::FHA-SpAGO4a_cDNA (#216842).

Splicing analysis by RT-PCR:

RNA and cDNA were produced as described above. Oligonucleotides were designed to amplify two different regions containing several introns in SpAGO4a. All fragments were amplified by PCR using 100ng of cDNA or 10ng of plasmid, as a template, and the primers described in Supplemental material ([Supplemental Fig. S39](#)). The resulting fragments were resolved in a 1X TBE 1% agarose gel, stained with peqGreen (Peqlab, #732-3196) and imaged using the Molecular Imager® Gel Doc™ XR System (Bio-Rad).

***Agrobacterium*-mediated transient expression:**

***N. benthamiana*:** Agrobacterium-mediated transient expression in *N. benthamiana* was performed as in ([Felippes and Weigel 2010](#)). In brief, *A. tumefaciens* strain GV3101 harbouring the vectors described below were cultured at 28°C in LB medium with appropriate antibiotics. After 36 hours, cultures were pelleted at 2000g, 10 minutes at 20°C and resuspended to an OD₆₀₀ of 0.5 in filtered sterilized agroinfiltration buffer: 2mM MES, 50mM NaH₂PO₄, 0.5% (w/v) glucose, pH 5.6. Acetosyringone was added prior to use at 100 µM. After 1 hour of incubation at room temperature in darkness, the bacterial solutions were infiltrated into the abaxial side of young *N. benthamiana* true leaves, using a 1ml syringe without needle. At 3 or 5 days after infiltration (dpi), leaf discs were collected, flash-frozen in liquid nitrogen and ground in liquid nitrogen using morter and pestle. The ground samples were stored at -80C.

***Spirodela polyrhiza*:** For Agrobacterium-mediated transient expression in *Spirodela*, *Agrobacterium* strain EHA105 was used. Bacteria cultures were prepared as for *N. benthamiana* infiltrations with the following modifications: Bacteria was resuspended to OD₆₀₀ 0.8 in *Spirodela* agroinfiltration media (10 mM MgCl₂, 5% sucrose (w/v), pH 5.6). *Spirodela* fronds were prepared as it follows: Cultures were initiated from axenic stocks by inoculating fronds into 2L glass beakers containing 0.5-1L of ½ SH media, covered with the lid of a 145 x 20 mm polystyrene culture dish (Greiner Bio-One #639102) sealed with 2.5 cm wide Leucopore tape (Duchefa Biochemie #L3301). Cultures were grown to 50-80% confluence (as surface occupancy). Prior to agroinfiltration, fronds were pretreated as in ([Yang et al. 2018](#)) by transferring them to an ice-cold 20 mg/L L-Glutamine (PanReac AppliChem #A1420) solution for 20 min. Following pretreatment, fronds were infiltrated with the *Vir*-induced Agrobacterium

solution either (i) manually, at the budding pouch area with a 1 mL syringe without needle by gently applying pressure with the plunger on the upper side of fronds or, (ii) trough vacuum infiltration by transferring the fronds to 100 mL agrobacterium solution complemented with 0.02% (v/v) Silwet L-77 (Kurt-Obermeier GmbH #7060-10) in a 200 mL beaker in a vacuum desiccator. -70 kPa vacuum was applied twice for 10 min. Following either manual or vacuum agroinfiltration, excess of bacteria was removed by rinsing the fronds in ddH₂O and plants transferred to 100 x 20 mm culture dishes (Greiner Bio-One #664160) containing 30-50 mL ½ SH media + 100 µM acetosyringone for a 3 day co-culture. 4 days post-infiltration (dpi) transfer fronds to plates containing ½ SH media. At 7 dpi agrobacterium elimination was initiated by or replacing the media with ½ SH + 250 µM ticarcillin (Duchefa #T0190.0010, lab stock at 250 mg/mL in H₂O) + 300 µM cefotaxime (Duchefa #C0111.0005, lab stock at 300 mg/mL in H₂O) for a week. Plants were cultured with regular (1/week) ½ SH media replacements. See Supplementary Fig. S36 for a graphic depiction of the protocol and workflow.

Immunoprecipitation of Flag-tagged AGO4:

100-150mg of *N. benthamiana* ground tissue was homogenized in 1 ml of IP buffer (50 mM Tris-HCl, pH 7.5, 150 mM NaCl, 10% glycerol, 0.1% NP-40) containing 2 µM MG-132 and cOmplete™ mini EDTA-free protease inhibitor cocktail (Roche, #04693159001) for 30 minutes at 4 °C. After lysis, debris were removed by centrifugation (12000g for 10 min at 4°C). An aliquot of lysate was kept as input, while the remainder was incubated with ANTI-FLAG® M2 Magnetic beads (20µl of slurry/sample) (Sigma-Aldrich, #M8823) for 3 hours at 4°C, on a orbital shaker. After incubation, the resin was separated from supernatant in a magnetic rack (DynaMag-5, ThermoFisher, #12321D) and washed with 1 ml of IP buffer for 20 minutes at 4°C, for 3 times. After the final wash, 100µl of PBS were added and 10µl put aside, used to check immunoprecipitation quality by western blot by adding Laemli buffer and boiling the sample for 10 min. at 95°C. The remaining 90µl was used to analyze the small RNA composition upon extraction using TRIzol™ (ThermoFisher, #15596018). The isolated small RNAs were used to generate libraries and sequenced as described above. TraPR purified small RNAs (described above) from not-infiltrated plants were used to asses *N. benthamiana* small RNA profile.

Small RNA blot analysis:

AGO-loaded small RNAs were purified from 100mg of starting material using TraPR columns, as described above. The resulting small RNAs were mixed with an equal volume of 2X Novex™ TBE-Urea sample buffer (ThermoFisher, #LLC6876), separated on a 17.5% polyacrylamide-urea gel, transferred onto Hybond-NX membrane (Cytiva, #RPN303T) and chemically crosslinked (12.5M 1-methylimidazol (Merk, #M50834), 31.25mg/mL N-(3-dimethylaminopropyl)-N'-ethylcarbodiimide hydrochloride (Merk, #E7750) as in (Pall and Hamilton 2008). Probes produced from PCR templates were radiolabelled with [α -³²P]-dCTP (Hartmann Analytic, #SRP-305) using Prime-it II Random Primer Labelling kit (Agilent, #300385) and oligonucleotides used as a probe were radiolabelled with [γ -³²P]-ATP (Hartmann analytic #SRP-501), using T4 Polynucleotide kinase (Thermofisher, #EK0031) (see Supplementary figures for a list of oligonucleotides used). The probes were incubated in PerfectHyb™ Plus Hybridization Buffer (Sigma Aldrich, #H7033) and washed with 2XSSC, 0.1%SDS. The signal was detected with the Amersham™Typhoon™ (Cytivia). Probes and oligonucleotides used are listed in [Supplemental Fig. S39](#).

Small RNA extraction:

Total RNA: For small RNA extraction from total RNA and TraPR input fraction, 10 μ g of total RNA (as described above) or RNA extracted as described above from TraPR inputs was separated on a 15% denaturing polyacrylamide-urea gel. For size reference, 20 μ l of microRNA marker (New Englad Biolabs, #N2102S) were loaded in the same gel. Following gel staining with peqGreen (Peqlab, #732-3196), and using the marker as reference, small RNAs ranging from 17-to-25 nt were excised and recovered using the ZR small-RNA PAGE Recovery Kit (Zymo Research, #R1070).

TraPR: Purification of Argonaute-loaded small RNAs was performed according to the protocol described in (Grentzinger et al. 2020). In brief, 100mg of flash-frozen plant tissue was ground to fine powder using a Silamat S6 (Ivoclar Vivadent) twice for 3s in 1.5 mL microcentrifuge tubes with ~20 1 mm ø glass beads (Carl Roth, #A554.1). Frozen powder was incubated with TraPR lysis buffer and the homogenate loaded into the TraPR columns. TraPR eluates were collected and small RNAs extracted by adding and mixing 1 volume of acidic Phenol:Chloroform:Isoamyl alcohol (50:49:1, pH 4.5-5) (Carl Roth, #X985.1). After centrifugation (12000g for 10 min at 4°C) RNA was precipitated from the aqueous phase with 1 volume of isopropanol and 10% (v/v) of

sodium acetate 3M pH 5.2, overnight at -20°C. RNA was collected by centrifugation (12000g for 30 min at 4°C) and the resulting pellet was washed with 75% ethanol and resuspended in 10-20 µL RNase free water.

Supplementary References to Supplementary Methods

Camacho C, Coulouris G, Avagyan V, Ma N, Papadopoulos J, Bealer K, Madden TL. 2009. BLAST+: architecture and applications. *BMC Bioinform* **10**: 421.

Consortium TU, Bateman A, Martin M-J, Orchard S, Magrane M, Ahmad S, Alpi E, Bowler-Barnett EH, Britto R, Bye-A-Jee H, et al. 2022. UniProt: the Universal Protein Knowledgebase in 2023. *Nucleic Acids Res* **51**: D523–D531.

Doblmann J, Dusberger F, Imre R, Hudecz O, Stanek F, Mechtler K, Dürnberger G. 2019. apQuant: Accurate Label-Free Quantification by Quality Filtering. *J Proteome Res* **18**: 535–541.

Dorfer V, Pichler P, Stranzl T, Stadlmann J, Taus T, Winkler S, Mechtler K. 2014. MS Amanda, a Universal Identification Algorithm Optimized for High Accuracy Tandem Mass Spectra. *J Proteome Res* **13**: 3679–3684.

Felippes FF de, Weigel D. 2010. Transient assays for the analysis of miRNA processing and function. *Methods in molecular biology (Clifton, NJ)* **592**: 255–264.

Galbraith DW, Harkins KR, Maddox JM, Ayres NM, Sharma DP, Firoozabady E. 1983. Rapid Flow Cytometric Analysis of the Cell Cycle in Intact Plant Tissues. *Science* **220**: 1049–1051.

Grentzinger T, Oberlin S, Schott G, Handler D, Svozil J, Barragan-Borrero V, Humbert A, Duharcourt S, Brennecke J, Voinnet O. 2020. A universal method for the rapid isolation of all known classes of functional silencing small RNAs. *Nucleic Acids Res* **48**: gkaa472-.

Käll L, Canterbury JD, Weston J, Noble WS, MacCoss MJ. 2007. Semi-supervised learning for peptide identification from shotgun proteomics datasets. *Nat Methods* **4**: 923–925.

Kanno T, Huettel B, Mette MF, Aufsatz W, Jaligot E, Daxinger L, Kreil DP, Matzke M, Matzke AJM. 2005. Atypical RNA polymerase subunits required for RNA-directed DNA methylation. *Nature Genetics* **37**: 761–765.

Mistry J, Chuguransky S, Williams L, Qureshi M, Salazar GA, Sonnhammer ELL, Tosatto SCE, Paladin L, Raj S, Richardson LJ, et al. 2020. Pfam: The protein families database in 2021. *Nucleic Acids Res* **49**: gkaa913-.

Otto FJ, Oldiges H, Göhde W, Jain VK. 1981. Flow cytometric measurement of nuclear DNA content variations as a potential in vivo mutagenicity test. *Cytometry* **2**: 189–191.

Pall GS, Hamilton AJ. 2008. Improved northern blot method for enhanced detection of small RNA. *Nature Protocols* **3**: 1077–1084.

Paysan-Lafosse T, Blum M, Chuguransky S, Grego T, Pinto BL, Salazar GA, Bileschi ML, Bork P, Bridge A, Colwell L, et al. 2022. InterPro in 2022. *Nucleic Acids Res* **51**: D418–D427.

Perez-Riverol Y, Bai J, Bandla C, García-Seisdedos D, Hewapathirana S, Kamatchinathan S, Kundu DJ, Prakash A, Frericks-Zipper A, Eisenacher M, et al. 2021. The PRIDE database resources in 2022: a hub for mass spectrometry-based proteomics evidences. *Nucleic Acids Res* **50**: D543–D552.

Rappaport J, Mann M, Ishihama Y. 2007. Protocol for micro-purification, enrichment, pre-fractionation and storage of peptides for proteomics using StageTips. *Nat Protoc* **2**: 1896–1906.

Sambrook J, Russell DW. 2001. *Molecular Cloning*. CSHL Press.

Scheid R, Dowell JA, Sanders D, Jiang J, Denu JM, Zhong X. 2022. Histone Acid Extraction and High Throughput Mass Spectrometry to Profile Histone Modifications in *Arabidopsis thaliana*. *Curr Protoc* **2**: e527.

Schwach F, Vaistij FE, Jones L, Baulcombe DC. 2005. An RNA-Dependent RNA Polymerase Prevents Meristem Invasion by Potato Virus X and Is Required for the Activity But Not the Production of a Systemic Silencing Signal. *Plant Physiol*.

Schwanhäusser B, Busse D, Li N, Dittmar G, Schuchhardt J, Wolf J, Chen W, Selbach M. 2011. Global quantification of mammalian gene expression control. *Nature* **473**: 337–342.

Taus T, Köcher T, Pichler P, Paschke C, Schmidt A, Henrich C, Mechtler K. 2011. Universal and Confident Phosphorylation Site Localization Using phosphoRS. *J Proteome Res* **10**: 5354–5362.

Yang G-L, Fang Y, Xu Y-L, Tan L, Li Q, Liu Y, Lai F, Jin Y-L, Du A-P, He K-Z, et al. 2018. Frond transformation system mediated by *Agrobacterium tumefaciens* for *Lemna minor*. *Plant Mol Biol* **98**: 319–331.